

CONTROL SYSTEM DESIGN AND IMPLEMENTATION OF A TILT ROTOR
UAV

A THESIS SUBMITTED TO
THE GRADUATE SCHOOL OF NATURAL AND APPLIED SCIENCES
OF
MIDDLE EAST TECHNICAL UNIVERSITY

BY

LEVENT CEVHER

IN PARTIAL FULFILLMENT OF THE REQUIREMENTS
FOR
THE DEGREE OF MASTER OF SCIENCE
IN
AEROSPACE ENGINEERING

SEPTEMBER 2019

Approval of the thesis:

**CONTROL SYSTEM DESIGN AND IMPLEMENTATION OF A TILT
ROTOR UAV**

submitted by **LEVENT CEVHER** in partial fulfillment of the requirements for the degree of **Master of Science in Aerospace Engineering Department, Middle East Technical University** by,

Prof. Dr. Halil Kalıpçılar
Dean, Graduate School of **Natural and Applied Sciences**

Prof. Dr. İsmail Hakkı Tuncer
Head of Department, **Aerospace Engineering**

Prof. Dr. Ozan Tekinalp
Supervisor, **Aerospace Engineering Department, METU**

Examining Committee Members:

Assoc. Prof. Dr. İlkey Yavrucuk
Aerospace Engineering Department, METU

Prof. Dr. Ozan Tekinalp
Aerospace Engineering Department, METU

Prof. Dr. Kemal Leblebicioğlu
Electrical and Electronics Engineering Department, METU

Assist. Prof. Dr. Ali Türker Kutay
Aerospace Engineering Department, METU

Assist. Prof. Dr. Kutluk Bilge Arıkan
Mechanical Engineering Department, TEDU

Date: 03.09.2019

I hereby declare that all information in this document has been obtained and presented in accordance with academic rules and ethical conduct. I also declare that, as required by these rules and conduct, I have fully cited and referenced all material and results that are not original to this work.

Name, Surname: Levent Cevher

Signature:

ABSTRACT

CONTROL SYSTEM DESIGN AND IMPLEMENTATION OF A TILT ROTOR UAV

Cevher, Levent

M.S., Department of Aerospace Engineering

Supervisor: Prof. Dr. Ozan Tekinalp

September 2019, 153 pages

In this thesis, a hybrid vertical take off and landing unmanned air vehicle platform is designed and developed. The platform uses tricopter configuration for takeoff and landing while it uses its fixed wings for forward flight. Control algorithms are developed for the VTOL aircraft. For this purpose, first nonlinear simulation code is developed in Matlab/Simulink environment. The simulation uses the wind tunnel experimental data for the propellers and aerodynamic data obtained from a package program XFLR 5 that uses panel method. The controller uses Linear Quadratic Tracking (LQT) algorithms for vertical takeoff, transition and forward flight cases. For different flight phases, trim flight conditions are obtained and controllers are designed. During transition, weighted pseudo inverse and blended inverse control allocation methods are employed and simulation results are compared. The obtained controller gains are tuned in the lab test setup and flight tests are performed for vertical takeoff and landing flight, demonstrating acceptable flight performance.

Keywords: Tricopter, tilt-rotor, unmanned air vehicle, attitude control, linear quadratic

tracking, flight test

ÖZ

DÖNER ROTORLU İHA KONTROL SİSTEM TASARIMI VE UYGULAMASI

Cevher, Levent

Yüksek Lisans, Havacılık ve Uzay Mühendisliği Bölümü

Tez Yöneticisi: Prof. Dr. Ozan Tekinalp

Eylül 2019 , 153 sayfa

Bu tez çalışmasında, hibrit bir dikey kalkış ve iniş yapabilen insansız hava aracı platformu tasarlanmış ve geliştirilmiştir. Platform, kalkış ve iniş için üç motorlu/pervaneli hava aracı (tricopter) konfigürasyonunu kullanırken, ileri uçuş için sabit kanatlarını kullanır. Dikey kalkış ve iniş yapabilen uçak için kontrol algoritmaları geliştirilmiştir. Bu amaçla, ilk doğrusal olmayan simülasyon kodu, Matlab/Simulink ortamında oluşturulmuştur. Simülasyon, pervaneler için rüzgar tüneli deney verilerini ve panel yöntemini kullanan bir paket program olan XFLR 5'ten elde edilen aerodinamik verileri kullanmaktadır. Kontrolcü, dikey kalkış, geçiş ve ileri uçuş durumları için Doğrusal Kuadratik İzleme (LQT) algoritmalarını kullanır. Farklı uçuş aşamaları için uçuş denge noktası koşulları elde edilmiş ve kontrolcülerini tasarlanmıştır. Geçiş sırasında, weighted pseudo inverse ve blended inverse kontrol tahsis yöntemleri kullanılmış ve simülasyon sonuçları karşılaştırılmıştır. Elde edilen kontrolcü kazançları, laboratuvar test düzeneğinde ayarlanmış ve kabul edilebilir uçuş performansını gösteren dikey kalkış ve iniş için uçuş testleri gerçekleştirilmiştir.

Anahtar Kelimeler: Üç motorlu/pervaneli hava aracı, döner rotor, durum kontrolü,

doğrusal kuadratik izleme, uçuş testi

To my family, and my love.

ACKNOWLEDGMENTS

I would like to thank and express my gratitude to my advisor Prof. Dr. Ozan Tekinalp for his guidance and support for so many years. His valuable ideas helped me to accomplish the thesis. Thus, I appreciate that he gave me a chance to study in aerospace engineering, of which I have been eager to learn for so many years since I was in high school.

I would like to thank Anıl Sami Önen, with whom I started thesis studies and I learned so many things from him. It was a starting point for me to study on experimental side. Furthermore, I would like to thank Murat Şenipek, who helped me for modeling part. He had been always willing to share his experience whenever I needed. I would like to thank İsmail Özdemir Uzunlar, Osman Güngör, Metehan Yayla, Talha Mutlu, Emre Can Suiçmez, Onur Güreş, Derya Kaya and Ali Onur Baykal for their company during the studies. It was always a pleasure for me to study with them and learn from them. I would like thank them all for their valuable time.

I would like to thank Dr. Saffet Gökuç, who has always helped me whenever I needed most. He is the one who never hesitates to help me. I would like to thank him for his valuable ideas and precious time. He helped me during the manufacturing part and the flight tests. After each flight test failure he was the one to make it fly again.

I would like to express my deepest gratitudes to my mother, my grandfather, and my grandmother who always believed in me and supported me through my life. I am also grateful for my wife Göksu. She is the one who gave me the courage to start the thesis. I would like to thank her for her patience and her endless love. Without her, I could not find enough strength to overcome all the difficulties.

TABLE OF CONTENTS

ABSTRACT	v
ÖZ	vii
ACKNOWLEDGMENTS	x
TABLE OF CONTENTS	xi
LIST OF TABLES	xvii
LIST OF FIGURES	xix
LIST OF SYMBOLS	xxvi
CHAPTERS	
1 INTRODUCTION	1
1.1 Motivation and Objectives	1
1.2 UAV Literature Survey	1
1.2.1 UAV Types	2
1.3 Thesis Content	4
2 DYNAMIC MODEL	7
2.1 Introduction	7
2.2 Propulsion System Model	7
2.3 Reference Frames and Transformations	20
2.3.1 Wind Frame from Body-Fixed Frame	21

2.3.1.1	Derivation of Velocity Angles	21
2.4	Forces and Moments	21
2.4.1	Aerodynamic Forces	22
2.4.2	Gravitational Force	25
2.5	Propeller Forces on Body Center of Mass	25
2.6	Propeller Moments on Body Center of Mass	26
2.7	Dynamic Model	28
2.7.1	Rotational Motion	29
2.7.2	Forces and Moments in Hover Flight	30
2.7.3	Forces and Moments in Forward Flight	32
3	TRIMMING AND LINEARIZATION	35
3.1	Introduction	35
3.2	Trimming Approach for Hover Position	35
3.3	Linearization of Hover Flight Equations	36
3.4	Trimming Approach for Forward Flight	37
3.5	Simplification of Aerodynamic Coefficients	37
4	CONTROL METHODS	41
4.1	Introduction	41
4.2	Tricopter Attitude Control Strategy	41
4.3	Forward Flight Control Strategy	44
4.4	Control Design Approach	45
4.4.1	Linear Quadratic Tracker (LQT) Control	46
4.4.1.1	Tricopter Mode Attitude Control Approach	47

4.4.1.2	Forward Flight Attitude Control Approach	49
4.5	Transition Control Allocation Methods	50
4.5.1	Weighted Moore-Penrose Pseudo Inverse	50
4.5.2	Blended Inverse	53
4.6	Flight Management Overview	54
5	MODEL ENVIRONMENT AND SIMULATION RESULTS	57
5.1	Introduction	57
5.2	Simulation Specifications	57
5.3	Tricopter Platform Attitude Control Simulations	59
5.3.1	Roll Control	59
5.3.2	Pitch Control	61
5.3.3	Yaw Control	63
5.4	VTOL Platform Tricopter Attitude Control Simulations	65
5.4.1	Roll Control	65
5.4.2	Pitch Control	67
5.4.3	Yaw Control	69
5.5	VTOL Platform Transition to Forward Flight Control Simulations	71
5.5.1	Transition Control	71
5.6	VTOL Platform Forward Flight Control Simulations	77
5.6.1	Roll Control	77
5.6.2	Pitch Control	79
5.6.3	Yaw Control	81

5.7	VTOL Platform Transition to Tri-coper Mode Attitude Control Simulations	83
5.7.1	Transition Control	83
6	HARDWARE COMPONENTS AND SOFTWARE ENVIRONMENT	89
6.1	Avionics	89
6.1.1	Autopilot Platform	90
6.1.2	Telemetry	91
6.1.3	GPS Module	92
6.2	Software Development Environment and Architecture	93
7	SYSTEM CONFIGURATION TESTS	95
7.1	Introduction	95
7.2	Lab Tests and Results	95
7.2.1	Tricopter Lab Tests	96
7.2.2	Dummy-Wing VTOL Configuration Lab Tests	98
7.3	Flight Tests and Results	101
7.3.1	Tricopter Flight Tests	101
7.3.2	VTOL Configuration Flight Tests	104
8	CONCLUSION	107
	REFERENCES	109
	APPENDICES	
A.1	Previous Platform Studies	113
A.1.1	Dynamic Model of Motor	113
A.1.2	Dynamic Model	115

A.1.3	Trimming Approach for Hover Position	116
A.1.4	Linearization of Hover Flight Equations	117
A.1.5	Linear Quadratic Tracking Control	118
A.1.5.1	Linear Quadratic Tracking (LQT) Controller	119
A.1.5.1.1	LQT Controller - Attitude Control	119
A.1.5.1.2	LQT Controller - Ground Speed Control	120
A.1.5.2	Linear Quadratic Regulator Control with Integral Action (LQR-I)	120
A.1.5.2.1	Attitude Controller	122
A.1.6	Control Allocation Approach	122
A.1.7	Simulation Tests and Results	124
A.1.7.1	Tricopter Roll Control	127
A.1.7.2	Tricopter Pitch Control	128
A.1.7.3	Tricopter Yaw Control	129
A.1.7.4	Tricopter Ground Speed Hold Control	130
A.1.8	Flight Tests and Results	132
A.1.8.1	Tricopter Flight Tests	132
A.1.8.1.1	LQT Tri-coper Attitude Controller - Approach-1	133
A.1.8.1.2	LQT Tricopter Attitude Controller - Approach-2	134
B.2	Dummy-wing Mass and Inertia Calculation	139
B.2.1	Mass Moment of Inertia of Prism	139
B.2.2	Dummy Weights	140
B.2.3	Mass Moment of Inertia of Hollow Cylinder	140

C.3	LQT - Weighting Matrices and Gains for Tricopter Attitude Control	141
C.4	LQT - Weighting Matrices and Gains for Forward Flight Control	142
C.5	Weighted Pseudo Inverse - Transition to Forward Flight Control	143
C.6	Blended Inverse - Transition to Forward Flight Control	143
C.7	Weighted Pseudo Inverse - Transition to Tricopter Attitude Control	144
C.8	Blended Inverse - Transition to Tricopter Attitude Control	144
D.9	LQT - Weighting Matrices and Gains for Tricopter Attitude Control	147
D.10	LQR-I - Weighting Matrices and Gains for Attitude Control	148
D.11	LQT - Weighting Matrices and Gains for Tricopter Ground Speed Hold Control	149
E.12	Coefficients of Motor-Propeller Surface Fit Equations	151
E.13	Aerodynamic Coefficients	152
E.14	VTOL and Tricopter Parameters	153

LIST OF TABLES

TABLES

Table 2.1	Fitness quality of surface data	16
Table 2.2	Thrust vs Angular speed of motor relation at vertical position for $F[N] = k.\Omega_i^2$	17
Table 2.3	Torque vs Angular speed of motor relation at vertical position for $F[N] = l.\Omega_i^2$	17
Table 2.4	Linear curve fit parameter values for motor-prop thrust at 90° tilt position	18
Table 2.5	Linear curve fit parameter values for motor-prop torque at 90° tilt position	19
Table 2.6	Second degree polynomial model for rpm to throttle command - Scorpion SII-3020-780Kv motor and 11x5.5 APC combination at 0[deg] tilt position	20
Table 2.7	Second degree polynomial model for rpm to throttle command - Scorpion SII-3020-780Kv motor and 11x5.5 APC combination at 90[deg] tilt position	20
Table 3.1	Trim values for hover with Scorpion 3020-780kv motor and APC 11x5.5 combination	36
Table 3.2	Trim flight results for forward flight	39
Table A.1	Trim values for hover with AXI 2826/10 - Xoar 11x4 combination	117

Table E.2	Coefficients of Force Surface Fit Equations	151
Table E.3	Coefficients of Torque Surface Fit Equations	151
Table E.4	Coefficients of RPM Surface Fit Equations	151
Table E.5	C_X aerodynamic coefficients	152
Table E.6	C_Y aerodynamic coefficient	152
Table E.7	C_Z aerodynamic coefficients	152
Table E.8	C_l aerodynamic coefficients	152
Table E.9	C_m aerodynamic coefficients	152
Table E.10	C_n aerodynamic coefficients	152
Table E.11	Position vectors of each motor according to Center of Gravity (CG) .	153

LIST OF FIGURES

FIGURES

Figure 1.1	Hybrid VTOL UAV examples	4
Figure 2.1	Wind Tunnel test setup	9
Figure 2.2	Experimental results for 90 [deg] propeller axis	10
Figure 2.3	Experimental results for 70 [deg] propeller axis	11
Figure 2.4	Experimental results for 50 [deg] propeller axis	12
Figure 2.5	Experimental results for 30 [deg] propeller axis	13
Figure 2.6	Experimental results for 0 [deg] propeller axis	14
Figure 2.7	Throttle to RPM conversion block	15
Figure 2.8	0 [deg] tilted motor test data and curve fit function of Scorpion SII-3020-780Kv motor and 11x5.5 APC combination	17
Figure 2.9	90 [deg] tilted motor test data and curve fit function of Scorpion SII-3020-780Kv motor and 11x5.5 APC combination	18
Figure 2.10	Throttle vs rpm curve fit function Scorpion SII-3020-780Kv mo- tor and 11x5.5 APC combination at hover	19
Figure 2.11	Tricopter - Tilt Rotor VTOL configuration	22
Figure 2.12	3D Panel method solution for flying wing model	22
Figure 2.13	Aerodynamic forces and moments model	24

Figure 4.1	Tricopter attitude control allocation	42
Figure 4.2	Heading control allocation	43
Figure 4.3	Attitude control allocation for tricopter mode flight	43
Figure 4.4	Attitude control allocation for forward flight	44
Figure 4.5	Forward flight control allocation	45
Figure 4.6	Modes and Phases	54
Figure 4.7	Plane mode - phase transition flow chart	55
Figure 4.8	Tricopter mode - phase transition flow chart	56
Figure 5.1	Simulation block - Dynamic model of platform	58
Figure 5.2	LQT control result for given roll command	59
Figure 5.3	Tricopter frame responses for LQT controller for given roll command	60
Figure 5.4	LQT control result for given pitch command	61
Figure 5.5	Tricopter frame responses for LQT controller for given pitch command	62
Figure 5.6	LQT control result for the given yaw command	63
Figure 5.7	Tricopter frame responses for LQT controller for given yaw command	64
Figure 5.8	LQT control result for the given roll command	65
Figure 5.9	VTOL frame responses for LQT controller for the given roll command	66
Figure 5.10	LQT control result for the given pitch command	67

Figure 5.11	VTOL frame responses for LQT controller for the given pitch command	68
Figure 5.12	LQT control result for the given yaw command	69
Figure 5.13	VTOL frame responses for LQT controller for given yaw command	70
Figure 5.14	Throttle outputs - Weighted pseudo inverse allocation	72
Figure 5.15	Throttle outputs - Blended inverse allocation	72
Figure 5.16	Theta Response - Weighed Pseudo Inverse allocation	73
Figure 5.17	Theta Response - Blended Inverse allocation	73
Figure 5.18	Commands and platform response histories for transition to forward flight attitude control phase	73
Figure 5.19	Front tilt servo command history during transition to forward flight attitude control phase	74
Figure 5.20	Ground position change histories for transition to forward flight attitude control phase	74
Figure 5.21	Actuator command histories for transition to forward flight attitude control phase	75
Figure 5.22	Body Velocities - Weighted pseudo inverse allocation	76
Figure 5.23	Body Velocities - Blended inverse allocation	76
Figure 5.24	Roll command and roll angle response during forward flight . . .	77
Figure 5.25	Aileron deflection command due to given roll command	77
Figure 5.26	VTOL frame responses during 15 [deg] roll command in forward flight	78
Figure 5.27	Pitch command and pitch angle response during forward flight .	79
Figure 5.28	Elevator deflection command due to pitch command forward flight	79

Figure 5.29	VTOL frame responses during 15 [deg] pitch command in forward flight	80
Figure 5.30	Yaw command and yaw angle response during forward flight . . .	81
Figure 5.31	Rudder deflection command due to yaw command during forward flight	81
Figure 5.32	VTOL frame responses during heading commands in forward flight	82
Figure 5.33	Throttle outputs - Weighted pseudo inverse allocation	84
Figure 5.34	Throttle outputs - Blended inverse allocation	84
Figure 5.35	Theta Response - Weighed Pseudo Inverse allocation	85
Figure 5.36	Theta Response - Blended Inverse allocation	85
Figure 5.37	Commands and platform response histories for transition to tri-copter attitude control phase	85
Figure 5.38	Front tilt servo command history during transition to tri-copter attitude control phase	86
Figure 5.39	Ground position change histories for transition to tri-copter mode attitude control phase	86
Figure 5.40	Actuator command histories for transition to tri-copter attitude control phase	87
Figure 5.41	Body Velocities - Weighted pseudo inverse allocation	88
Figure 5.42	Body Velocities - Blended inverse allocation	88
Figure 6.1	Avionic Setup	90
Figure 6.2	Pixhawk board	90
Figure 6.3	GPS+Mag module	92

Figure 6.4	Pixhawk board	94
Figure 7.1	Tricopter lab test result for the given roll command	96
Figure 7.2	Tricopter lab test photo	96
Figure 7.3	Tricopter lab test result for the given theta command	97
Figure 7.4	Tricopter lab test result for the given yaw command	97
Figure 7.5	Tricopter lab test - throttle input command	97
Figure 7.6	Tricopter lab test throttle responses of motors	98
Figure 7.7	Dummy-Wing configuration lab test photo	99
Figure 7.8	Dummy-Wing configuration lab test result for the given roll command	99
Figure 7.9	Dummy-Wing configuration lab test result for the given theta command	99
Figure 7.10	Dummy-Wing configuration lab test result for the given yaw command	100
Figure 7.11	Dummy-Wing configuration lab test - throttle input command . .	100
Figure 7.12	Dummy-Wing configuration lab test - throttle responses of motors	100
Figure 7.13	Tricopter flight test photo	102
Figure 7.14	Tricopter flight test result for the given roll command	102
Figure 7.15	Tricopter flight test result for the given theta command	102
Figure 7.16	Tricopter flight test result for the given yaw command	103
Figure 7.17	Tricopter flight test - throttle input command	103
Figure 7.18	Tricopter flight test - throttle responses of motors	103
Figure 7.19	VTOL tricopter mode attitude control flight test photo	104

Figure 7.20	VTOL tricopter mode attitude control flight test result for the given roll command	105
Figure 7.21	VTOL tricopter mode attitude control flight test result for the given theta command	105
Figure 7.22	VTOL tricopter mode attitude control flight test result for the given yaw command	105
Figure 7.23	VTOL tricopter mode attitude control flight test - throttle input command	106
Figure 7.24	VTOL tricopter mode attitude control flight test - throttle responses of motors	106
Figure A.1	Torque[N.m] vs. RPM relation with Axi 2826/10 motor and Xoar 11x4 propeller	113
Figure A.2	Thrust[N] vs. RPM relation with Axi 2826/10 motor and Xoar 11x4 propeller	114
Figure A.3	RPM vs. Throttle[%] relation with Scorpion 3020-780kv and APC 11x5.5 propeller combination	115
Figure A.4	Dynamic model of tricopter	125
Figure A.5	System model of ground speed hold and attitude controllers	126
Figure A.6	Simulation results of LQT and LQR-I controllers for roll command	127
Figure A.7	Simulation results of LQT and LQR-I controllers for pitch command	128
Figure A.8	Simulation results of LQT and LQR-I controllers for yaw command	129
Figure A.9	LQT-Tricopter ground velocity responses for given reference commands	130

Figure A.10	LQT-Tricopter ground position changes for given reference commands	130
Figure A.11	Simulation results of LQT ground speed hold and attitude controllers for given speed commands	131
Figure A.12	Tricopter (Axi-Xoar configuration) flight test photo	132
Figure A.13	Tricopter flight test result for given roll command	133
Figure A.14	Tricopter flight test result for given pitch command	133
Figure A.15	Tricopter flight test result for given yaw command	133
Figure A.16	Tricopter flight test - throttle input command	134
Figure A.17	Tricopter flight test - throttle responses of motors	134
Figure A.18	Tricopter flight test result for given roll command	135
Figure A.19	Tricopter flight test result for given pitch command	135
Figure A.20	Tricopter flight test result for given yaw command	135
Figure A.21	Tricopter flight test - throttle input command	136
Figure A.22	Tricopter flight test - throttle responses of motors	136
Figure B.23	Dummy-wing configuration layout	139

LIST OF SYMBOLS

SYMBOLS

α, β	Angle of attack, angle of side slip
b	Wing span
A, B	System Matrix, Input Matrix
C, D	Output Matrix, Feed-through Matrix
\bar{c}	Mean chord length
C_L, C_Y, C_D	Lift, side-force, drag coefficients
C_X, C_Y, C_Z	Body-axis aerodynamic force coefficients
C_l, C_m, C_n	Body-axis aerodynamic moment coefficients
$\delta_{ail}, \delta_{elev}, \delta_{rud}$	Aileron, elevator, rudder control surface deflections
δ_{thi}	Throttle input for i^{th} motor
F_i	Thrust force generated by i^{th} motor on body-fixed frame
F_i^b	Thrust force generated by i^{th} motor
F_B	Body-fixed frame
F_E	Earth-fixed frame
g	Gravitational acceleration
γ	Aft tilt servo angle
i	Presents which motor is referred i=1: Front-left motor i=2: Front-right motor i=3: Aft motor
Ω_i	Rotational speed generated by i^{th} motor
k	Constant relates Ω_i to F_i
l	Constant relates Ω_i to Q_i

L_{EB}	Transformation matrix from earth-fixed frame to body-fixed frame
L_{EB}	Transformation matrix from body-fixed frame to earth-fixed frame
L_{WB}	Transformation matrix from body-axis to wind-axis
m_{tri}	Mass of tricopter
m_{vtol}	Mass of VTOL
M^P	Moment vector generated by motor in body-fixed frame
M^R	Induced moment vector generated by motor
$\phi_{cmd}, \theta_{cmd}, \psi_{cmd}$	Control commands in euler angles (roll, pitch, yaw)
ϕ, θ, ψ	Navigation euler angles (roll, pitch, yaw)
I_x, I_y, I_z	Body inertia in x, y and z axes
p, q, r	Body angular velocities
$\dot{p}, \dot{q}, \dot{r}$	Body angular acceleration components
Q_i	Reactive torque generated by i^{th} motor
r_i	Distance vector of i^{th} motor from CG
r_x, r_y, r_z	Distances between i^{th} motor between and CG
σ	Front tilt servo angle
S	Wing area
T_{C2M}	Transformation matrix from control commands to moments and force inputs.
U_E, V_E, W_E	Velocity vector in earth fixed frame
U_d, V_d, W_d	Desired velocity vector in earth fixed frame
V_w	Wind velocity
V_∞	Air speed of the platform
ω	Angular velocity
x_B, y_B, z_B	Positions in body-axis frame
x_E, y_E, z_E	Positions in earth-axis frame

CHAPTER 1

INTRODUCTION

1.1 Motivation and Objectives

The scope of this thesis is to develop a vertical take-off and landing (VTOL) air vehicle and design an attitude controller. It is aimed to implement flight tests to observe the performance of the platform. VTOL system can take-off and land vertically by thrust vectoring of motors and it tilts front motors to enable wing and control surfaces to create lift and sustain control on platform to hold desired forward flight regime. The platform can be used as a test-bed by providing configuration choices for both tricopter and winged assembly. Therefore, developments for platform approaches conducted firstly on tricopter and then for the winged VTOL configuration. Beside tricopter mode attitude controller and plane mode forward flight controller design, transition control methodology also requires detailed analysis [28].

In this chapter, brief information about UAVs and UAV types are given. Thus detailed information about VTOL concepts and recent development approaches are presented. Comparison between rotary and fixed wing UAVs and VTOL concepts are discussed and advantages of VTOL systems are highlighted.

1.2 UAV Literature Survey

UAV is a flying vehicle without a pilot, which can be remotely controlled from a ground control station. It gives the ability of semi or full autonomous capabilities [12]. It is equipped with electronic sensors and control devices. UAV provides flexibility in mobility and response time, and eliminates safety concerns. Its contribution

emerges as lower mission costs and enables acquisition of information in a shorter time frame [32]. UAVs are being used for surveying, delivering goods to customers, conducting inspection at hard-to-reach places, traffic monitoring, disaster monitoring and mitigation, as well as for search and rescue operations.

UAV systems are mostly used for military purposes and have tended to be driven by military applications, which is also true for many technology areas such that civilian practices tends to follow the development and testing had been carried out in military [25]. Their advantages come in sight depending on the vitality of task. For instance, long hours of surveillance can be tiring for the aircrew, which can lead to loss of effectiveness of given task. Monitoring chemical and nuclear pollution, and crop-spraying with chemicals without putting aircrew into risk is another advantage of UAVs. They are also advantageous in military usages as they are more difficult to detect due to their smaller size and stealth capabilities. During mission, valuable avionics and payloads may be damaged, but beside these pilots do not need to think about the consequences of their choices which leads to stress. Thus, they can focus only on the task in hand [4].

1.2.1 UAV Types

Differentiation in UAV types emerged due to mission requirements of a desired task. Therefore, it is more useful to categorize UAVs according to their mission types. Considering this UAVs can be classified as fixed-wing horizontal takeoff landing (HTOL), Rotary-wing VTOL and hybrid configurations (tilt-wing, tilt-rotor, tilt-body and ducted fan) and unconventional.

HTOL UAVs are categorized into four subtypes such as tailplane-aft, tailplane forward, tail-aft on booms, and tailless or flying wing UAVs. Lift is generated by wing and as the name suggest these UAVs mainly require a runway to take-off and land. They are advantageous on long range and endurance capabilities. Due to their design characteristics, they have simpler mechanism and consume less energy than rotary-wings UAVs.

Rotary-wing VTOL configurations can be seen in many different provisions. Single

main rotor with tail rotor helicopter is the well known type of it. Other configurations are mainly driven by counter-action rotor torque. Beside helicopters, rotary-wing configurations can be categorized as co-axial rotor, tandem rotor and multi rotor configurations (tricopter, quadcopter, hexacopter, etc.). These type of UAVs do not require runways. Thus they can hang in the air for desired altitude, which is important for monitoring and surveillance. They are not as fast as fixed wing configurations, and can not stay in the air for a long time.

Those winged UAVs enjoy longer flight time and endurance and they have a capability to carry heavier payload. On the other hand, helicopters are good for hovering over a location for a long time, and takeoff and land vertically. Similarly, multi-copters can also take-off and land vertically, with lower flight efficiency than helicopter. However, they are simpler to construct. Vertical take-off and landing fixed winged UAVs such as tilt-rotor, tilt-duct, tilt-wing configurations offer advantages of helicopters in terms of operational flexibility and winged aircraft in terms of reaching longer ranges, and capacity to carry heavier payload [27], [3].

Recent studies mainly focus on combining best parts of rotary-wing and fixed-wing configurations. Hybrid VTOL configurations are categorized into tilt-rotor, tilt-wing, tilt-body, and ducted fan UAVs [14, 4]. Tilt rotor VTOLs work in vertical position for take-off and landing; but in forward flight main rotors tilt 90 degrees, till they are positioned horizontally. Moreover, in tilt-wing configuration logic is the same with tilt-rotor configurations, but they tilt the wing instead of motors. It is stated that tilt-rotors are efficient in hover flight whereas tilt-wing configurations are more successful in forward flight [14]. Tilt-body UAV is a combination of previous two configurations. This type can change incidence angle through rotating around shaft. Ducted fan UAVs has enclosed thrust regions which are composed of most likely contra-rotating mounts to eliminate reactive torque effect on the body. Approaches and examples of some hybrid VTOL platforms can be seen in Figure (1.1)



(a) Cypher II [6]



(b) Scorpion Model 100 [31]



(c) NASA GL-10 Greased Lightning [1]



(d) The Lilium Jet five-seat VTOL aircraft [18]



(e) AeroVironment SkyTote [13]



(f) Bell Eagle Eye [7]

Figure 1.1: Hybrid VTOL UAV examples

1.3 Thesis Content

In this thesis, modelling and transition flight control of a tilt-rotor UAV is addressed. It consists of a tricopter configuration with fixed flying wing. A mathematical model and a non-linear simulation code for all three phases of flight are developed. Trimming and linearization are carried out for hover and forward flight conditions. Transition is controlled by tilting front motors to the horizontal position and activating aerodynamic control surfaces to achieve a stable forward flight. Following chapters describe the platform operation. In Chapter 2, dynamic model of the motor and platform

is described and propulsion, aerodynamic and flight mechanics model are presented. In Chapter 3, trimming and linearization methodologies are presented. In Chapter 4, the flight controller, control allocation strategies for both tricopter and VTOL configurations are presented. Flight management system state-flow charts are presented. In Chapter 5, simulation results for tricopter mode attitude control flight, transition and plane mode forward flight are given. In Chapter 6, system avionic components and software development environment are explained. Developed and modified software components are highlighted. In Chapter 7, lab and flight test results are presented which validate simulation tests and describes how system is emerged. Finally, the conclusion and future work are explained for system evaluation.

CHAPTER 2

DYNAMIC MODEL

2.1 Introduction

Tilt rotor tricopter-VTOL consists of two main parts, tricopter and wing. Tricopter have three motors, such that front motors are positioned on the same shaft and they are tilted by front tilt servo. Aft motor is tilted by aft servo motor. Wing have two elevons and two rudders. In this chapter, dynamic model of a tilt rotor tricopter VTOL platform is described. Simulation model includes platform aerodynamics, front and aft propeller dynamics, and gravity model. These models are developed in Matlab-Simulink environment with use of built-in 6-Degree of Freedom (DoF) equation model. Simulation model also includes control equation blocks, pilot input signal generation blocks, logger blocks to observe and understand system responses. Aerodynamic sub-system model includes wing static coefficients. Propulsion sub-system model includes lookup tables which are obtained from experimental test data. Since front and aft motors and propellers are same, same lookup tables are used for each of them. Propulsion model is used to get RPM, thrust and torque outputs for given tilt position and instant velocity for desired collective inputs for each motor.

2.2 Propulsion System Model

Propulsion system characteristics should be defined in order to find thrust and moment relations of tricopter. In tricopter frame, all three motor-propeller combinations are the same, so that set-up constructed according to one motor. Tests are performed in the wind tunnel of METU Aerospace Engineering Department as it is shown in

Figure (2.1a). Besides motor and propeller, experimental setup contains electrical speed controller (ESC), optical revolutions per minute (RPM) sensor, load-cell, power supply and throttle command control card as shown in Figure (2.1b).

ESC is used to drive motor according to the pulse width modulation (PWM) signal generated by Pixhawk microcontroller which is configured as a command control card. It monitors throttle input percentage coming from the radio controller. Optical RPM sensor is used to measure the angular speed of rotor for given throttle input position. Load-cell is used to measure the thrust and moments generated by rotor in three axes. According to commanded throttle input corresponding, thrust, torque and RPM values are collected. For motor-propeller combination Scorpion SII-3020-780Kv motor and 11x5.5 APC propellers are used. Mathematical model can be derived for thrust, torque, throttle and rotation speed of motor using experimental data.



(a) Wind Tunnel

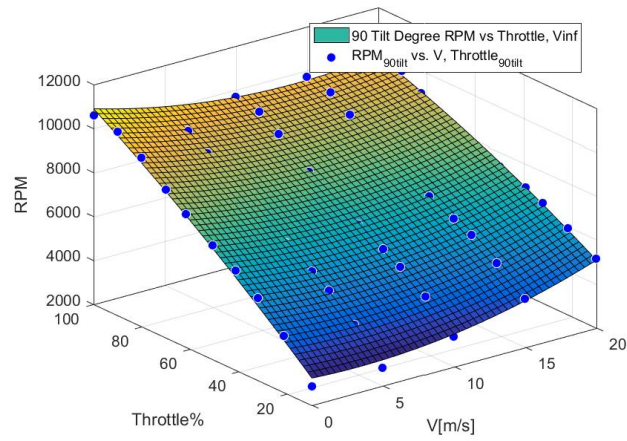


(b) Experimental Setup

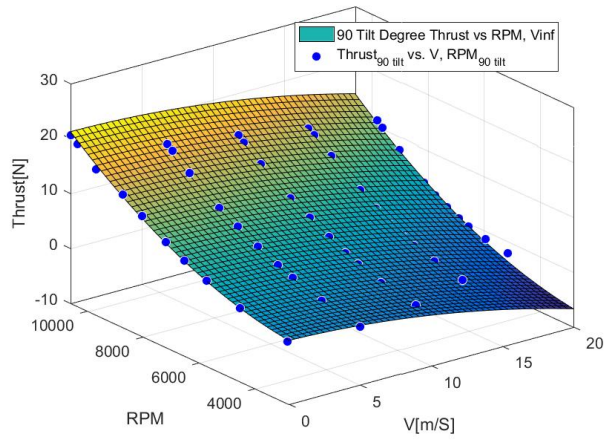
Figure 2.1: Wind Tunnel test setup

Real platform will be driven by control card which converts controller output to throttle command, in other words PWM. Moreover, experiments are conducted at different air speed and rotor axis tilt angles based on throttle command values. Desired airspeed generated by wind tunnel. The torque, thrust and angular speed data are recorded.

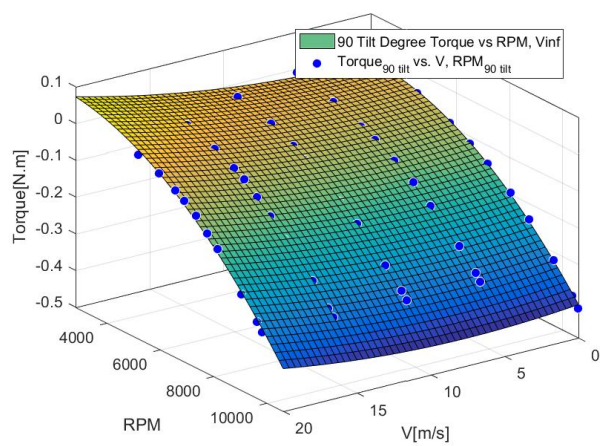
Wind tunnel tests are performed based on five tilt position [90° , 70° , 50° , 30° , 0°], and for each tilted position five wind tunnel speeds [0, 5, 10, 15, 20](m/s) are applied. Thus, for each tunnel speed, varying range of throttle commands are given. Surface fitting data for relevant study is presented in Figure (2.2), Figure (2.3), Figure (2.4), Figure (2.5) and Figure (2.6).



(a) RPM vs. throttle and wind speed plot

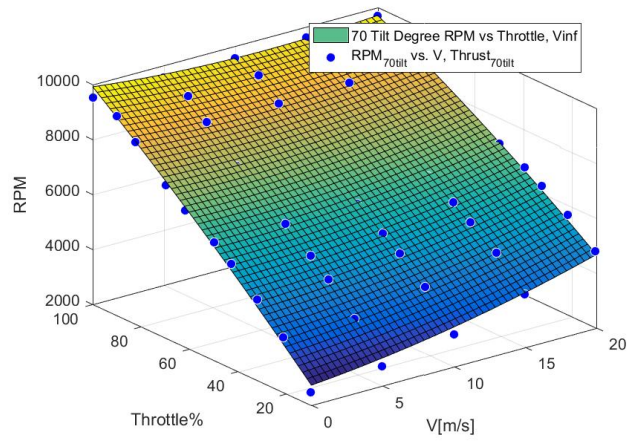


(b) Thrust vs RPM and wind speed plot

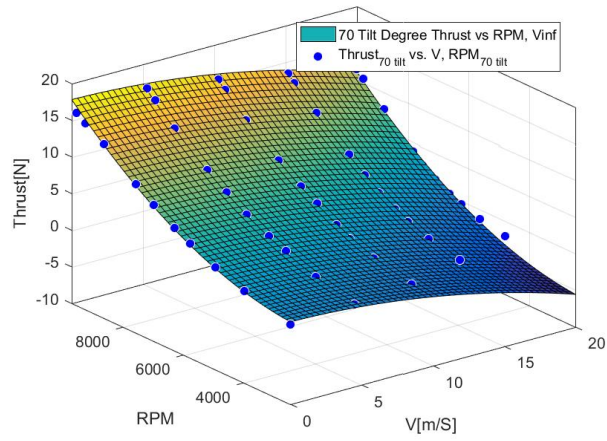


(c) Torque vs. RPM and wind speed plot

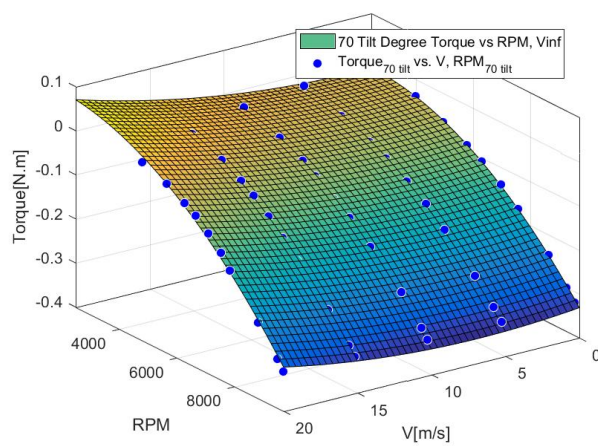
Figure 2.2: Experimental results for 90 [deg] propeller axis



(a) RPM vs. throttle and wind speed plot

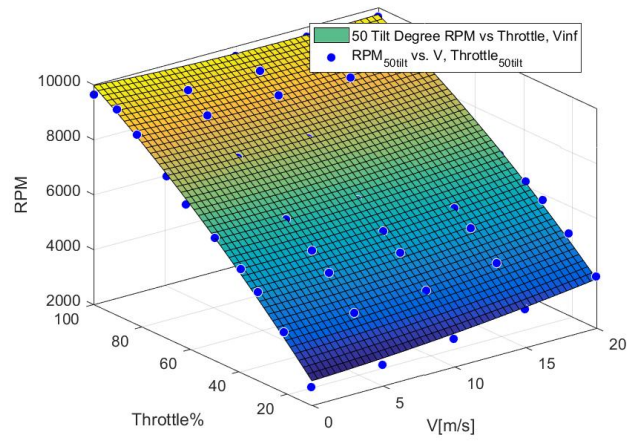


(b) Thrust vs RPM and wind speed plot

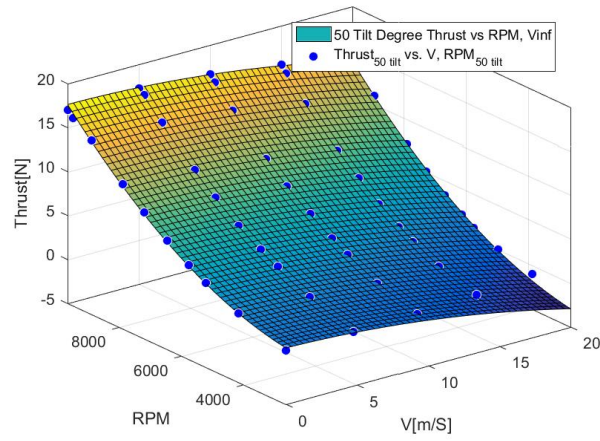


(c) Torque vs. RPM and wind speed plot

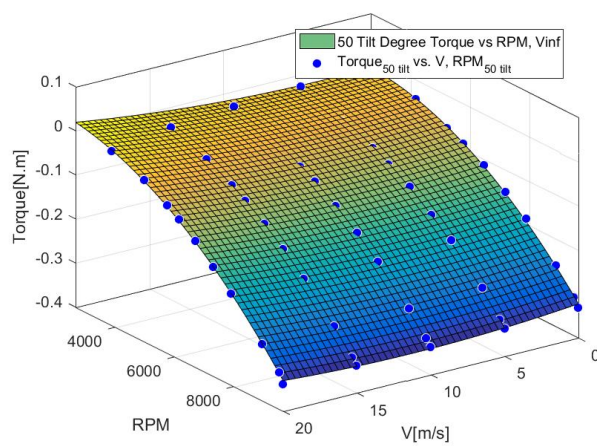
Figure 2.3: Experimental results for 70 [deg] propeller axis



(a) RPM vs. throttle and wind speed plot

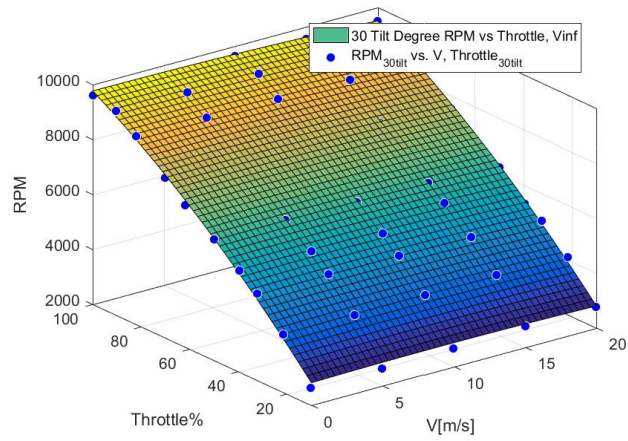


(b) Thrust vs RPM and wind speed plot

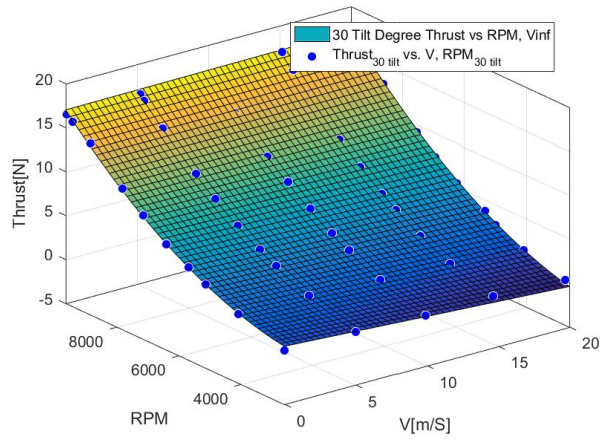


(c) Torque vs. RPM and wind speed plot

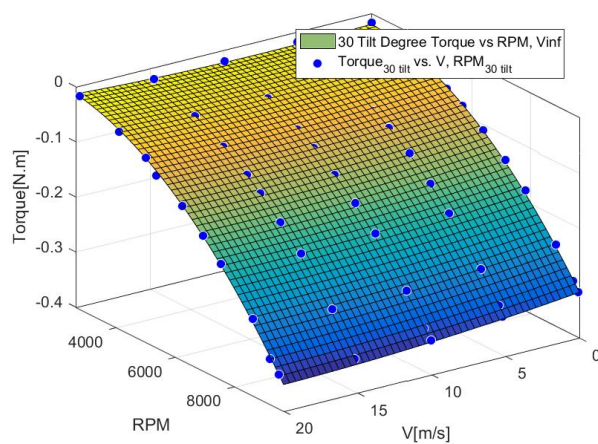
Figure 2.4: Experimental results for 50 [deg] propeller axis



(a) RPM vs. throttle and wind speed plot

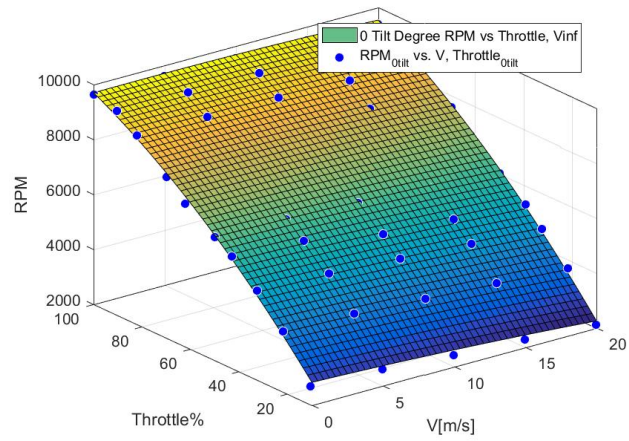


(b) Thrust vs RPM and wind speed plot

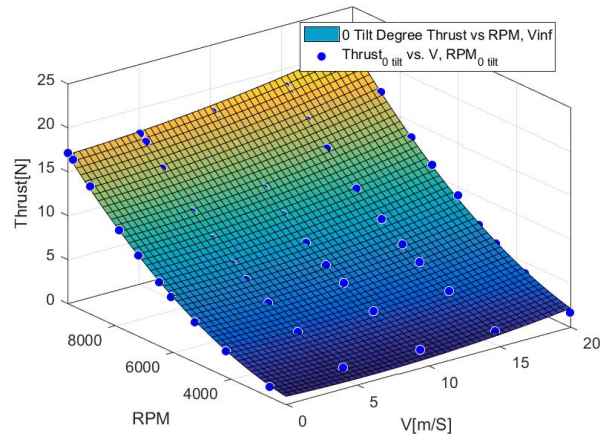


(c) Torque vs. RPM and wind speed plot

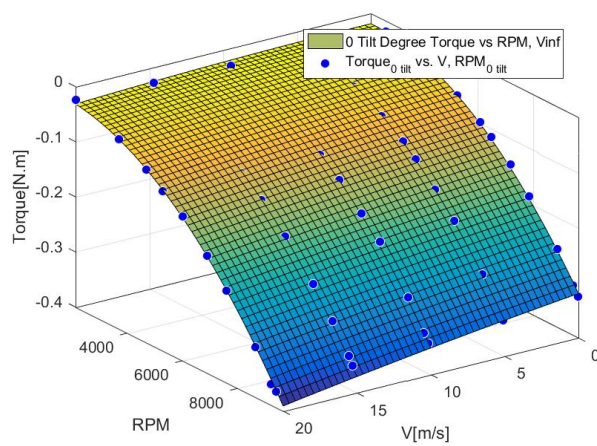
Figure 2.5: Experimental results for 30 [deg] propeller axis



(a) RPM vs. throttle and wind speed plot



(b) Thrust vs RPM and wind speed plot



(c) Torque vs. RPM and wind speed plot

Figure 2.6: Experimental results for 0 [deg] propeller axis

Data obtained from the tests is used to create look-up table in simulation block as given in Figure (2.7) below:

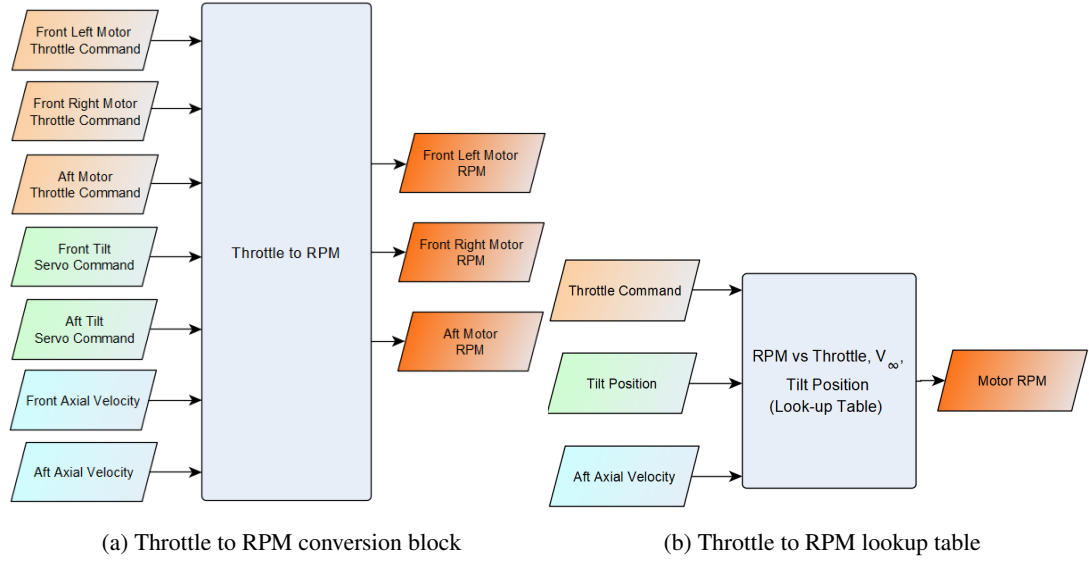


Figure 2.7: Throttle to RPM conversion block

As it is suggested in [17], blade element theory can not predict accurately the changes in rotor loads generated due to free stream velocity; multi-variable polynomial functions are used to fit the test data. The curve fitting is used to generate second order functions. Additional to the reference, rotational speed variation due to given throttle input is also obtained for simulation environment. Therefore, surface fit functions at given tilt angle configuration for force and moment can be defined as follows:

$$F^P(V_w, \Omega) = a_0(\sigma) + a_1(\sigma)V_w + a_2(\sigma)\Omega + a_3(\sigma)V_w^2 + a_4(\alpha)V_w\Omega + a_5(\sigma)\Omega^2 \quad (2.1)$$

$$M^P(V_w, \Omega) = b_0 + b_1V_w + b_2\Omega + b_3V_w^2 + b_4V_w\Omega + b_5\Omega^2 \quad (2.2)$$

$$\Omega(V_w, \delta_{th}) = c_0(\sigma) + c_1(\sigma)V_w + c_2(\sigma)\delta_{th} + c_3(\sigma)V_w^2 + c_4(\sigma)V_w\delta_{th} + c_5(\sigma)\delta_{th}^2 \quad (2.3)$$

Motor characterization will be defined for given surface fit function that meets the closest to experimental data combinations. For thrust and torque models, second order multivariable polynomial is selected, where function parameters are defined as

angular speed [RPM], Ω and wind tunnel velocity [m/s], V_w . Second order polynomial fits better to the experimental data. Throttle command and angular velocity of motor relation are also required in order to understand controller output of autopilot system on plant. Function variables were chosen as angular speed and wind tunnel speed since motor-propeller generated forces and moments are direct results of angular speed, and wind speed which can be implemented in 6 DoF model of tricopter and hybrid VTOL platforms. Coefficients that are used in Function (2.1), Function (2.2) and Function (2.3) are given in Appendix E.

Fitness quality are defined by the r-squared values of function outputs which are defined in Equation (2.1), Equation (2.2) and Equation (2.3). Results can be seen in table as follows:

	Thrust vs RPM, V	Torque vs RPM, V	RPM vs Throttle, V
90 [deg] tilt	0,9948	0,9963	0,9884
70 [deg] tilt	0,9963	0,9969	0,9906
50 [deg] tilt	0,9984	0,9986	0,9931
30 [deg] tilt	0,9971	0,9985	0,9947
0 [deg] tilt	0,9985	0,9987	0,9949

Table 2.1: Fitness quality of surface data

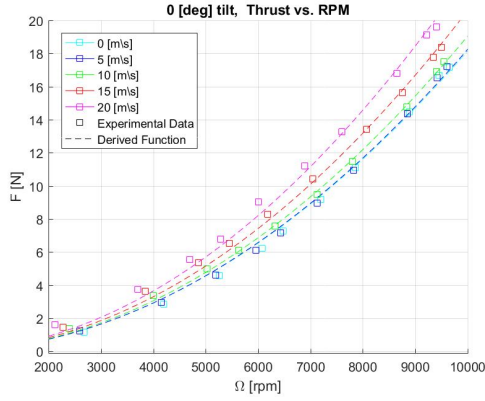
Besides surface model, simplified relation is required for the controller part. Considering fixed pitch rigid propellers angular velocity and thrust relation, at hover flight, relation can be taken, using the linear least squares curve fits as shown in Figure (2.8), and can be expressed as below [8, 16]:

$$F_i = k.\Omega_i^2[N] \quad (2.4)$$

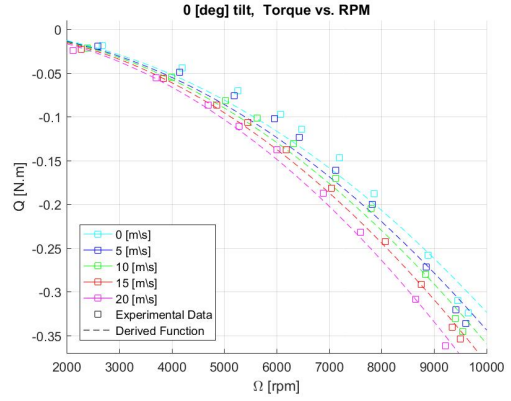
Relation between angular velocity and torque relation can be given as follows:

$$Q_i = l.\Omega_i^2 \quad (2.5)$$

Where Ω_i is the angular velocity of the i_{th} motor. Thrust and torque are represented as F_i and Q_i respectively. Squared input of angular speed motor is related to force by thrust coefficient $k [N/rpm^2]$ and to torque by drag coefficient $l [N.m/rpm^2]$



(a) Surface fit for rpm data



(b) Experimental vs. Derived throttle function

Figure 2.8: 0 [deg] tilted motor test data and curve fit function of Scorpion SII-3020-780Kv motor and 11x5.5 APC combination

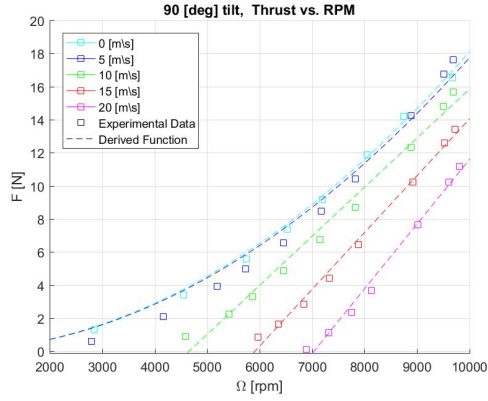
Table 2.2: Thrust vs Angular speed of motor relation at vertical position for $F[N] = k \cdot \Omega_i^2$

	Vertical Position - 0° tilt				
Wind Speed [m/s]	0	5	10	15	20
k [N/rpm^2]	-3.24e-09	-3.44e-09	-3.60e-09	-3.82e-09	-4.13e-09
r-squared	0.9962	0.9970	0.9989	0.9961	0.9936

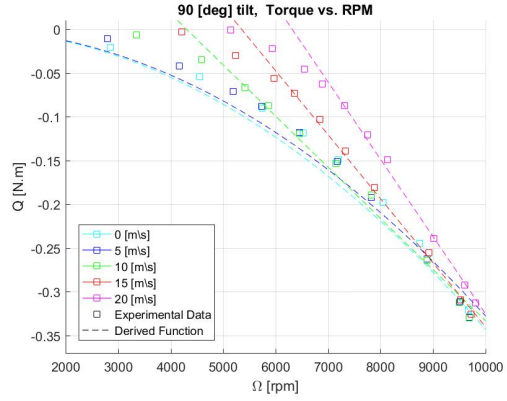
Table 2.3: Torque vs Angular speed of motor relation at vertical position for $F[N] = l \cdot \Omega_i^2$

	Vertical Position - 0° tilt				
Wind Speed [m/s]	0	5	10	15	20
l [$N.m/rpm^2$]	1.817e-07	1.826e-07	1.905e-07	2.061e-07	2.278e-07
r-squared	0.9719	0.9821	0.9897	0.9971	0.9969

The same approach is used for forward flight, as wind speed increased over propeller, it is observed that relations between angular velocity and thrust/torque can be taken as linear. Figure (2.9) shows the functional dependency over test data as follows:



(a) Surface fit for rpm data



(b) Experimental vs. Derived throttle function

Figure 2.9: 90 [deg] tilted motor test data and curve fit function of Scorpion SII-3020-780Kv motor and 11x5.5 APC combination

Considering linear curve fit results in Table (2.4) and Table (2.5), linear least squares curve fits as it is shown in Figure (2.9). Thus, it can be defined for force/torque and angular speed of the motor as given below:

$$F = k_1 \cdot \Omega + k_0 \quad (2.6)$$

$$Q = l_1 \cdot \Omega + l_0 \quad (2.7)$$

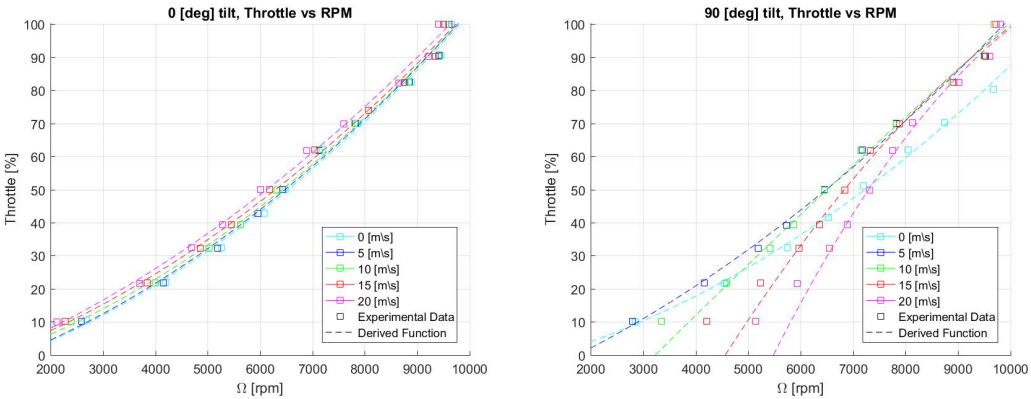
Table 2.4: Linear curve fit parameter values for motor-prop thrust at 90° tilt position

Horizontal Position - 90° tilt			
Wind Speed [m/s]	k_1	k_0	r-squared
10	0.0029684	-13.826	0.9870
15	0.0034373	-20.3181	0.9940
20	0.0039157	-27.5488	0.9899

Table 2.5: Linear curve fit parameter values for motor-prop torque at 90° tilt position

Horizontal Position - 90° tilt			
Wind Speed [m/s]	l_1	l_0	r-squared
10	-6.1412e-05	0.27608	0.9919
15	-7.5508e-05	0.41198	0.9984
20	-9.2266e-05	0.59372	0.9979

Throttle is defined as a second degree multivariable polynomial with RPM and wind velocity inputs. As the curve fit data indicates, which is given in Figure (2.10), throttle - RPM relations show similar behaviours, such that wind speed may be negligible, and this relation can be used for RPM to throttle conversions in autopilot algorithms. In other words, angular velocity output of controller for each motor can be converted into PWM signal which is used to drive motors through ESC. Conversion is established by scaling throttle percentage into corresponding PWM range.



(a) Experimental vs. Derived function for 0[deg] tilt (b) Experimental vs. Derived function for 90[deg] tilt

Figure 2.10: Throttle vs rpm curve fit function Scorpion SII-3020-780Kv motor and 11x5.5 APC combination at hover

In Figure (2.10), it is shown that derived function in second degree polynomial over varying airspeed acting on propeller fits.

$$\delta_{th} = c_{10}\Omega^2 + c_{01}\Omega + c_{00} \quad (2.8)$$

Fit quality of the Equation (2.8) with parameter constants are presented in Table (2.6) and Table (2.7).

Table 2.6: Second degree polynomial model for rpm to throttle command - Scorpion SII-3020-780Kv motor and 11x5.5 APC combination at 0[deg] tilt position

90° tilt position				
Wind Speed [m/s]	c_{10}	c_{01}	c_{00}	r-squared
0	6.5881e-07	0.0044649	0.0044649	0.9945
5	6.4613e-07	0.0046649	0.0046649	0.9946
10	6.4759e-07	0.0044468	0.0044468	0.9944
15	5.9369e-07	0.0050027	0.0050027	0.9950
20	5.4105e-07	0.0057464	0.0057464	0.9949

Table 2.7: Second degree polynomial model for rpm to throttle command - Scorpion SII-3020-780Kv motor and 11x5.5 APC combination at 90[deg] tilt position

0° tilt position				
Wind Speed [m/s]	c_{10}	c_{01}	c_{00}	r-squared
10	-1.187e-07	0.016417	0.016417	0.9932
15	-1.185e-07	0.035533	0.035533	0.9895
20	-2.107e-07	0.054492	0.054492	0.9868

2.3 Reference Frames and Transformations

Before writing equations to define dynamics, reference frames must be specified to find relative forces, velocities and moments. The equations of motion should be specified such that specific observer can be formulated to transform one frame to another. In the thesis, body fixed frame, F_B and earth fixed frame F_E will be used.

2.3.1 Wind Frame from Body-Fixed Frame

Aerodynamic forces generated by wing contribute to all three axes of body fixed frame. Contribution of lift, drag and side forces to body fixed frame related by α , angle of attack and β , angle of side-slip. Transformation matrix can be defined as follows [20]:

$$L_{WB} = \begin{bmatrix} \cos(\beta) & \sin(\beta) & 0 \\ -\sin(\beta) & \cos(\beta) & 0 \\ 0 & 0 & 1 \end{bmatrix} \cdot \begin{bmatrix} \cos(\alpha) & 0 & \sin(\alpha) \\ 0 & 1 & 0 \\ -\sin(\alpha) & 0 & \cos(\alpha) \end{bmatrix} \quad (2.9)$$

2.3.1.1 Derivation of Velocity Angles

Angles between body-fixed coordinate system and its relative velocities are angle of attack α , and angle of side-slip β can be derived from following equations [15]:

$$\alpha = \arctan(w_B/u_B) \quad (2.10)$$

$$V_\infty = \sqrt{v_B^2 + u_B^2 + w_B^2} \quad (2.11)$$

$$\beta = \arcsin(v_B/V_\infty) \quad (2.12)$$

Relative velocity equations for tricopter mode attitude control introduces problems due to small changes in relative velocity vector angles. Workaround solution is introduced in the model environment such that angle of attack and angle of side-slip are assumed to be 0 when V_∞ is below 5[m/s].

2.4 Forces and Moments

In the following sections, force and moment derivations are explained. Dynamic models for the effective forces and moments are defined. Moreover, force and moment equations is expressed in body fixed frame(F_B).

2.4.1 Aerodynamic Forces

Wing is modelled for transition and forward flight phases, and flying wing concept is chosen since it is a simpler configuration to adapt to the system. Moreover, it does not require additional frame. The airfoil section is chosen as MH60 profile for the wing and the airfoil cross section on the winglets is chosen as NACA008. Aerodynamic model is designed in XFLR5 which uses 3D panel method [5]. Panel method analysis is applied on wing surfaces to obtain aerodynamic coefficients. Control deflection limits are used for analysis constraints. Analyses are applied separately for each control control surfaces with varying angle of attack angles.



Figure 2.11: Tricopter - Tilt Rotor VTOL configuration

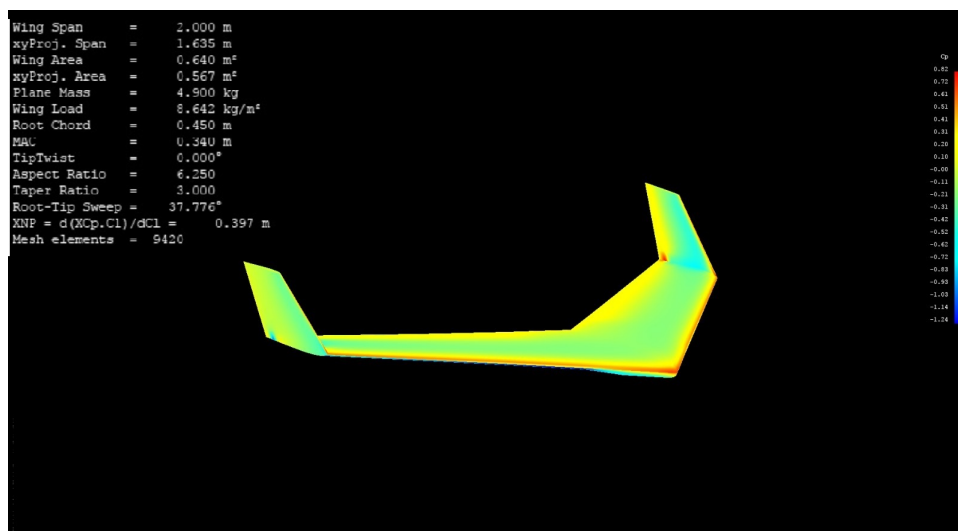


Figure 2.12: 3D Panel method solution for flying wing model

Nondimensional aerodynamic force and moment coefficients in the body fixed frame

according to point on which aerodynamic loads act may be expressed as following [30]:

$$C_L = C_{L_0} + C_{L_\alpha}\alpha + C_{L_{\delta_{elev}}}\delta_{elev} \quad (2.13)$$

where C_L is lift coefficient and C_{L_0} is lift coefficient with zero angle of attack. Variation of lift coefficient with respect to angle of attack is given as C_{L_α} and variation of lift coefficient with respect to δ_{elev} , elevator deflection angle is given as $C_{L_{\delta_{elev}}}$.

$$C_Y = C_{Y_\beta}\beta + C_{Y_{\delta_{rud}}}\delta_{rud} \quad (2.14)$$

where C_{Y_β} is variation of side force coefficient with respect to β , side slip angle and $C_{Y_{\delta_{rud}}}$ is variation of side force with respect to δ_{rud} , rudder deflection angle.

$$C_D = C_{D_0} + C_{D_\alpha}\alpha + C_{D_{\alpha^2}}\alpha^2 + C_{D_\beta}\beta + C_{D_{\delta_{ail}}}\delta_{ail} + C_{D_{\delta_{rud}}}\delta_{rud} + C_{D_{\delta_{elev}}}\delta_{elev} \quad (2.15)$$

where C_{D_0} is drag force coefficient for zero angle of attack. C_{D_α} and $C_{D_{\alpha^2}}$ are variations of drag force coefficient with respect to angle of attack. C_{D_β} is variation of drag coefficient with respect to side slip angle. $C_{D_{\delta_{ail}}}$, $C_{D_{\delta_{rud}}}$ and $C_{D_{\delta_{elev}}}$ are variations of drag coefficients with respect control surface deflections, which are aileron, elevator and drag respectively.

$$C_l = C_{l_{\delta_{ail}}}\delta_{ail} + C_{l_{\delta_{rud}}}\delta_{rud} + C_{l_p}p \quad (2.16)$$

where $C_{l_{\delta_{ail}}}$ and $C_{l_{\delta_{rud}}}$ are variations of rolling moment coefficients with respect to control surface deflections, aileron and rudder respectively.

$$C_m = C_{m_\alpha}\alpha + C_{m_{\delta_{elev}}}\delta_{elev} \quad (2.17)$$

where $C_{m_\alpha}\alpha$ is variation of pitch moment coefficient with respect to angle of attack and $C_{m_{\delta_{elev}}}$ is variation of pitch moment coefficient with respect to elevator deflection angle

$$C_n = C_{n_\beta}\beta + C_{n_{\delta_{rud}}}\delta_{rud} + C_{n_r}r \quad (2.18)$$

where $C_{n_\beta}\beta$ is variation of yaw moment coefficient with respect to side slip angle and $C_{n_{\delta_{rud}}}$ is variation of yaw moment coefficient with respect to rudder deflection

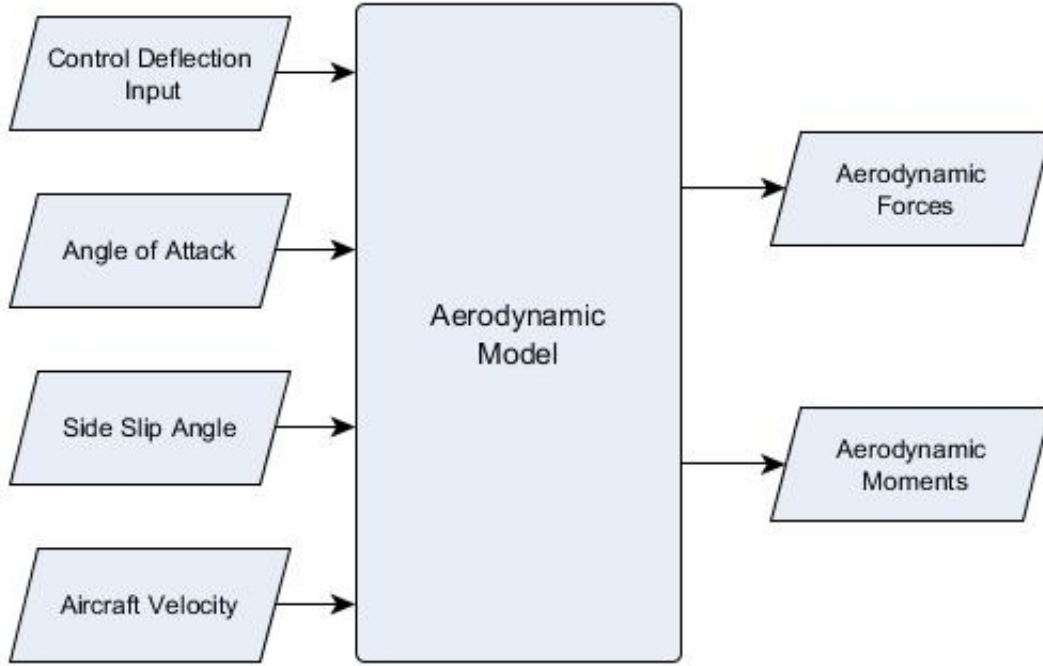


Figure 2.13: Aerodynamic forces and moments model

Forces and moments generated by the wing are given in wind coordinate system. In order to present them in body fixed frame, F_B^A transformation matrix, which is defined in Equation (2.9), is used [10]:

$$F_B^A = \begin{bmatrix} \cos(\beta)\cos(\alpha) & -\cos(\alpha)\sin(\beta) & -\sin(\alpha) \\ \sin(\beta) & \cos(\beta) & 0 \\ \sin(\alpha)\cos(\beta) & -\sin(\alpha)\sin(\beta) & \cos(\alpha) \end{bmatrix} \cdot \frac{1}{2}\rho V_\infty^2 S \begin{bmatrix} -C_D \\ C_Y \\ -C_L \end{bmatrix} \quad (2.19)$$

$$F_B^{aero} = \frac{1}{2}\rho V_\infty^2 S \begin{bmatrix} C_X \\ C_Y \\ C_Z \end{bmatrix} \quad (2.20)$$

Where S stands for wing area and ρ , local density of atmosphere and V_∞ , airspeed of platform measured by pitot tube. Moments generated by wing using Equation (2.16),

Equation (2.17) and Equation (2.18) yields as follows:

$$M_B^A = \begin{bmatrix} \frac{1}{2}\rho V_\infty^2 S b C_l \\ \frac{1}{2}\rho V_\infty^2 S \bar{c} C_m \\ \frac{1}{2}\rho V_\infty^2 S b C_n \end{bmatrix} \quad (2.21)$$

Where b presents wing span and \bar{c} presents mean aerodynamic chord.

2.4.2 Gravitational Force

Force acts on tricopter due to gravity is expressed in earth fixed frame since it is obvious that $mg[kg.m/s^2]$ is directed along z_E axis on F_E frame. For the thesis, gravity acceleration is taken as constant with parameter value of $g = 9.81[m/s^2]$ and gravitational force in earth fixed frame may be expressed as follows:

$$F_E^{grav} = m \cdot \begin{bmatrix} 0 \\ 0 \\ g \end{bmatrix} \quad (2.22)$$

Using transformation matrix L_{BE} , relative force can be expressed in body fixed frame, F_B as follows [11]:

$$\begin{aligned} F_B^G &= L_{BE} \cdot \begin{bmatrix} 0 \\ 0 \\ mg \end{bmatrix} \\ &= \begin{bmatrix} -mg \sin(\theta) \\ mg \cos(\theta) \sin(\phi) \\ mg \cos(\theta) \cos(\phi) \end{bmatrix} \end{aligned} \quad (2.23)$$

2.5 Propeller Forces on Body Center of Mass

Forces acting on body are F_1 , F_2 and F_3 , which are respectively the front left, front right and aft motor. σ is the front tilt angle of front motors and its direction is in pitch

axis. When σ is zero, it means that front motors are perpendicular to x-axis of body fixed frame. γ is tilt angle of aft motor, of which direction in roll axis. When α is zero, aft motor is in vertical position. Forces acting by each motor on body axes may be given as below [8]:

$$\begin{aligned}
 F_1^P &= \begin{bmatrix} F_1.\sin(\sigma) \\ 0 \\ -F_1.\cos(\sigma) \end{bmatrix} \\
 F_2^P &= \begin{bmatrix} F_2.\sin(\sigma) \\ 0 \\ -F_2.\cos(\sigma) \end{bmatrix} \\
 F_3^P &= \begin{bmatrix} 0 \\ F_3.\sin(\gamma) \\ -F_3.\cos(\alpha) \end{bmatrix}
 \end{aligned} \tag{2.24}$$

Forces generated by the propellers in the body fixed frame F_B^P , using Equation (2.24), yields as follows:

$$F_B^P = \begin{bmatrix} (F_1 + F_2).\sin(\sigma) \\ F_3.\sin(\gamma) \\ -(F_1 + F_2).\cos(\sigma) - F_3.\cos(\gamma) \end{bmatrix} \tag{2.25}$$

2.6 Propeller Moments on Body Center of Mass

Using Equation (2.24), expression of moment generated by motors is given as follows [8]:

$$M_B = \sum_{i=1}^3 r_i x F_i^P + \sum_{i=1}^3 \tau_i \tag{2.26}$$

Where, r_i is the position vector of i_{th} motor in the body fixed frame and τ_i is the induced moment generated by i_{th} motor. Moment arm of i_{th} motor is composed of distances in x, y and z directions according to Center of Gravity (CG) of the platform. Position vector of each motor is given in Appendix E. Position vector r_i can be defined

as below:

$$r_i = \begin{bmatrix} r_{x,i} \\ r_{y,i} \\ r_{z,i} \end{bmatrix} \quad (2.27)$$

By using the Equation (2.26) and Equation (2.27), propeller forces acting on the body are expressed as torque, according to axis of rotation, and relative torque equations are calculated as given below:

$$\begin{aligned} & \begin{bmatrix} M_x^P \\ M_y^P \\ M_z^P \end{bmatrix} = [r_1 x F_1^P] + [r_2 x F_2^P] + [r_3 x F_3^P] \\ = & \begin{bmatrix} -F_1 \cos(\sigma) r_{y,1} - F_2 \cos(\sigma) r_{y,2} - F_3 \cos(\gamma) r_{y,3} - F_3 \sin(\gamma) r_{z,3} \\ F_1 \sin(\sigma) r_{z,1} + F_1 \cos(\sigma) r_{x,1} + F_2 \sin(\sigma) r_{z,2} + F_2 \cos(\sigma) r_{x,2} + F_3 \cos(\gamma) r_{x,3} \\ -F_1 \sin(\sigma) r_{y,1} - F_2 \sin(\sigma) r_{y,2} + F_3 \sin(\gamma) r_{x,3} \end{bmatrix} \end{aligned} \quad (2.28)$$

Rotating machines always create equal/opposite reactive torques on stationary parts reactive torques generated by motors. Such reaction moments may be written as below:

$$\begin{aligned} \tau_1 &= \begin{bmatrix} -Q_1 \cdot \sin(\sigma) \\ 0 \\ Q_1 \cdot \cos(\sigma) \end{bmatrix} \\ \tau_2 &= \begin{bmatrix} Q_2 \cdot \sin(\sigma) \\ 0 \\ -Q_2 \cdot \cos(\sigma) \end{bmatrix} \\ \tau_3 &= \begin{bmatrix} 0 \\ -Q_3 \cdot \sin(\gamma) \\ Q_3 \cdot \cos(\gamma) \end{bmatrix} \end{aligned} \quad (2.29)$$

Induced moments generated by propeller in body frame M_x^R , M_y^R and M_z^R according to Equation (2.24) yields as follows:

$$\begin{bmatrix} M_x^R \\ M_y^R \\ M_z^R \end{bmatrix} = \sum_{i=1}^3 \tau_i = \begin{bmatrix} (Q_2 - Q_1) \cdot \sin(\sigma) \\ -Q_3 \cdot \sin(\gamma) \\ (Q_1 - Q_2) \cdot \cos(\sigma) + Q_3 \cdot \cos(\gamma) \end{bmatrix} \quad (2.30)$$

In Equation (2.30), moments generated by reactive torque of each motor is defined. M_x^R is the differential induced moment between left and right motor in the x_B direction. Thus, M_y^R is induced moment of aft motor in the y_B direction, whereas M_z^R is the differential induced moment between all three motors in the z_B direction.

2.7 Dynamic Model

Newton's second law for translational motion in body frame is presented for all external forces acting on the body frame can be expressed as follows:

$$F_B^{ext} = m \cdot \left(\frac{dV_B}{dt} + \omega_B \times V_B \right) \quad (2.31)$$

Where ω_B is angular velocity of the platform, relative to the body frame, is presented as follows:

$$\omega_B = [p \quad q \quad r]^T \quad (2.32)$$

Furthermore, when it is expressed in coordinates, body velocities and their relative rate of change parameters can be written as follows:

$$V_B = [u_B \quad v_B \quad w_B] \quad (2.33)$$

$$\frac{dV_B}{dt} = \dot{V}_B = \begin{bmatrix} \dot{u}_B \\ \dot{v}_B \\ \dot{w}_B \end{bmatrix} \quad (2.34)$$

Angular velocity, defined according to body fixed frame, represents the particles' velocities. This means that time derivative of euler angles do not directly refer to angular velocity. In order to sustain it, proper coordinate frame conversions must be derived. Recall from the notational convention that yaw, pitch and roll represent sequential rotations about inertial frame. Thus, z, y and x axes euler angles are used

to describe the rotation of platform. The relation between euler angles and angular velocity vector can be described as follows [11]:

$$\begin{bmatrix} p \\ q \\ r \end{bmatrix} = \begin{bmatrix} 1 & 0 & -\sin(\theta) \\ 0 & \cos(\phi) & \sin(\phi).\cos(\theta) \\ 0 & -\sin(\phi) & \cos(\phi).\cos(\theta) \end{bmatrix} \cdot \begin{bmatrix} \dot{\phi} \\ \dot{\theta} \\ \dot{\psi} \end{bmatrix} \quad (2.35)$$

Inverting the Equation (2.35), euler rates are represented as follows:

$$\begin{bmatrix} \dot{\phi} \\ \dot{\theta} \\ \dot{\psi} \end{bmatrix} = \begin{bmatrix} 1 & \sin(\phi).\tan(\theta) & \cos(\phi).\tan(\theta) \\ 0 & \cos(\phi) & -\sin(\phi) \\ 0 & \sin(\phi).\sec(\theta) & \cos(\phi).\sec(\theta) \end{bmatrix} \cdot \begin{bmatrix} p \\ q \\ r \end{bmatrix} \quad (2.36)$$

External forces include, gravitation, propulsive and aerodynamic forces. Thus, F_B^{ext} can be expressed also as follows:

$$F_B^{ext} = F_B^G + F_B^P + F_B^A \quad (2.37)$$

By substituting Equation (2.23), Equation (2.25) and Equation (2.20) into Equation (2.37), F_B^{ext} yields as follows:

$$F_B^{ext} = \begin{bmatrix} -mgsin(\theta) \\ mg.\cos(\theta).\sin(\phi) \\ mg.\cos(\theta).\cos(\phi) \end{bmatrix} + \begin{bmatrix} (F_1 + F_2).\sin(\sigma) \\ F_3.\sin(\gamma) \\ -(F_1 + F_2).\cos(\sigma) - F_3.\cos(\gamma) \end{bmatrix} + \begin{bmatrix} \frac{1}{2}\rho V_\infty^2 SC_X \\ \frac{1}{2}\rho V_\infty^2 SC_Y \\ \frac{1}{2}\rho V_\infty^2 SC_Z \end{bmatrix} \quad (2.38)$$

2.7.1 Rotational Motion

Moment generated by rotational motion of platform can be expressed in body fixed frame as below:

$$M_B^{ext} = \frac{dH_B}{dt} + \omega_B \times H_B \quad (2.39)$$

Where H_B is angular momentum calculated as a dot product of I , moment of platform's inertia and ω_B , angular velocity in body fixed frame.

$$H_B = \begin{bmatrix} I_x & 0 & 0 \\ 0 & I_y & 0 \\ 0 & 0 & I_z \end{bmatrix} \cdot \begin{bmatrix} p \\ q \\ r \end{bmatrix} \quad (2.40)$$

Derivative of H_B is derived using time derivative of angular velocity ω_B and I . Using the property $\omega_B x \omega_B = 0$, applying this information and Equation (2.40) into Equation (2.39), total moment can be expressed as follows[11]:

$$H_B = \begin{bmatrix} I_x & 0 & 0 \\ 0 & I_y & 0 \\ 0 & 0 & I_z \end{bmatrix} \cdot \begin{bmatrix} \dot{p} \\ \dot{q} \\ \dot{r} \end{bmatrix} + \begin{bmatrix} p \\ q \\ r \end{bmatrix} \times \left(\begin{bmatrix} I_x & 0 & 0 \\ 0 & I_y & 0 \\ 0 & 0 & I_z \end{bmatrix} \cdot \begin{bmatrix} \dot{p} \\ \dot{q} \\ \dot{r} \end{bmatrix} \right) \quad (2.41)$$

Total moments acting on body fixed frame are generated by forces acting on axis rotation and reactive torques. Since gravity acts on CG, no moments are produced by the gravitational forces. Total moments can be expressed of summation of M^P body moments generated by propeller forces, M^R reactive torques due resistance to rotation of rotors and M^A moments generated by wing, which are defined in Equation (2.30), Equation (2.28) and Equation (2.21) respectively. External moments apply on body fixed frame can be represented as follows:

$$\begin{bmatrix} L_T \\ M_T \\ N_T \end{bmatrix} = \begin{bmatrix} M_x^P + M_x^R + M_x^A \\ M_y^P + M_y^R + M_y^A \\ M_z^P + M_z^R + M_z^A \end{bmatrix} \quad (2.42)$$

Using Equation (2.41) and Equation (2.42), $\dot{\omega}_B$ can be reexpressed as following:

$$\begin{bmatrix} \dot{p} \\ \dot{q} \\ \dot{r} \end{bmatrix} = \begin{bmatrix} (I_y - I_z).q.r/I_x \\ (I_z - I_x).p.r/I_y \\ (I_x - I_y).p.q/I_z \end{bmatrix} + \begin{bmatrix} L_T/I_x \\ M_T/I_y \\ N_T/I_z \end{bmatrix} \quad (2.43)$$

Inertia parameters for tricopter and winged VTOL configurations are given in Appendix E.

2.7.2 Forces and Moments in Hover Flight

Control allocation of the system is designed based on simplified model for rotational and translational dynamics obtained. Recalling relations between angular velocity of motor and thrust stated in Equation (2.4), and angular velocity of motor and torque stated in Equation (2.5), external force and moment can be expressed.

Substituting Equation (2.4) and Equation (2.5) into total external force equation defined in Equation (2.38), forces acting on body fixed frame can be reexpressed as

follows:

$$\begin{aligned}
F_B^{ext} = & \begin{bmatrix} -mgsin(\theta) \\ mg.cos(\theta).sin(\phi) \\ mg.cos(\theta).cos(\phi) \end{bmatrix} + \begin{bmatrix} k.(\Omega_1^2 + \Omega_2^2).sin(\sigma) \\ k.\Omega_3^2.sin(\gamma) \\ -k.(\Omega_1^2 + \Omega_2^2).cos(\sigma) - k.\Omega_3^2.cos(\gamma) \end{bmatrix} \\
& + \begin{bmatrix} \frac{1}{2}\rho V_\infty^2 SC_X \\ \frac{1}{2}\rho V_\infty^2 SC_Y \\ \frac{1}{2}\rho V_\infty^2 SC_Z \end{bmatrix} \tag{2.44}
\end{aligned}$$

Substituting Equation (2.4) and Equation (2.5) into Equation (2.28) and Equation (2.30) respectively to reexpress total moment, M^P as following:

$$k \begin{bmatrix} -\Omega_1^2 cos(\sigma)r_{y,1} - \Omega_2^2 cos(\sigma)r_{y,2} - \Omega_3^2 (cos(\gamma)r_{y,3} + sin(\gamma)r_{z,3}) \\ \Omega_1^2 (sin(\sigma)r_{z,1} + cos(\sigma)r_{x,1}) + \Omega_2^2 (sin(\sigma)r_{z,2} + cos(\sigma)r_{x,2}) + \Omega_3^2 cos(\gamma)r_{x,3} \\ -\Omega_1^2 sin(\sigma)r_{y,1} - \Omega_2^2 sin(\sigma)r_{y,2} + \Omega_3^2 sin(\gamma)r_{x,3} \end{bmatrix} \tag{2.45}$$

$$M^R = \begin{bmatrix} l(\Omega_2^2 - \Omega_1^2)sin(\sigma) \\ -l\Omega_3^2.sin(\gamma) \\ l(\Omega_1^2 - \Omega_2^2).cos(\sigma) + l\Omega_3^2.cos(\gamma) \end{bmatrix} \tag{2.46}$$

When the tricopter/VTOL configuration is in hover position, front motors should be positioned vertically, such that σ is zero. At hover position, it is assumed that wing does not generate forces, due to the reason that the aerodynamic forces are assumed to be zero. Forces acting on the body fixed frame are given in Equation (2.44) in hover flight can be expressed as below:

$$F_{B_{hover}}^{ext} = \begin{bmatrix} -mgsin(\theta) \\ mg.cos(\theta).sin(\phi) \\ mg.cos(\theta).cos(\phi) \end{bmatrix} + \begin{bmatrix} 0 \\ k\Omega_3^2.sin(\gamma) \\ -k(\Omega_1^2 + \Omega_2^2) - k\Omega_3^2.cos(\gamma) \end{bmatrix} \tag{2.47}$$

Moments acting on the body, generated by propellers are given in Equation (2.45)

and Equation (2.46) becomes as following:

$$M_{hover}^P = \begin{bmatrix} -k\Omega_1^2 r_{y,1} - k\Omega_2^2 r_{y,2} - k\Omega_3^2 (\cos(\gamma)r_{y,3} + \sin(\gamma)r_{z,3}) \\ k.\Omega_1^2 r_{x,1} + k\Omega_1^2 r_{x,2} + k\Omega_3^2 \cos(\gamma)r_{x,3} \\ k\Omega_3^2 \sin(\gamma)r_{x,3} \end{bmatrix} \quad (2.48)$$

$$M_{hover}^R = \begin{bmatrix} 0 \\ -l\Omega_3^2 \sin(\gamma) \\ l(\Omega_1^2 - \Omega_2^2) + l\Omega_3^2 \cos(\gamma) \end{bmatrix} \quad (2.49)$$

2.7.3 Forces and Moments in Forward Flight

When the VTOL configuration is at forward flight, front motors are positioned horizontally, such that σ is 90 [deg]. Aft motor will not generate force, also it is positioned vertically. Lift is sustained in this mode by wing, which is defined in $F_{B_f}^{ext}$. Moreover, attitude control is sustained by wing generated moments which is obtained by control surfaces. More information about $F_{B_f}^{ext}$ and $M_{B_f}^{ext}$ will be given in Chapter 3. Recalling relation between angular velocity of motor and thrust, which is stated in Equation (2.6), and relation between angular velocity of motor and torque, which is stated in Equation (2.7), external force and moment can be expressed.

Substituting Equation (2.6) and Equation (2.7) into Equation (2.38), total external force equation can be defined as following:

$$F_{B_f}^{ext} = mg \begin{bmatrix} -\sin(\theta) \\ \cos(\theta).\sin(\phi) \\ \cos(\theta).\cos(\phi) \end{bmatrix} + \begin{bmatrix} \frac{1}{2}\rho V_\infty^2 SC_X \\ \frac{1}{2}\rho V_\infty^2 SC_Y \\ \frac{1}{2}\rho V_\infty^2 SC_Z \end{bmatrix} \quad (2.50)$$

$$+ \begin{bmatrix} 2(k_1\Omega_{1,2} + k_0)\sin(\sigma) \\ (k_1\Omega_3 + k_0)\sin(\gamma) \\ -2(k_1\Omega_{1,2} + k_0)\cos(\sigma) - (k_1\Omega_3 + k_0)\cos(\gamma) \end{bmatrix}$$

Substituting Equation (2.6) into Equation (2.28) to reexpress moments generated by

propellers, M_f^R can be defined as following:

$$\begin{bmatrix} -(k_1\Omega_{1,2} + k_0)\cos(\sigma)(r_{y,1} + r_{y,2}) - (k_1\Omega_3 + k_0)(\sin(\gamma)r_{z,3} + \cos(\gamma)r_{y,3}) \\ (k_1\Omega_{1,2} + k_0)(\cos(\sigma)(r_{x,1} + r_{x,2}) + \sin(\sigma)(r_{z,1} + r_{z,2})) + (k_1\Omega_3 + k_0)\cos(\gamma)r_{x,3} \\ -(k_1\Omega_{1,2} + k_0)\sin(\sigma)(r_{y,1} + r_{y,2}) + (k_1\Omega_3 + k_0)\sin(\gamma)r_{x,3} \end{bmatrix} \quad (2.51)$$

It should be noted that in forward flight, front motors will rotate at same RPM. Moreover, reactive torques generated by front motors will omit each other. Also it is assumed that aft motor will not generate thrust and wind-mill effect is neglected. Considering these assumptions, reactive torque in forward flight can be reexpressed by substituting Equation (2.7) into Equation (2.30) as following:

$$M_f^R = \begin{bmatrix} 0 \\ 0 \\ 0 \end{bmatrix} \quad (2.52)$$

According to forces acting on the body fixed frame, given in Equation (2.50), forward flight external forces can be expressed as following:

$$F_{B_f}^{ext} = mg \begin{bmatrix} -\sin(\theta) \\ \cos(\theta).\sin(\phi) \\ \cos(\theta).\cos(\phi) \end{bmatrix} + \begin{bmatrix} 2(k_1\Omega_{1,2} + k_0) \\ 0 \\ 0 \end{bmatrix} + \begin{bmatrix} \frac{1}{2}\rho V_\infty^2 SC_X \\ \frac{1}{2}\rho V_\infty^2 SC_Y \\ \frac{1}{2}\rho V_\infty^2 SC_Z \end{bmatrix} \quad (2.53)$$

Moments acting on the body that are generated by propellers and wing in forward flight are expressed in Equation (2.51), Equation (2.52) and Equation (2.21) respectively. Considering Equation (2.42), moments can be expressed as following:

$$M^P + M^R + M^A = \begin{bmatrix} 0 \\ (k_1\Omega_{1,2} + k_0)(r_{z,1} + r_{z,2}) \\ -(k_1\Omega_{1,2} + k_0)(r_{y,1} + r_{y,2}) \end{bmatrix} + \frac{1}{2}\rho V_\infty^2 S \begin{bmatrix} bC_l \\ \bar{c}C_m \\ bC_n \end{bmatrix} \quad (2.54)$$

CHAPTER 3

TRIMMING AND LINEARIZATION

3.1 Introduction

Trimming approach which is applied for hover and forward flight is chosen as *fmincon*, the function of Optimization Toolbox of MATLAB. This is used to find minimum value of bounded parameters of multi-variable function. Initial values of parameters are passed, upper and lower boundary values of parameters are given to function so that it tries to minimize function within constrained region with specified iteration trials.

3.2 Trimming Approach for Hover Position

It is desired for hover case that the platform holds in the air steady and straight, so that ground speed is zero and it is not accelerating in any directions [20]. Considering these circumstances, it can be assumed that:

$$\dot{\Phi}_0 = u_0 = v_0 = w_0 = p_0 = q_0 = r_0 = \dot{u}_0 = \dot{v}_0 = \dot{w}_0 = \dot{p}_0 = \dot{q}_0 = \dot{r}_0 = 0 \quad (3.1)$$

Simplified equations can be obtained by applying conditions given in Equation (3.1) with perturbations. Before applying perturbed values, unknown trim values in the equations should be obtained. For the rest of parameter values, equations can be written using trim conditions, such that Equation (2.43) simply becomes as below:

$$\begin{bmatrix} \dot{p}_0 \\ \dot{q}_0 \\ \dot{r}_0 \end{bmatrix} = \begin{bmatrix} (I_y - I_z).(q_0.r_0)/I_x \\ (I_z - I_x).(p_0.r_0)/I_y \\ (I_x - I_y).(p_0.q_0)/I_z \end{bmatrix} + \begin{bmatrix} L_{T0}/I_x \\ M_{T0}/I_y \\ N_{T0}/I_z \end{bmatrix} \quad (3.2)$$

Applying assumptions in Equation (3.1) into the Equation (2.48) and Equation (2.49), total moment equation becomes as following:

$$\begin{bmatrix} L_{T0} \\ M_{T0} \\ N_{T0} \end{bmatrix}_{\sigma=0} = \begin{bmatrix} -k\Omega_{0,1}^2 r_{y,1} - k\Omega_{0,2}^2 r_{y,2} - k\Omega_{0,3}^2 (\cos(\gamma_0) r_{y,3} + \sin(\gamma_0) r_{z,3}) \\ k\Omega_{0,1}^2 r_{x,1} + k\Omega_{0,1}^2 r_{x,2} + k\Omega_{0,3}^2 \cos(\gamma_0) r_{x,3} - l\Omega_{0,3}^2 \sin(\gamma_0) \\ k\Omega_{0,3}^2 \sin(\gamma_0) r_{x,3} + l(\Omega_{0,1}^2 - \Omega_{0,2}^2) + l\Omega_{0,3}^2 \cos(\gamma_0) \end{bmatrix} \quad (3.3)$$

Applying assumptions, $\dot{u} = \dot{v} = \dot{w} = 0$ in Equation (3.1) and substituting Equation (3.3) into Equation (2.31), the equation becomes as following:

$$m \cdot \begin{bmatrix} \dot{u}_0 \\ \dot{v}_0 \\ \dot{w}_0 \end{bmatrix}_{\sigma=0} = \begin{bmatrix} 0 \\ 0 \\ 0 \end{bmatrix} = L_{EB} \cdot \begin{bmatrix} 0 \\ k\Omega_{0,3}^2 \sin(\gamma_0) \\ -k\Omega_{0,1}^2 - k\Omega_{0,2}^2 - k\Omega_{0,3}^2 \cos(\gamma_0) \end{bmatrix} + \begin{bmatrix} 0 \\ 0 \\ mg \end{bmatrix} \quad (3.4)$$

Right side of the Equation (3.3) and Equation (3.4) are used to construct function F such that, minimum of the function subject to constraints for given limits. Function minimized in a circle with a value c_{min} given as below:

$$c_{min} = F.F' \quad (3.5)$$

Solving equation for characteristics of Scorpion 3020-780kv motor and APC 11x5.5 propeller combination gives results as following:

Table 3.1: Trim values for hover with Scorpion 3020-780kv motor and APC 11x5.5 combination

Φ_0 [deg]	Θ_0 [deg]	Ψ_0 [deg]	γ_0 [deg]	$\Omega_{0,1}$ [rpm]	$\Omega_{0,2}$ [rpm]	$\Omega_{0,3}$ [rpm]
0.604	2.732e-09	0.0246	-1.8127	7445	7436	7489

3.3 Linearization of Hover Flight Equations

Assumptions given in Equation (3.1) are combined with derived trim values as given in Table (3.1). Moreover, small perturbation is applied to relative parameters, such

that equations can be linearized around trimmed values. Perturbations are so small that any product of perturbed variables of two parameters are zero [11]. In transformation matrices, trigonometric functions, cosine and sine can be presented by following notations:

$$\begin{aligned} \sin(\gamma_0 + \Delta\gamma) &\doteq \sin(\gamma_0) + \Delta\gamma \cos(\gamma_0) \\ \cos(\gamma_0 + \Delta\gamma) &\doteq \cos(\gamma_0) - \Delta\gamma \sin(\gamma_0) \end{aligned} \quad (3.6)$$

Considering the given information, Equation (2.43) and Equation (2.36) can be expressed as following:

$$\begin{bmatrix} \Delta\dot{\phi} \\ \Delta\dot{\theta} \\ \Delta\dot{\psi} \end{bmatrix} = \begin{bmatrix} 1 & 0 & 0 \\ 0 & 1 & -\Phi_0 \\ 0 & \Phi_0 & 1 \end{bmatrix} \cdot \begin{bmatrix} \Delta p \\ \Delta q \\ \Delta r \end{bmatrix} \quad (3.7)$$

$$\begin{bmatrix} \Delta\dot{p} \\ \Delta\dot{q} \\ \Delta\dot{r} \end{bmatrix} = \begin{bmatrix} \Delta L_T/I_x \\ \Delta M_T/I_y \\ \Delta N_T/I_z \end{bmatrix} \quad (3.8)$$

3.4 Trimming Approach for Forward Flight

In aircraft mode, platform is trimmed for straight, symmetric and wing level flight conditions. Time derivatives of all parameters are taken zero in equations of motion. As a result of it, angular velocities also become zero. It is assumed that there is no side slip manoeuvre and bank angle. Besides all time derivatives, trimmed values for rest of the parameters may be given as follows:

$$\Phi_0 = \Psi_0 = \beta_0 = v_0 = p_0 = q_0 = r_0 = 0 \quad (3.9)$$

3.5 Simplification of Aerodynamic Coefficients

Aerodynamic forces and moments obtained from different angle of attack, angle of side slip and deflected control surface input results are analysed. Assumption from this analysis was made that rate of change for varying parameters may be taken constant, such that when applying it into Equation (2.20) and Equation (2.21), aerody-

dynamic coefficients C_X , C_Y , C_Z , C_l , C_m and C_n may be presented in following equations. Thus, coefficients that are defined for each equation is presented in Appendix E.

$$C_{X_d} = C_{X_0} + \frac{\Delta C_X}{\Delta \delta_{elev}} \delta_{elev} + \frac{\Delta C_X}{\Delta \delta_{ail}} \delta_{ail} + \frac{\Delta C_X}{\Delta \alpha} \alpha + \frac{\Delta C_X}{\Delta \alpha^2} \alpha^2 \quad (3.10)$$

$$C_{Y_d} = \frac{\Delta C_Y}{\Delta \beta} \beta \quad (3.11)$$

$$C_{Z_d} = C_{Z_0} + \frac{\Delta C_Z}{\Delta \delta_{elev}} \delta_{elev} + \frac{\Delta C_Z}{\Delta \alpha} \alpha \quad (3.12)$$

$$C_{l_d} = \frac{\Delta C_l}{\Delta \delta_{ail}} \delta_{ail} + \frac{\Delta C_l}{\Delta \beta} \beta \quad (3.13)$$

$$C_{m_d} = C_{m_0} + \frac{\Delta C_m}{\Delta \delta_{elev}} \delta_{elev} + \frac{\Delta C_m}{\Delta \alpha} \alpha \quad (3.14)$$

$$C_{n_d} = \frac{\Delta C_n}{\Delta \delta_{rud}} \delta_{rud} + \frac{\Delta C_n}{\Delta \beta} \beta \quad (3.15)$$

Forces acting on body for trimmed forward flight which is defined in Equation (2.53) can be rewritten using trim conditions which are stated in Equation (3.9) as following:

$$F_{B0_f} = \begin{bmatrix} -mg \sin(\theta_0) \\ 0 \\ mg \cos(\theta_0) \end{bmatrix} + \begin{bmatrix} 2(k_1 \Omega_{1,2_0} + k_0) \\ 0 \\ 0 \end{bmatrix} + \frac{1}{2} \rho V_\infty^2 S \left(\begin{bmatrix} C_{X_0} \\ 0 \\ C_{Z_0} \end{bmatrix} + \begin{bmatrix} \Delta C_{X_{\delta_{ail}}} & \Delta C_{X_{\delta_{elev}}} & 0 & \Delta C_{X_\alpha} & \Delta C_{X_{\alpha^2}} \\ 0 & 0 & 0 & 0 & 0 \\ 0 & \Delta C_{Z_{\delta_{elev}}} & 0 & \Delta C_{Z_\alpha} & 0 \end{bmatrix} \begin{bmatrix} \delta_{ail_0} \\ \delta_{elev_0} \\ \delta_{rud_0} \\ \alpha_0 \\ \alpha_0^2 \end{bmatrix} \right) \quad (3.16)$$

Moments acting on body for trimmed forward flight which are defined in Equation (2.51) and Equation (2.21) can be rewritten using assumptions that are given in Equations (3.10) through (3.15).

tion (3.9) as follows:

$$M_{B0_f} = \frac{1}{2} \rho V_\infty^2 S \begin{bmatrix} b & \bar{c} & b \end{bmatrix} \left(\begin{bmatrix} 0 \\ C_{M_0} \\ 0 \end{bmatrix} + \begin{bmatrix} \Delta C_{l_{\delta_{ail}}} & 0 & 0 & 0 \\ 0 & \Delta C_{m_{\delta_{elev}}} & 0 & \Delta C_{m_\alpha} \\ 0 & 0 & \Delta C_{n_{\delta_{rud}}} & 0 \end{bmatrix} \begin{bmatrix} \delta_{ail_0} \\ \delta_{elev_0} \\ \delta_{rud_0} \\ \alpha_0 \end{bmatrix} \right) \quad (3.17)$$

Equation (3.16) and Equation (3.17) are used to find local minimum such that trimming constraints for level flight are met. Results for trimmed values are given in Table (3.2). Trimmed results showed that to hold platform in forward flight, elevator control deflection should be applied heavily for relatively low speeds, and required aileron and rudder control deflections are close to zero. Cruise speed of the VTOL platform is chosen as 20 [m/s] and related trimmed results for that airspeed are used for linearization of the system.

Table 3.2: Trim flight results for forward flight

V_∞ [m/s]	$\Omega_{1,2_0}$ [rpm]	δ_{elev_0} [deg]	Θ_0 [deg]	Max Error
19	5777.35	-15.83	9.89	2.0692e-11
20	6199.99	-14.22	8.85	1.4643e-11
21	6602.54	-12.84	7.95	1.008e-11
22	6989.01	-11.65	7.16	1.0096e-11
23	7362.32	-10.63	6.47	1.3404e-11
24	7724.65	-9.74	5.86	1.0495e-11
25	8077.64	-8.97	5.33	9.9884e-12
26	8422.56	-8.30	4.85	9.8505e-12
27	8760.44	-7.72	4.42	9.2089e-12
28	9092.07	-7.21	4.04	9.5578e-12

Applying the trim results given in Table (3.2), Equation (2.36) can be expressed as

follows for the forward flight:

$$\begin{bmatrix} \Delta\dot{\phi} \\ \Delta\dot{\theta} \\ \Delta\dot{\psi} \end{bmatrix} = \begin{bmatrix} 1 & 0 & \Theta_0 \\ 0 & 1 & -\Phi_0 \\ 0 & \Phi_0 & 1 \end{bmatrix} \cdot \begin{bmatrix} \Delta p \\ \Delta q \\ \Delta r \end{bmatrix} \quad (3.18)$$

Angular rate change will be derived from perturbed moments as it is defined in Equation (3.8), perturbed motion of moment generated by control deflections can be derived by substituting Equation (3.9) and function output of Equation (3.5) according to desired control surface deflection combinations into relevant parts to hold the system in desired level trim condition. Motor reactive torque has no effect on total moment, since rotation speed of front motors are the same. Thus, constant parts of the each equations are neglected. After simplification, function becomes as following:

$$\begin{bmatrix} \Delta\dot{p} \\ \Delta\dot{q} \\ \Delta\dot{r} \end{bmatrix} = \begin{bmatrix} \frac{\rho V_\infty^2 S b \Delta C_{l_{\delta_{ail}}}}{2I_x} & 0 & 0 \\ 0 & \frac{\rho V_\infty^2 S \bar{c} \Delta C_{m_{\delta_{elev}}}}{2I_y} & 0 \\ 0 & 0 & \frac{\rho V_\infty^2 S b \Delta C_{n_{\delta_{rud}}}}{2I_z} \end{bmatrix} \begin{bmatrix} \Delta\delta_{ail} \\ \Delta\delta_{elev} \\ \Delta\delta_{rud} \end{bmatrix} \quad (3.19)$$

CHAPTER 4

CONTROL METHODS

4.1 Introduction

In this chapter, control strategies and control algorithms are proposed to handle platform configurations. Control strategy is proposed to define control allocation of the system, such that states, inputs and outputs can be related to each other. Controller outputs for tricopter attitude control case are designated by motor outputs and aft angle command. Thus, controller outputs for forward flight are designated by wing control surface deflections and front motor outputs. Considering control strategy, algorithms can be derived for transition methodology between tricopter attitude control and forward flight regimes. LQT controller is explained and formulated for these purposes. Previous studies for attitude and speed controller are also mentioned in Appendix A. LQT and LQR with integral action controllers are explained and formulated also for proposed approaches in Appendix A.

4.2 Tricopter Attitude Control Strategy

Tricopter control is sustained by differential thrust of motors and aft motors tilt position. Control is divided into roll, pitch, yaw and throttle control. Control commands are given by pilot through Radio Frequency (RF) controller stick commands. Commands are converted into allocated commands as input to controller. Autopilot controller stabilizes stick commands and designates the desired flight regime. When pilot wants to pitch-up (Θ_{cmd}) the system, longitudinal command, δ_{lon} is given as shown in Figure (4.1)(a).

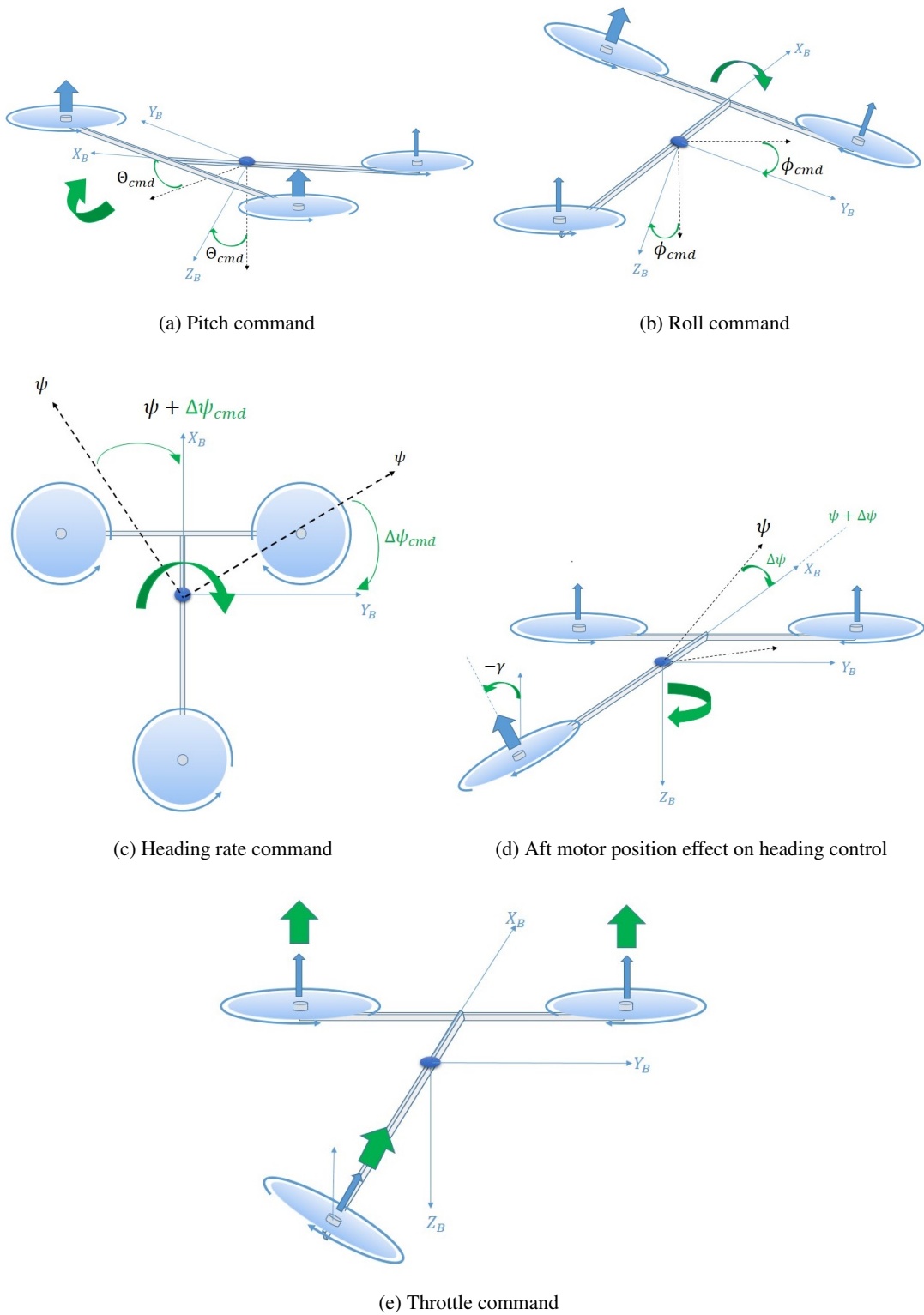


Figure 4.1: Tricopter attitude control allocation

When it is desired to turn system left or right (Φ_{cmd}), latitude command is directed by

δ_{lat} as shown in Figure (4.1)(b). Frame gains altitude by increasing angular velocity of all three motors using throttle command, δ_{th} shown in Figure (4.1)(e).

Yaw control is sustained as heading hold, such that when pilot does not give any pedal command δ_{ped} controller holds the heading in current position. When pilot gives rudder command in desired direction, $\Delta\Psi_{cmd}$ reference heading settles around current navigation heading with varying rate change, $\Psi_{nav} \pm \Delta\Psi_{cmd}$ as shown in Figure (4.1)(c) and Figure (4.1)(d) with logic presented in Figure (4.2). Aft servo motor plays an important role in this scenario. It tilts the aft motor in opposite direction of rotation.

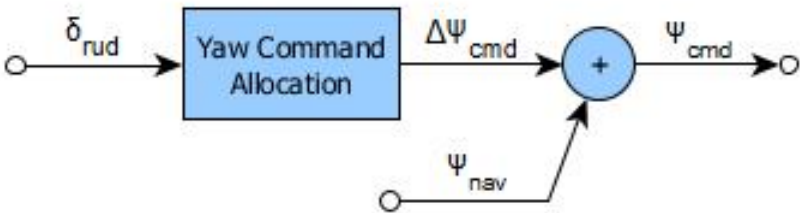


Figure 4.2: Heading control allocation

Using all the information for control strategy for state, input and output information the attitude control approach for control can be presented as shown in Figure (4.3)

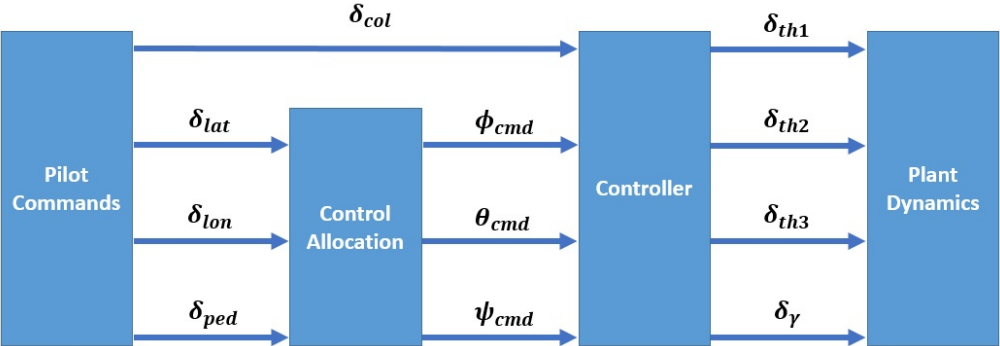


Figure 4.3: Attitude control allocation for tricopter mode flight

4.3 Forward Flight Control Strategy

Plane control is sustained by front motors and control surfaces. Inputs can be divided into roll, pitch, yaw and throttle control commands. These are given by pilot through RF controller stick commands. Autopilot controller stabilizes stick commands and designates the desired forward flight regime. When pilot wants to nose-down (Θ_{cmd}) the system, longitudinal command, δ_{lon} is given as shown in Figure(4.5)(a). When it is desired to turn system left or right (Φ_{cmd}), latitude command is directed by δ_{lat} as shown in Figure (4.5)(b). Heading control is sustained by rate command, such that when pilot does not give any pedal command δ_{ped} controller holds the heading in current position. When pilot gives rudder command in desired direction, $\Delta\Psi_{cmd}$ reference heading settles around current navigation heading with varying rate change as shown in Figure (4.5)(c). Control logic is same as it is presented in Figure (4.2). Forward flight controller does not produce throttle command. When pilot gives the collective input δ_{col} , plane gains altitude by increasing angular speed of front motors (Ω_1 and Ω_2) at same amount and wing generates more lift for the level flight regime.

Using control strategy for given state, input and output information the forward flight approach for control can be presented as shown in Figure (4.4) :

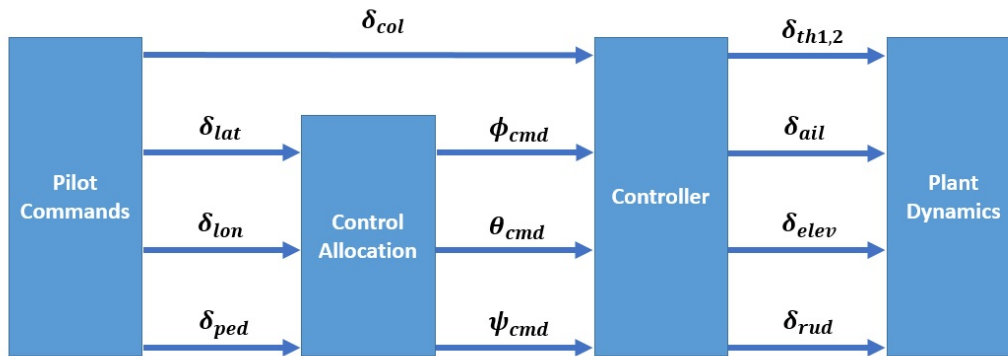


Figure 4.4: Attitude control allocation for forward flight

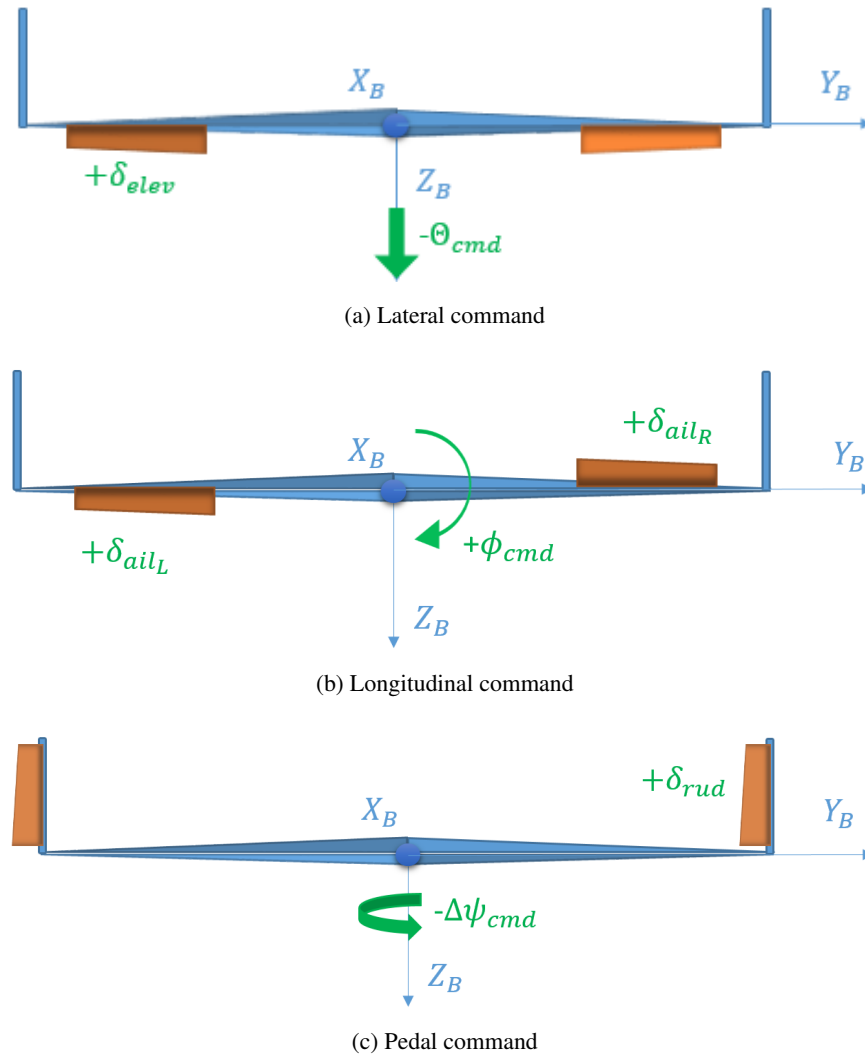


Figure 4.5: Forward flight control allocation

4.4 Control Design Approach

It is stated in the introduction that LQT is used for the controller design. Since it is a linear controller, linear state space approach is needed to be followed. Control approach is implemented in embedded system, so that discrete time domain is chosen as design approach. As control strategy guided, attitude commands are fed into attitude controller to hold system in desired states. The state space approach used for linearized solutions obtained in Equation (3.7) and Equation (3.8), states and inputs

of the system at tricopter attitude control can be defined as follows:

$$\Delta x = \left[\Delta p \quad \Delta q \quad \Delta r \quad \Delta \Phi \quad \Delta \Theta \quad \Delta \Psi \right]' \quad (4.1)$$

$$\Delta u_h = \left[\Delta L \quad \Delta M \quad \Delta N \right]' \quad (4.2)$$

Linearized solutions obtained for forward flight from Equation (3.18) and Equation (3.19) showed that states for forward flight can be defined as proposed in tricopter attitude control state vector which is given in Equation (4.1). Since throttle stick command is directed by the pilot, input vector for forward flight can be defined as follows:

$$\Delta u_f = \left[\Delta \delta_{ail} \quad \Delta \delta_{elev} \quad \Delta \delta_{rud} \right]' \quad (4.3)$$

Discretization applied on dynamic equations result as below:

$$\begin{aligned} \Delta \dot{x}(t) &= A_d \Delta x(t) + B_d \Delta u(t) \\ \Delta y(t) &= C_d \Delta x(t) + D_d \Delta u(t) \end{aligned} \quad (4.4)$$

4.4.1 Linear Quadratic Tracker (LQT) Control

Linear quadratic controller is chosen to get desired output with minimum control energy. As it is proposed in Equation (4.4), $x(t)$ is a $[nx1]$ state vector, $u(t)$ is a $[mx1]$ control vector, and $y(t)$ is a $[kx1]$ output vector. Desired trajectory, $z(t)$ has the same dimension as output vector. The aim is to follow/track desired output as much as possible with system output during flight.

The error between desired output and system output is tried to be controlled and minimized to hold system in desired attitude.

$$\Delta e_h(t) = \Delta z(t) - C_d \Delta x(t) \quad (4.5)$$

Performance index is chosen for infinite time case such that there is no terminal cost is given as specified in [23, 33].

$$J_d = \frac{1}{2} \sum_{t=t_0}^{\infty} \left\{ \left[\Delta z(t) - C_d \Delta x(t) \right]^T Q \left[\Delta z(t) - C_d \Delta x(t) \right] + \left[\Delta u(t) \right]^T R \left[\Delta u(t) \right] \right\} \quad (4.6)$$

where Q is positive semi-definite [kxk] state weight matrix, R is positive definite [mxm] control weight matrix. Stability of system is sustained using optimal weight matrices. Solution to the linear quadratic tracker is constructed using stable eigenvectors of Hamiltonian form. The optimal control obtained from this approach is given as following:

$$u^*(t) = -R^{-1}B^T\lambda^*(t) \quad (4.7)$$

State and optimal costate equation are related as following:

$$\lambda^*(t) = Px^*(t) - g(t) \quad (4.8)$$

Equation (4.8) is satisfied by eliminating the costat, by $P(t)$ square matrix as a solution to the matrix differential ricatti equation and $g(t)$ vector as a solution to vector differential equation.

$$0 = -PA_d - A_d^T P + PBR^{-1}B_d^T P - C_d^T Q C_d \quad (4.9)$$

$$0 = [P(t)E - A_d^T]g(t) + Wz(t) \quad (4.10)$$

Where $E = B_d R^{-1} B_d^T$ and $W = C_d^T Q$. Applying Equation (4.9) and Equation (4.10) into optimal control Equation (4.7) eliminates costate $\lambda^*(t)$, and function becomes as following:

$$u^*(t) = -R^{-1}B_d^T \left[Px(t) - [PE - A_d^T]^{-1}Wz(t) \right] \quad (4.11)$$

Controller gains can be group into corresponding vectors as follows:

$$\begin{aligned} u^*(t) &= -Kx(t) + K_z z(t) \\ K &= R^{-1}B_d^T P \\ K_z &= R^{-1}B_d^T \left[PE - A_d^T \right]^{-1} W \end{aligned} \quad (4.12)$$

4.4.1.1 Tricopter Mode Attitude Control Approach

Using Equation (4.4), attitude control can be defined also as follows, where state and input vectors are Equation (4.1) and Equation (3.8) respectively. The command atti-

tudes are converted into roll, pitch and yaw moments.

$$\Delta \dot{x}_h(t) = \begin{bmatrix} A_{h_d} \end{bmatrix} \begin{bmatrix} \Delta p(t) \\ \Delta q(t) \\ \Delta r(t) \\ \Delta \Phi(t) \\ \Delta \Theta(t) \\ \Delta \Psi(t) \end{bmatrix} + \begin{bmatrix} B_{h_d} \end{bmatrix} \begin{bmatrix} \Delta L(t) \\ \Delta M(t) \\ \Delta N(t) \end{bmatrix} \quad (4.13)$$

LQT optimal control approach for tricopter attitude control case can be derived by applying Equation (4.12) into Equation (4.13) as follows:

$$u_h(t) = \begin{bmatrix} \Delta L(t) \\ \Delta M(t) \\ \Delta N(t) \end{bmatrix} = \begin{bmatrix} -K_H \end{bmatrix} \begin{bmatrix} \Delta p(t) \\ \Delta q(t) \\ \Delta r(t) \\ \Delta \Phi(t) \\ \Delta \Theta(t) \\ \Delta \Psi(t) \end{bmatrix} + \begin{bmatrix} K_{z_H} \end{bmatrix} \begin{bmatrix} \Delta \Phi(t) \\ \Delta \Theta(t) \\ \Delta \Psi(t) \end{bmatrix} \quad (4.14)$$

Using moment and force equations, Equation (2.45), Equation (2.46) and Equation (2.44), respectively for tricopter frame, relation between control inputs and motors and aft servo parameters can be derived:

$$\begin{bmatrix} L \\ M \\ N \\ Z \end{bmatrix} = \begin{bmatrix} -k \cos(\sigma) r_{y,1} - l \sin(\sigma) & -k \cos(\sigma) r_{y,2} + l \sin(\sigma) & -k r_{y,3} & -k r_{z,3} \\ k(\sin(\sigma) r_{z,1} + \cos(\sigma) r_{x,1}) & k(\sin(\sigma) r_{z,2} + \cos(\sigma) r_{x,2}) & k r_{x,3} & -l \\ -k \sin(\sigma) r_{y,1} + l \cos(\sigma) & -k \sin(\sigma) r_{y,2} - l \cos(\sigma) & l & k r_{x,3} \\ -k \cos(\sigma) & -k \cos(\sigma) & -k & 0 \end{bmatrix} \cdot \begin{bmatrix} \Omega_1^2 \\ \Omega_2^2 \\ \Omega_3^2 \cos(\gamma) \\ \Omega_3^2 \sin(\gamma) \end{bmatrix} \quad (4.15)$$

Pilot's collective input is converted to relative force value; such that when full stick input for δ_{col} is given, corresponding Z force is obtained as maximum force that all

three motors can be produced.

$$\begin{bmatrix} \Omega_1^2 \\ \Omega_2^2 \\ \Omega_3^2 \cos(\gamma) \\ \Omega_3^2 \sin(\gamma) \end{bmatrix} = [T_{C2M}] \begin{bmatrix} L \\ M \\ N \\ Z \end{bmatrix} \quad (4.16)$$

where T_{C2M} is a [4x4] transformation matrix. Aft servo angle is derived from vectorial force components of aft motor, of which is a result of change in aft servo angle:

$$\gamma = \text{atan}\left(\frac{\Omega_3^2 \sin(\gamma)}{\Omega_3^2 \cos(\gamma)}\right) \quad (4.17)$$

The gain matrices for attitude control are given in Appendix C.

4.4.1.2 Forward Flight Attitude Control Approach

From Equation (4.4), forward flight attitude control, where state and input vectors are stated in Equation (4.1) and Equation (4.3) respectively. Pilot's collective input δ_{col} is fed as throttle input to front motors. As collective input increases, due to generated lift force, platform gains altitude. If the pitch attitude is hold as throttle increases, speed of the platform also increases.

$$\Delta \dot{x}_l(t) = [A_{df}] \begin{bmatrix} \Delta p(t) \\ \Delta q(t) \\ \Delta r(t) \\ \Delta \Phi(t) \\ \Delta \Theta(t) \\ \Delta \Psi(t) \end{bmatrix} + [B_{df}] \begin{bmatrix} \Delta \delta_{ail}(t) \\ \Delta \delta_{elev}(t) \\ \Delta \delta_{rud}(t) \end{bmatrix} \quad (4.18)$$

LQT optimal control approach for forward flight case can be derived by applying Equation (4.12) into Equation (4.18) as follows:

$$u_l(t) = \begin{bmatrix} \Delta \delta_{ail}(t) \\ \Delta \delta_{elev}(t) \\ \Delta \delta_{rud}(t) \end{bmatrix} = [-K_F] \begin{bmatrix} \Delta p(t) \\ \Delta q(t) \\ \Delta r(t) \\ \Delta \Phi(t) \\ \Delta \Theta(t) \\ \Delta \Psi(t) \end{bmatrix} + [K_{zF}] \begin{bmatrix} \Delta \Phi(t) \\ \Delta \Theta(t) \\ \Delta \Psi(t) \end{bmatrix} \quad (4.19)$$

The gain matrices for forward flight control are given in Appendix C.

4.5 Transition Control Allocation Methods

4.5.1 Weighted Moore-Penrose Pseudo Inverse

Attitude control is sustained using controller gains to hold system in desired state determining the required control inputs. At tricopter mode, this is sustained by using motors and aft motor. However, in forward flight transition case, platform gains speed in order to use wing as a lift source. Control approach for the forward flight transition is using the attitude controller for tricopter mode. At early stages, when speed of platform is small, motors and aft servo angle becomes more effective. Increment in speed of the platform makes change in control surface deflections and makes them more important.

The thrust and control surface allocation block decides how the controller is divided amongst control surfaces and motors as follows:

$$v = T_a u_{out} \quad (4.20)$$

Where v is allocated control input and u_{out} controller output. In tricopter mode attitude control flight, front motors are positioned vertically, thus relation of angular velocity between thrust and torque have a quadratic relation as proposed in Equation (2.4) and Equation (2.5). Thus, it is assumed that relations apply the same for all three motors. Using the information given in Equation (4.20), transition from tricopter mode to plane mode can be defined as following:

$$\begin{bmatrix} L \\ M \\ N \\ Z \end{bmatrix} = \begin{bmatrix} T_{atri} \end{bmatrix} \begin{bmatrix} \Omega_1^2 \\ \Omega_2^2 \\ \Omega_3^2 \cos(\gamma) \\ \Omega_3^2 \sin(\gamma) \\ \delta_{ail} \\ \delta_{elev} \\ \delta_{rud} \end{bmatrix} \quad (4.21)$$

In forward flight, front motors are positioned horizontally, thus relation of angular velocity, using curve fit simplifications between thrust and torque relation at forward flight shows that these relations are linear as proposed in Equation (2.6) and Equation

(2.7), and it is assumed that relations apply the same for all three motors. Control allocation is carried out for forward flight between the control surface deflections, propeller thrusts, front and aft propeller tilt angles can be represented as follows:

$$\begin{bmatrix} L \\ M \\ N \\ Z \end{bmatrix} = [T_{a_{fwd}}] \begin{bmatrix} \Omega_1 \\ \Omega_2 \\ \Omega_3 \cos(\gamma) \\ \Omega_3 \sin(\gamma) \\ \delta_{ail} \\ \delta_{elev} \\ \delta_{rud} \end{bmatrix} \quad (4.22)$$

Where T_a is control out arrangement matrix and it is shown in Equation (4.24).

$$T_a = [T_{a_1} \ T_{a_2}] \quad (4.23)$$

$$T_{a_1} = \begin{bmatrix} -k \cos(\sigma) r_{y,1} - l \sin(\sigma) & -k \cos(\sigma) r_{y,2} + l \sin(\sigma) & -k r_{y,3} & -k r_{z,3} \\ k(\sin(\sigma) r_{z,1} + \cos(\sigma) r_{x,1}) & k(\sin(\sigma) r_{z,2} + \cos(\sigma) r_{x,2}) & k r_{x,3} & -l \\ -k \sin(\sigma) r_{y,1} + l \cos(\sigma) & -k \sin(\sigma) r_{y,2} - l \cos(\sigma) & l & k r_{x,3} \\ -k \cos(\sigma) & -k \cos(\sigma) & -k & 0 \end{bmatrix}$$

$$T_{a_2} = \begin{bmatrix} \frac{1}{2} \rho V_\infty^2 S b \Delta C_{l_{\delta_{ail}}} & 0 & 0 \\ 0 & \frac{1}{2} \rho V_\infty^2 S \bar{c} \Delta C_{m_{\delta_{elev}}} & 0 \\ 0 & 0 & \frac{1}{2} \rho V_\infty^2 S b \Delta C_{n_{\delta_{rud}}} \\ 0 & \frac{1}{2} \rho V_\infty^2 S \Delta C_{Z_{\delta_{elev}}} & 0 \end{bmatrix} \quad (4.24)$$

Equation (4.24) represents undetermined set of equations so that there are many possible solutions that satisfies it. T_a matrix is used for both plane and tricopter transition, and k and l constants assumed to be same for all three motors. For forward flight, k and l constants are taken from Table (2.4) and Table (2.5) respectively for 20 [m/s] airspeed. For tricopter attitude control, k and l constants, are taken from Table (2.2) and Table (2.3) respectively for hover condition. Approach is chosen as minimum norm [22] to find the solution and it requires Moore-Penrose generalized inverse of T_a which is defined as T_a^* . However, Moore-Penrose generalized inverse technique is not be sufficient to handle control, since it is desired to increase effectiveness of

$$w_{fwd} = \text{diag}\left(\frac{1}{\Omega_{1max}^2}, \frac{1}{\Omega_{2max}^2}, \frac{1}{\Omega_{3max}^2 \cos(\gamma)^2}, \frac{1}{\Omega_{3max}^2 \sin(\gamma)^2}, \frac{1}{\delta_{ailmax}^2}, \frac{1}{\delta_{elevmax}^2}, \frac{1}{\delta_{rudmax}^2}\right) \quad (4.30)$$

Weight costs for both transition to plane mode and transition to tricopter mode are given in Appendix C. If the weight costs are selected equal, Equation (4.32) becomes pseudo inverse matrix. Such that weight can be represented as $W = c_w I$, where I is identity matrix and c_w is cost coefficient.

$$T_a^* = c_w T_a^T (T_a T_a^T)^{-1} \quad (4.31)$$

4.5.2 Blended Inverse

Blended Inverse approach is proposed to handle steering control allocation problems [34]. Desired control outputs are used to weight required control inputs to hold system in desired states. Required control inputs may be used for system allocation using controller generated moments and user defined thrust force to generate motor, control surface and tilt commands. Algorithm can be defined as follows:

$$v_{bl} = [qI_{n \times n} + T_a^T R T_a]^{-1} [q v_{des} + T_a^T R u_{out}] \quad (4.32)$$

Where v_{bl} is the allocated control input vector for actual system, q is smoothing coefficient which is chosen as scalar, and u_{out} is controller output. Desired control input is chosen as trimmed values as suggested in [36] for desired flight regime within varying front tilt angle range. Moreover, desired control input values are assigned dynamically such that each control input is a function of V_∞ . R matrix weights moments and thrust values. Thus, n is equal to the number of rows in u_{out} vector. Equation (4.32) is reexpressed as following:

$$\begin{aligned} v_{bl} &= [Wq + T_a^T R T_a]^{-1} [Wq v_{des} + T_a^T R u_{out}] \\ &= [q + W^{-1} T_a^T R T_a]^{-1} [q v_{des} + W^{-1} T_a^T R u_{out}] \end{aligned} \quad (4.33)$$

Where W is the cost matrix, as defined in Equation (4.26). R matrix is chosen as an identity matrix for this study and Equation (4.33) becomes as following:

$$v_{bl} = [qI_{n \times n} + W^{-1} T_a^T T_a]^{-1} [q v_{des} + W^{-1} T_a^T u_{out}] \quad (4.34)$$

Desired input vectors and smoothing coefficients for both transition to plane mode and transition to tricopter mode are given in Appendix C.

4.6 Flight Management Overview

In order to be directed by pilot, platform is required to handle attitude control as it takes-off, holds attitude commands and transits to forward flight in tricopter mode; and whereas it flies with wing generated lift in forward flight and transit to tricopter mode attitude control in plane mode. Since control approach is chosen such that it is capable of handling the tricopter attitude control, forward flight and control allocation for transition stages from and to forward/tricopter attitude control flight, linear quadratic controller method is sufficient. Control strategy is planned according to phases using change of controller states and inputs. Phase changes occur for given conditions in predefined time limits. Considering platform, control modes separated into Tricopter and Plane modes, where each of them has two flight phases as it is proposed in Figure (4.6).

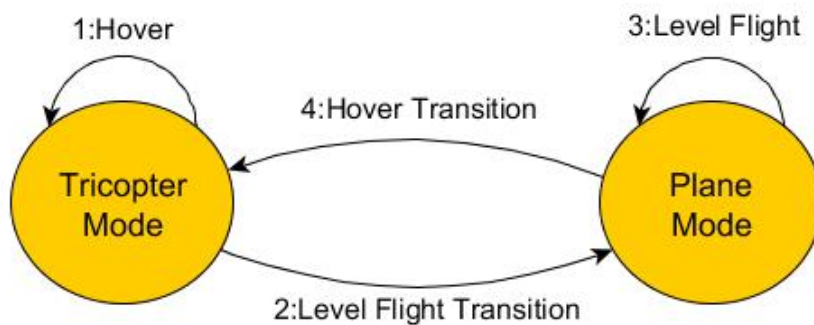


Figure 4.6: Modes and Phases

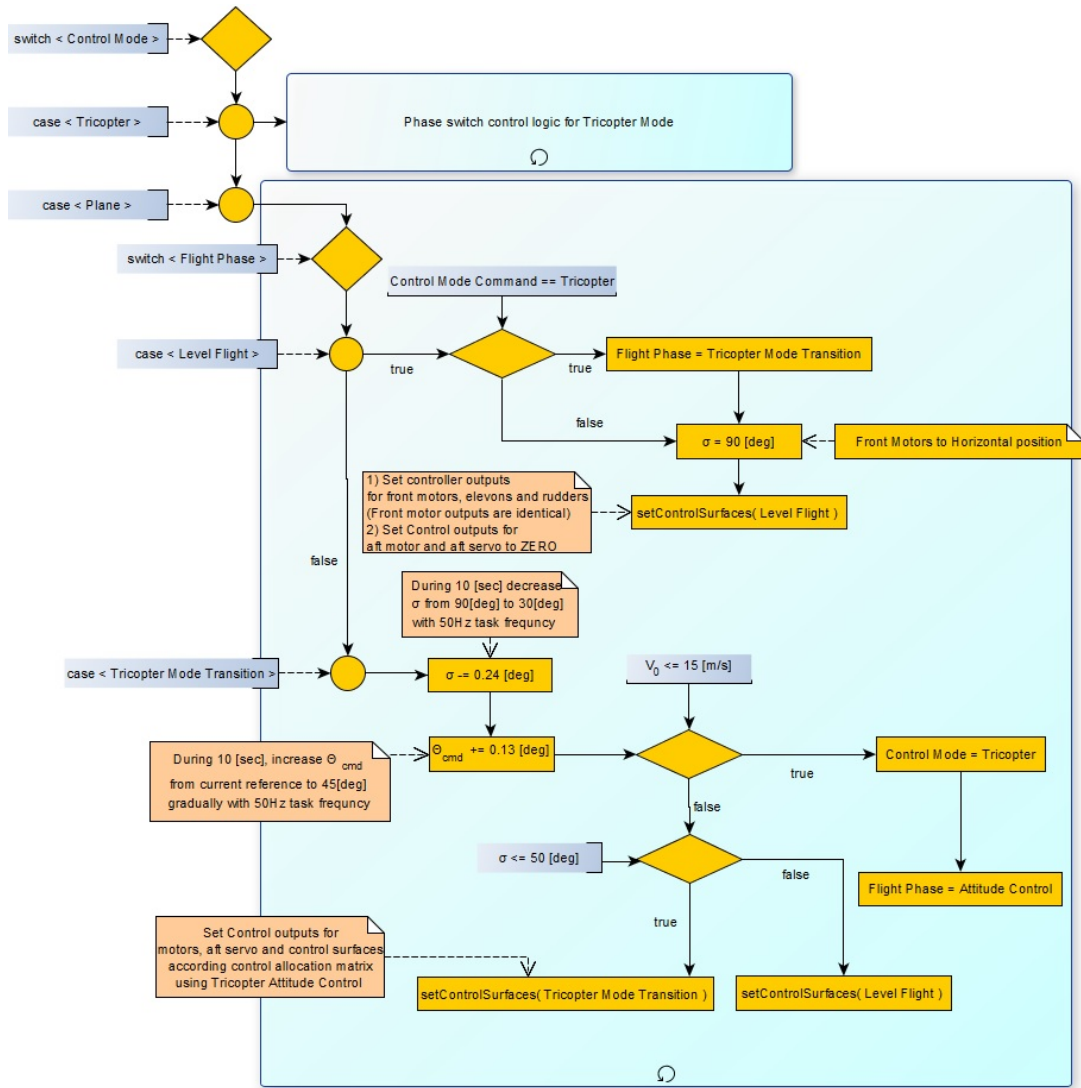


Figure 4.7: Plane mode - phase transition flow chart

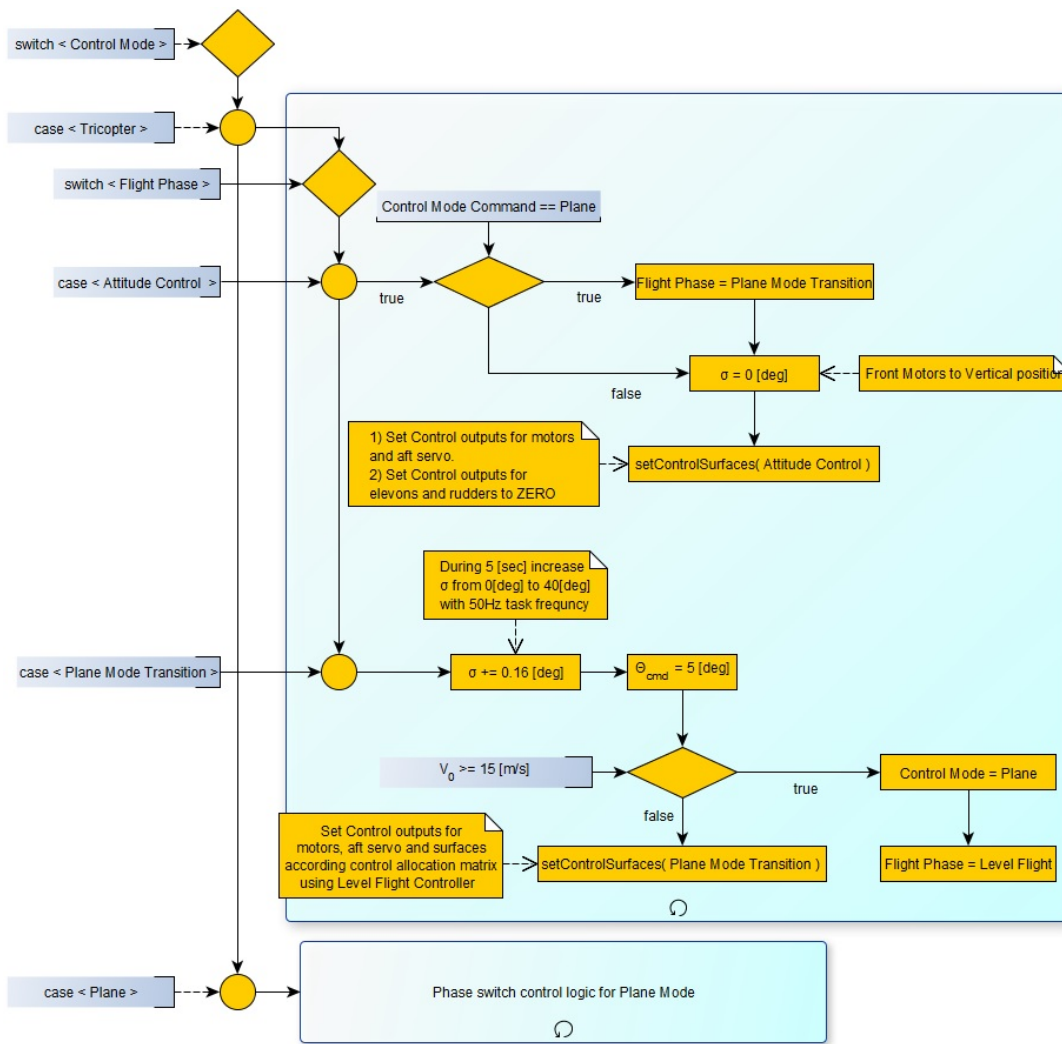


Figure 4.8: Tricopter mode - phase transition flow chart

CHAPTER 5

MODEL ENVIRONMENT AND SIMULATION RESULTS

5.1 Introduction

In the previous chapter, controllers are introduced for attitude control of tricopter and plane modes. In this section, simulation results is obtained and controller outputs are compared. Equations for platform dynamics, obtained in Chapter 2, are modelled. Forces and moments generated by motors are defined as lookup tables as obtained from wind tunnel test results. LQT controller disturbance rejection is performed and analysed.

5.2 Simulation Specifications

Controller methodologies derived in Chapter 4 are applied to the models and gain corrections is made around trimmed system. The aim of the simulations mentioned in this chapter is to test and analyse the system performance for given reference commands against dynamics. System model runs at 50Hz and test scenarios are created to observe LQT controller performance.

According subsystem models defined in Chapter 2, the overall picture of the system model is shown in Figure 5.1.

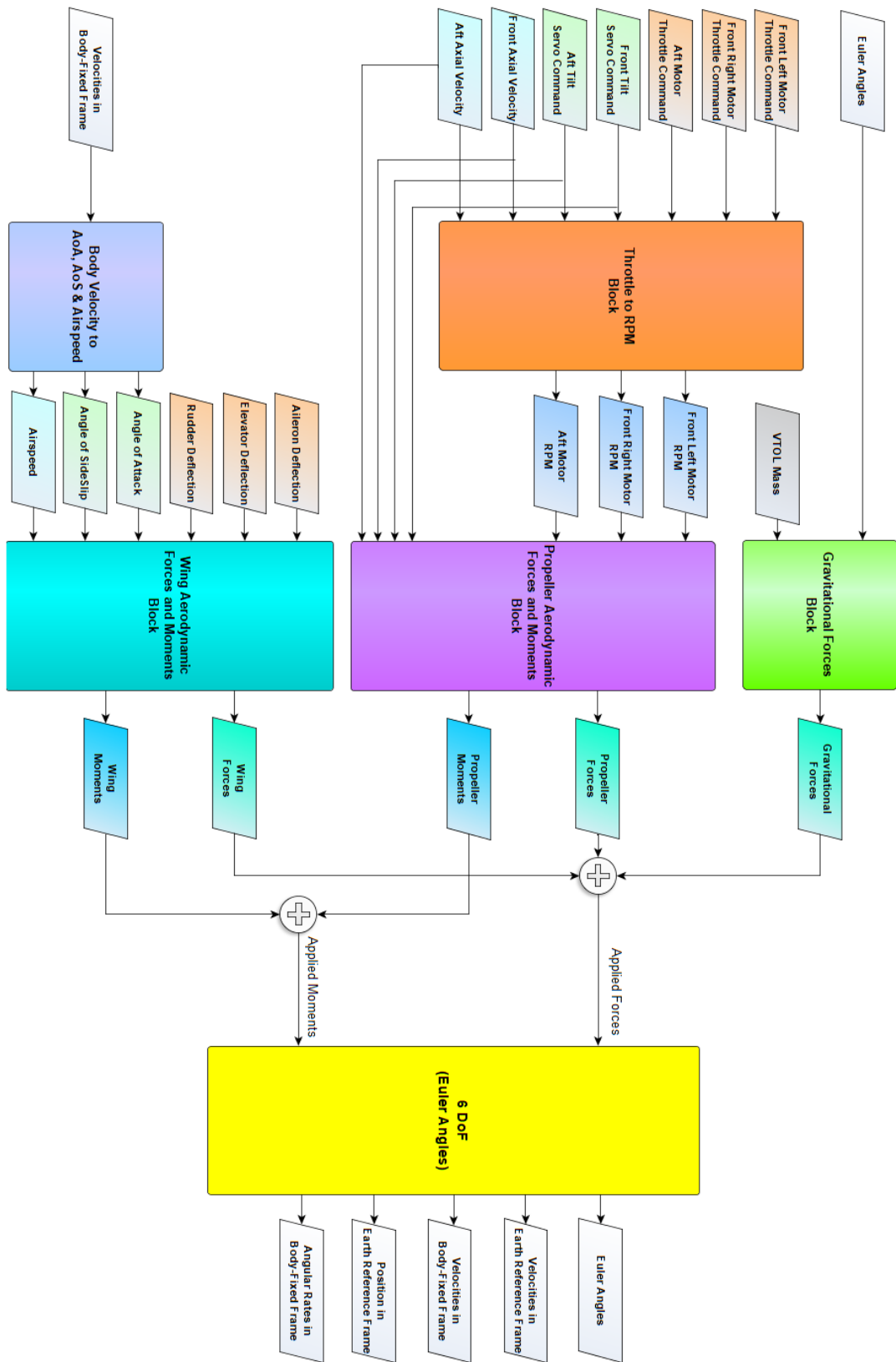


Figure 5.1: Simulation block - Dynamic model of platform

5.3 Tricopter Platform Attitude Control Simulations

5.3.1 Roll Control

Attitude controller simulation results for 10 [deg] roll command with 75% collective input and response of the tricopter frame are given in the following figures. In the Figure (5.2), it is observed that tricopter tracks the given rolling commands while sustaining zero pitch and yaw commands as in the Figure (5.3.a) and Figure (5.3.b). It is also observed in the Figure (5.3.c) that differential thrust of front motor outputs creates rolling moment as intended.

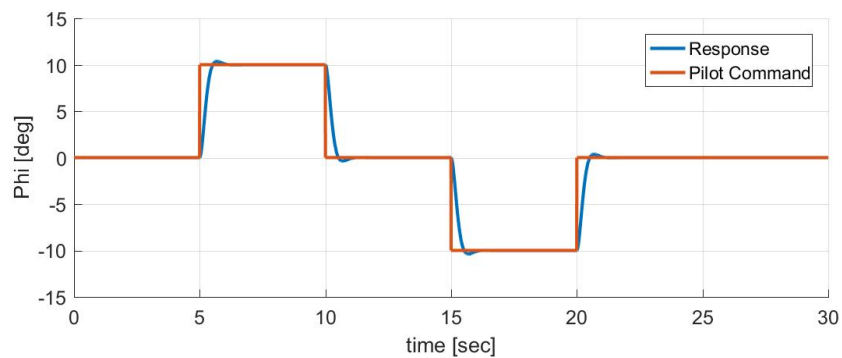
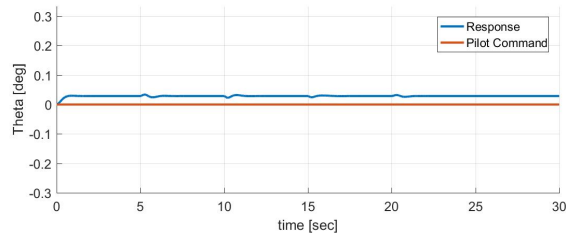
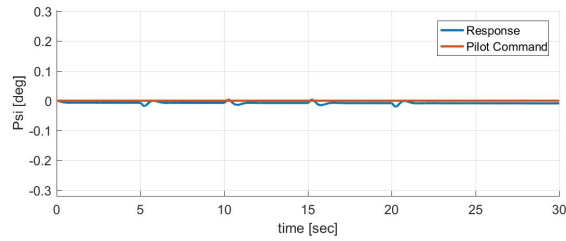


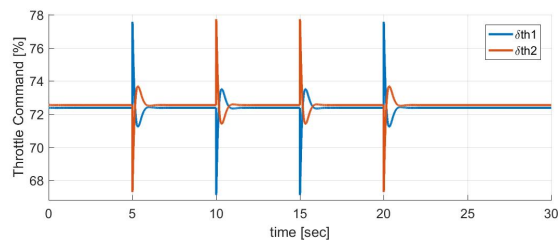
Figure 5.2: LQT control result for given roll command



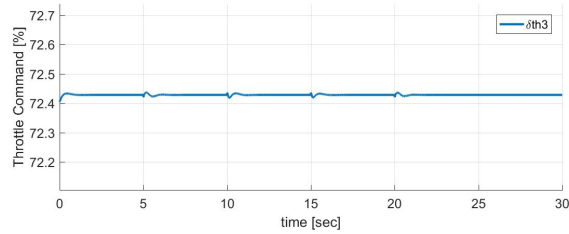
(a) LQT control result for the given zero pitch command



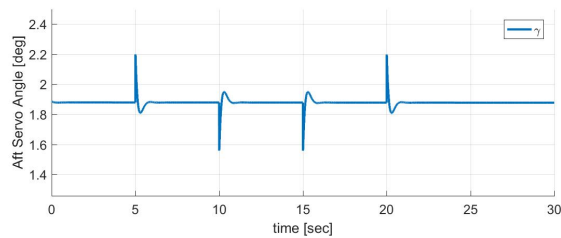
(b) LQT control result for the given zero yaw command



(c) Throttle outputs of front motors for the given roll command



(d) Throttle output of aft motor for the given roll command



(e) Aft servo angle output for the given roll command

Figure 5.3: Tricopter frame responses for LQT controller for given roll command

5.3.2 Pitch Control

Attitude controller simulation results for 10 [deg] pitch command with 75% collective input and response of the tricopter frame are given in the following figures. In the Figure (5.4), it is observed that tricopter tracks the given pitching commands while sustaining to hold zero roll and yaw commands as it is shown in the Figure (5.5.a) and Figure (5.5.b). It is also observed in the Figure (5.5.c) and Figure (5.5.d) that front motors characteristics are similar such that differential thrust of front and aft motors' output creates pitching moment as intended.

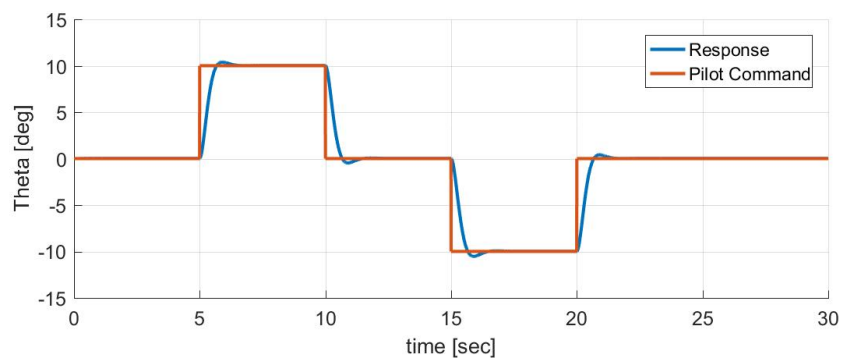
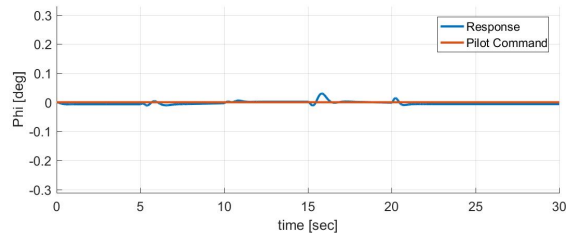
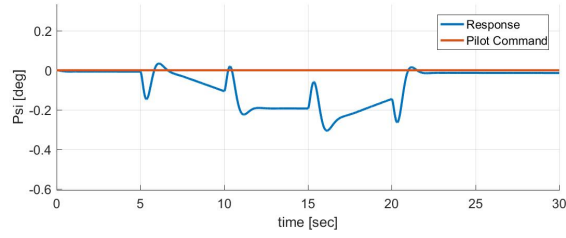


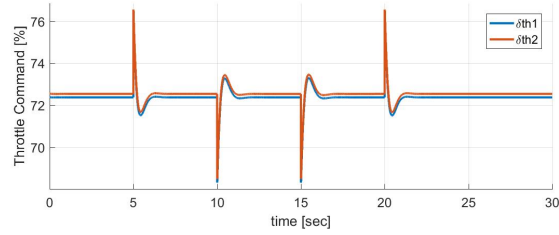
Figure 5.4: LQT control result for given pitch command



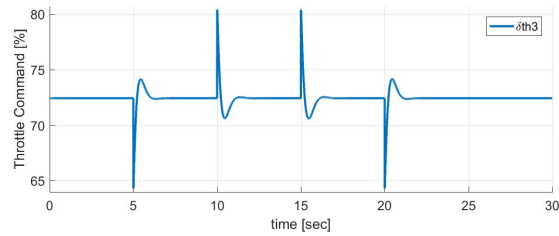
(a) LQT control result for the given zero roll command



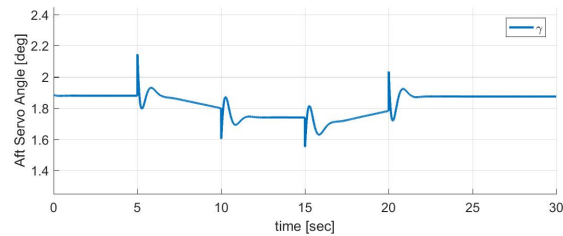
(b) LQT control result for the given zero yaw command



(c) Throttle outputs of front motors for the given pitch command



(d) Throttle output of aft motor for the given pitch command



(e) Aft servo angle output for the given pitch command

Figure 5.5: Tricopter frame responses for LQT controller for given pitch command

5.3.3 Yaw Control

Attitude controller simulation results for 5.73 [deg/s] yaw rate command with 75% collective input and response of the tricopter frame are given in the following figures. In the Figure (5.6), it is observed that tricopter tracks the given yawing commands while sustaining to hold zero roll and pitch commands as shown in the Figure (5.7.a) and Figure (5.7.b). It is also observed in the Figure (5.7.c), Figure (5.7.d) and Figure (5.7.e) with the help of front motors' differential thrust, aft servo directs aft motor to track the given yawing moment as intended.

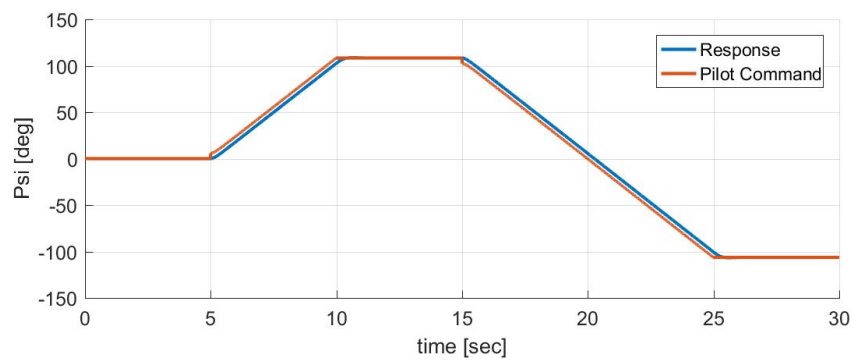
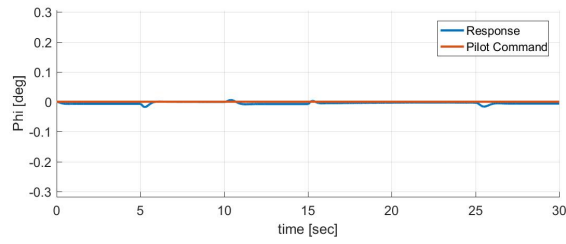
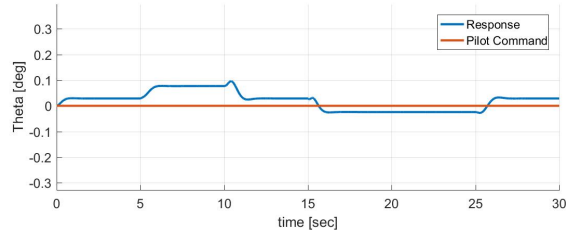


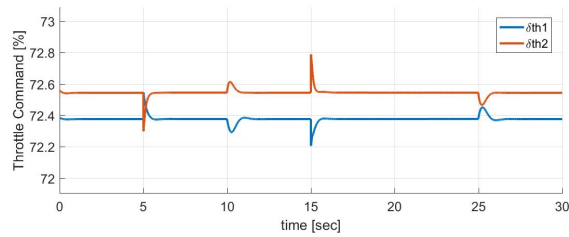
Figure 5.6: LQT control result for the given yaw command



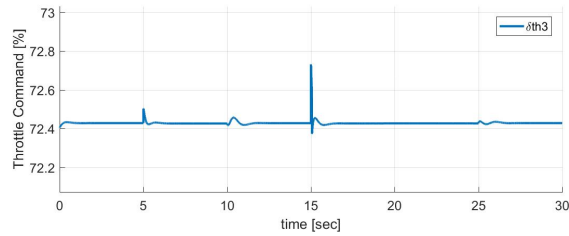
(a) LQT control result for the given zero roll command



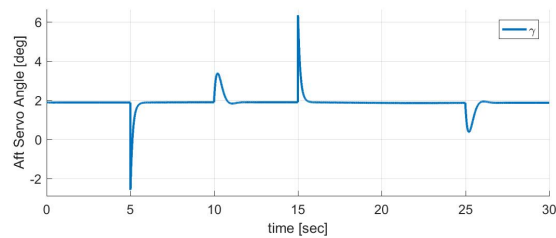
(b) LQT control result for the given zero pitch command



(c) Throttle outputs of front motors for the given yaw command



(d) Throttle output of aft motor for the given yaw command



(e) Aft servo angle output for the given yaw command

Figure 5.7: Tricopter frame responses for LQT controller for given yaw command

5.4 VTOL Platform Tricopter Attitude Control Simulations

5.4.1 Roll Control

Attitude controller simulation results for 5 [deg] roll command with 75% collective input and response of the VTOL frame are given in the following figures. In the Figure (5.8), it is observed that VTOL tracks the given rolling commands with some overshoot while it tries to sustain zero pitch and yaw commands as in the Figure (5.9.a) and Figure (5.9.b). Theta response drifts away from desired command, comparing with tricopter simulation results given in Figure (5.3,a), it is due to wing aerodynamic effects. In Figure (5.9.a), it can be seen that rolling motion causes small pitch variances. It is also observed in the Figure (5.9.c) that differential thrust of front motor outputs creates rolling moment as intended.

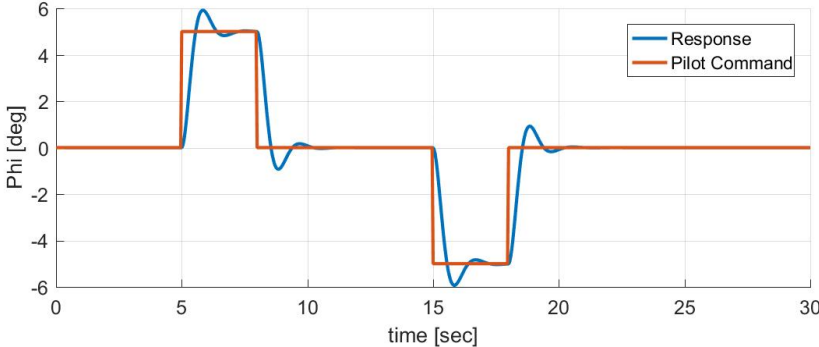
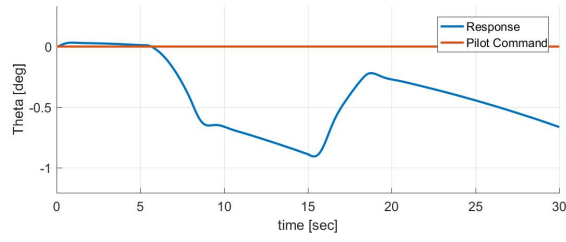
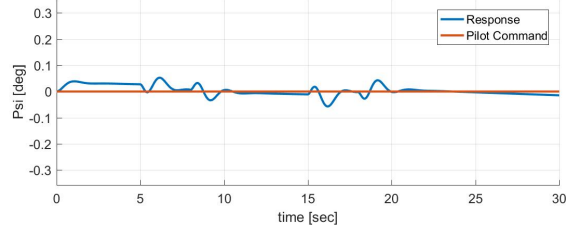


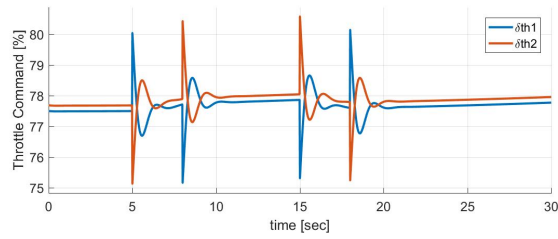
Figure 5.8: LQT control result for the given roll command



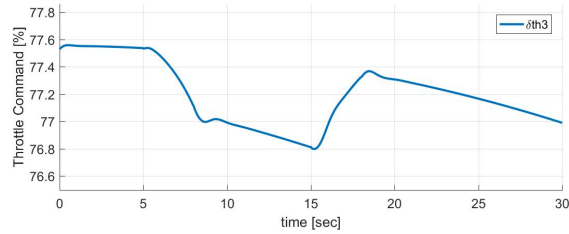
(a) LQT control result for the given zero pitch command



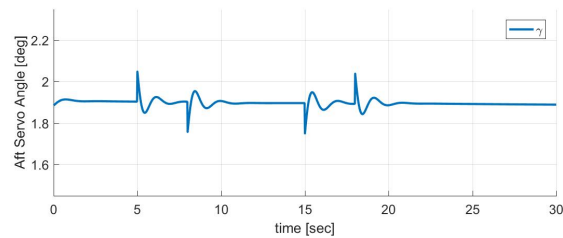
(b) LQT control result for the given zero yaw command



(c) Throttle outputs of front motors for the given roll command



(d) Throttle output of aft motor for the given roll command



(e) Aft servo angle output for the given roll command

Figure 5.9: VTOL frame responses for LQT controller for the given roll command

5.4.2 Pitch Control

Attitude controller simulation results for 5 [deg] pitch command with 75% collective input and response of the VTOL frame are given in the following figures. In the Figure (5.10), it is observed that VTOL tracks the given pitching commands while sustaining to hold zero roll and pitch commands as shown in the Figure (5.11.a) and Figure (5.11.b). It is also observed in the Figure (5.11.c) and Figure (5.11.d), front motors characteristics are similar such that differential thrust of front and aft motors' output creates pitching moment as intended. Theta response drifts away from desired command, comparing with tricopter simulation results given in Figure (5.4), it is due to the wing aerodynamic effects.

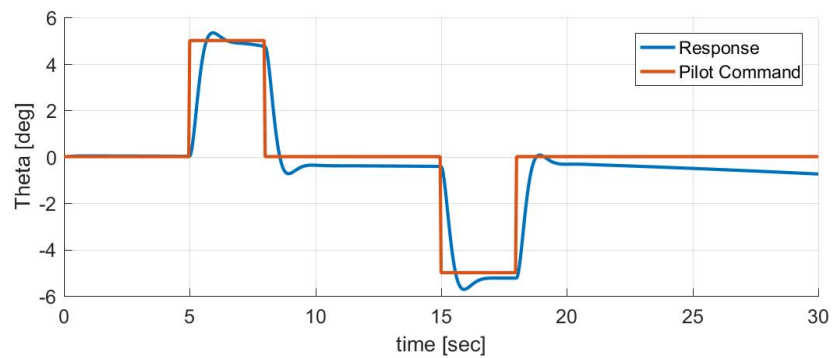
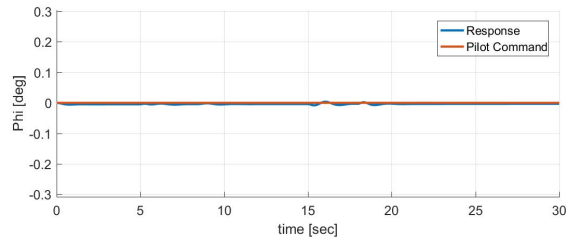
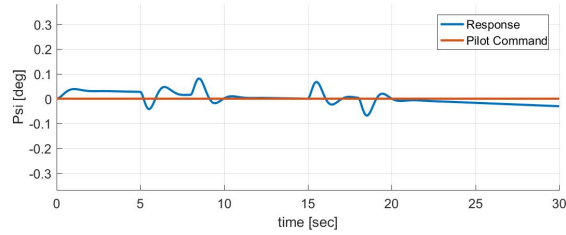


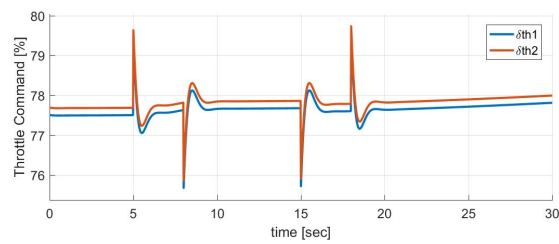
Figure 5.10: LQT control result for the given pitch command



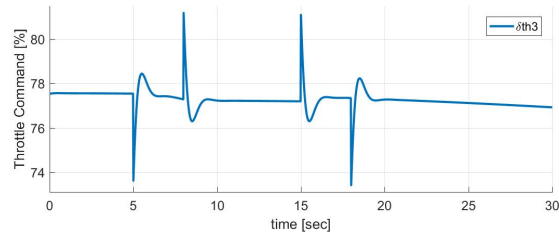
(a) LQT control result for the given zero roll command



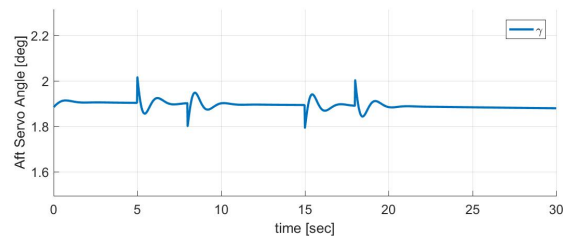
(b) LQT control result for the given zero yaw command



(c) Throttle outputs of front motors for the given pitch command



(d) Throttle output of aft motor for the given pitch command



(e) Aft servo angle output for the given pitch command

Figure 5.11: VTOL frame responses for LQT controller for the given pitch command

5.4.3 Yaw Control

Attitude controller simulation results for 5.73 [deg/s] yaw rate command with 75% collective input and response of the VTOL frame are in the following figures. In the Figure (5.12), it is observed that VTOL tracks the given yawing commands while sustaining to hold zero roll and pitch commands as shown in the Figure (5.13.a) and Figure (5.13.b). It is also observed in the Figure (5.13.c), Figure (5.13.d) and Figure (5.13.e) with the help of front motors' differential thrust, aft servo directs aft motor to track the given yawing moment as intended.

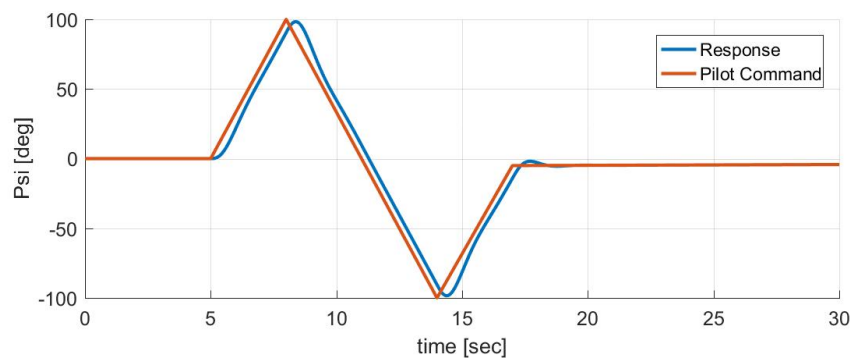
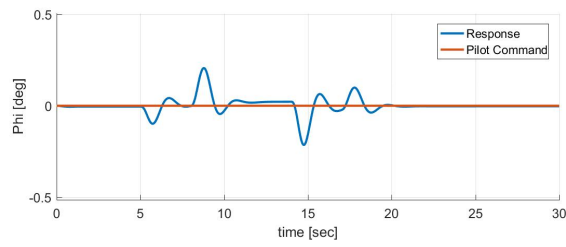
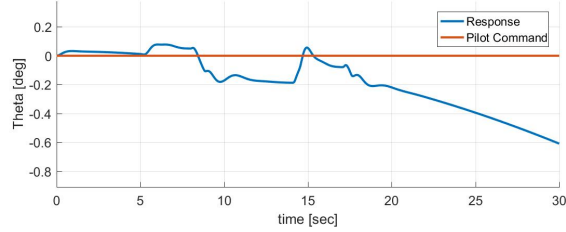


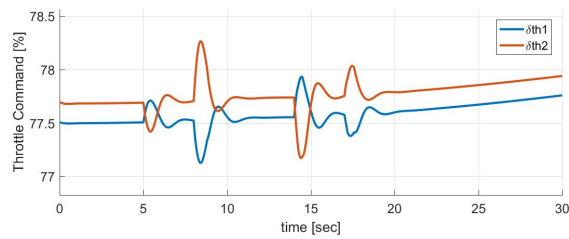
Figure 5.12: LQT control result for the given yaw command



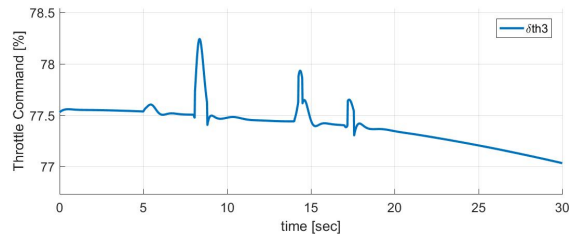
(a) LQT control result for the given zero roll command



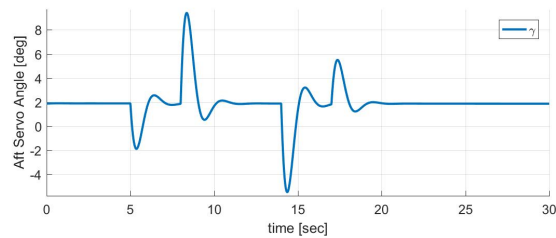
(b) LQT control result for the given zero pitch command



(c) Throttle outputs of front motors for the given yaw command



(d) Throttle output of aft motor for the given yaw command



(e) Aft servo angle output for the given yaw command

Figure 5.13: VTOL frame responses for LQT controller for given yaw command

5.5 VTOL Platform Transition to Forward Flight Control Simulations

5.5.1 Transition Control

Forward flight transition is controlled by given 5 [deg] pitch command and by holding platform at level flight and sustaining current heading. Control allocation is applied at transition phase. During transition front motors tilt from vertical position, $\sigma = 0$ [deg] to $\sigma = 40$ [deg] as specific in flight management tricopter mode in Figure (4.8). Tricopter attitude control is active till transition phase ends. Starting from transition phase, control surface deflections become active. In simulation, transition pulse is triggered at 15 seconds. It may observed from the results that as the system gains speed, wing creates more lift, and control surfaces become effective then, and aft motor output is not required. Consequently, front motors output characteristics become the same. Simulations results showed that both weighted pseudo inverse (WPI) and blended inverse (BI) transition responses are enough to hold system stable. During transition phase front motors' throttle outputs increase and aft motor's throttle output decreases gradually. Transition ends at 21 seconds and it may observed that during the transition phase both of the control allocation approaches hold the system almost at the same altitude as shown in Figure (5.20). Although WPI and BI response characteristics for theta command are different, system can hold the desired roll and yaw commands with some small variations for both approaches as shown in Figure (5.18).

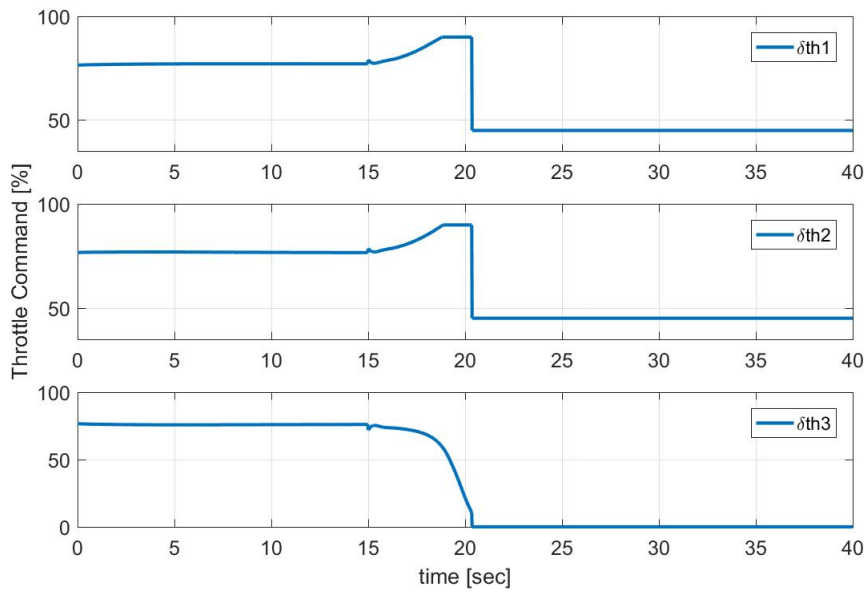


Figure 5.14: Throttle outputs - Weighted pseudo inverse allocation

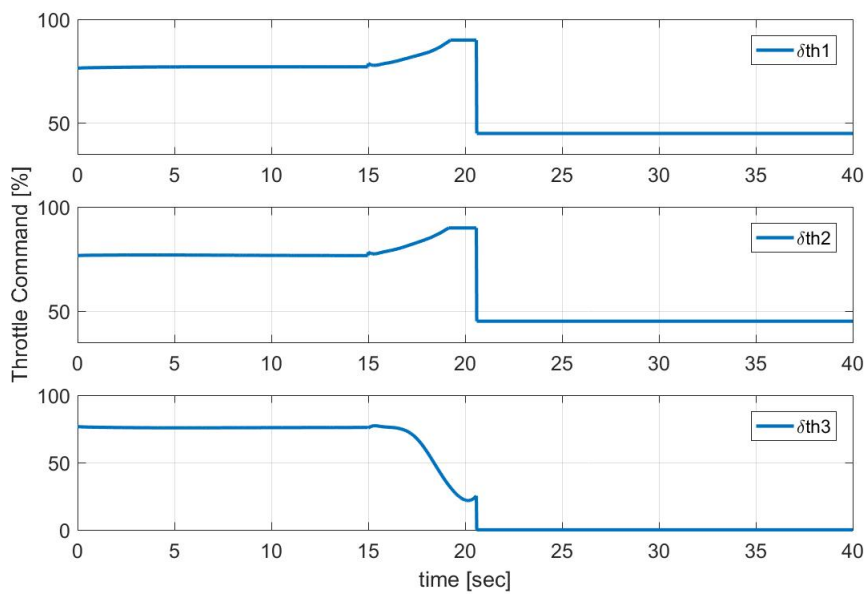


Figure 5.15: Throttle outputs - Blended inverse allocation

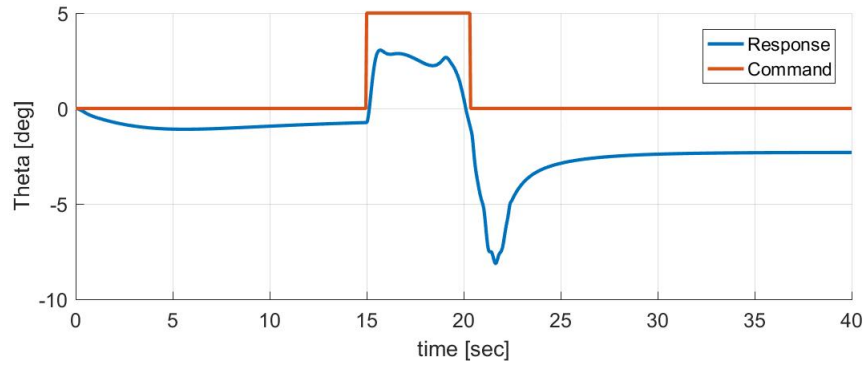


Figure 5.16: Theta Response - Weighed Pseudo Inverse allocation

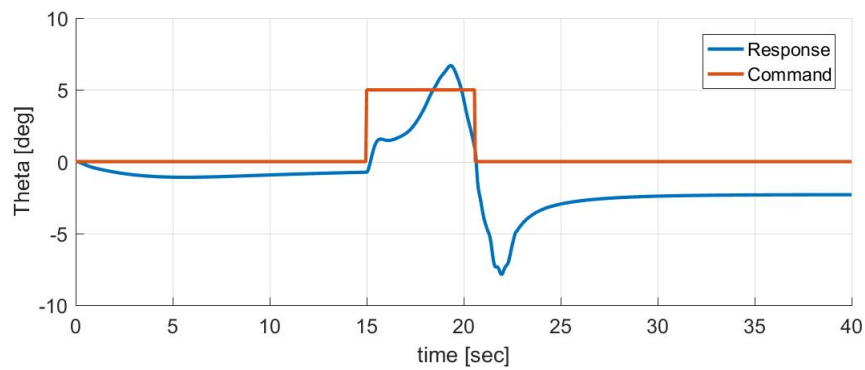
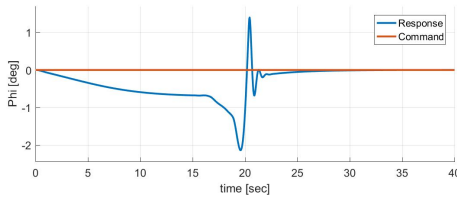
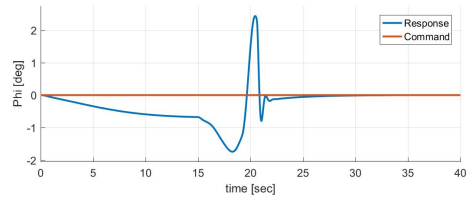


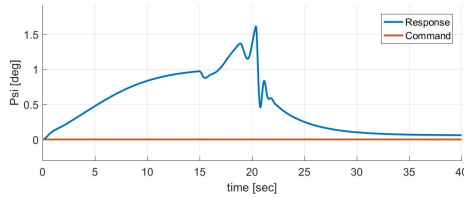
Figure 5.17: Theta Response - Blended Inverse allocation



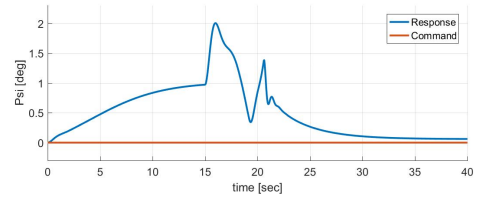
(a) Phi response - Weighted pseudo inverse allocation



(b) Phi response - Blended inverse allocation



(c) Psi response - Weighted pseudo inverse allocation



(d) Psi response - Blended inverse allocation

Figure 5.18: Commands and platform response histories for transition to forward flight attitude control phase

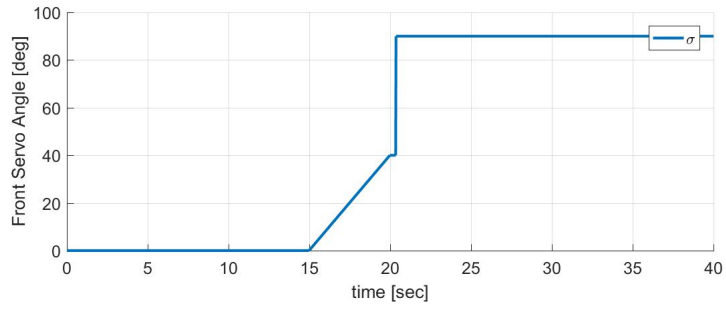
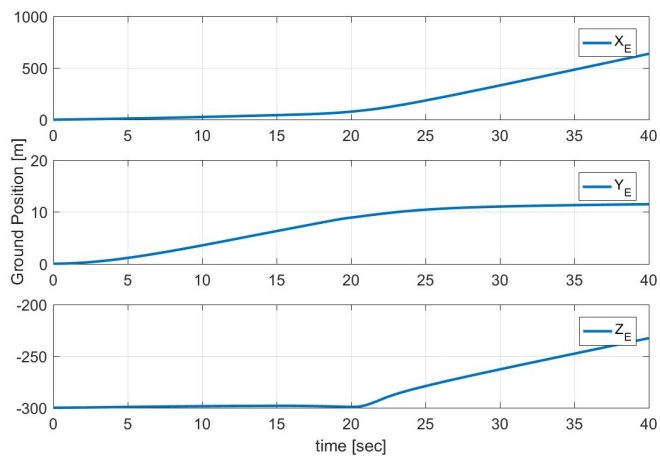
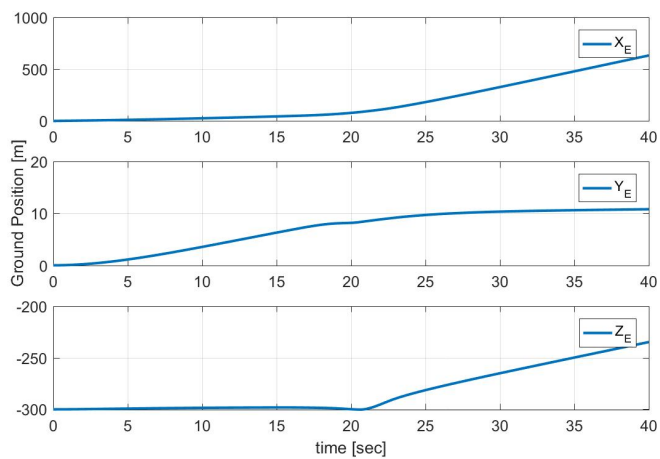


Figure 5.19: Front tilt servo command history during transition to forward flight attitude control phase

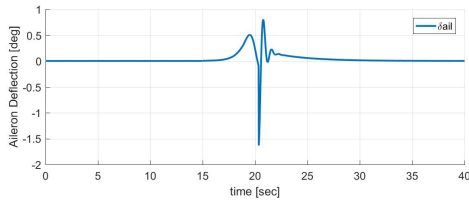


(a) Ground Position - Weighted pseudo inverse allocation

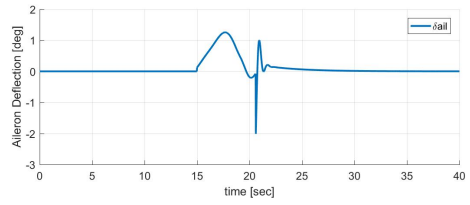


(b) Ground Position - Blended inverse allocation

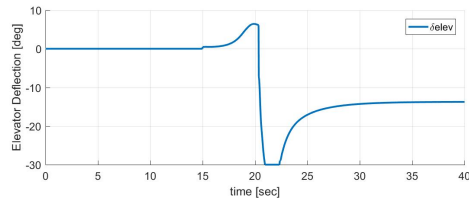
Figure 5.20: Ground position change histories for transition to forward flight attitude control phase



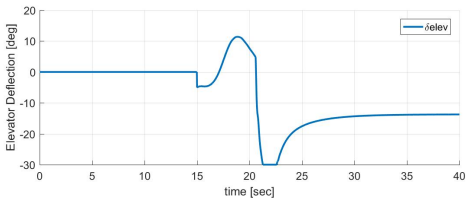
(a) Aileron command - Weighted pseudo inverse allocation



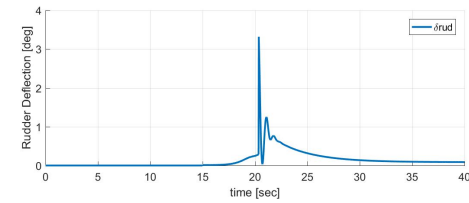
(b) Aileron command - Blended inverse allocation



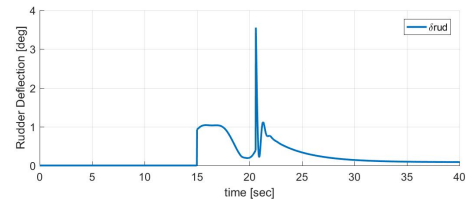
(c) Elevator command - Weighted pseudo inverse allocation



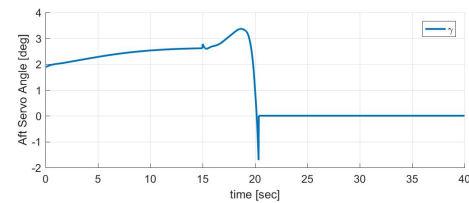
(d) Elevator command - Blended inverse allocation



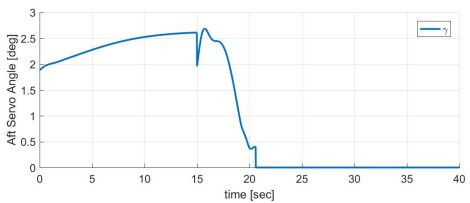
(e) Rudder command - Weighted pseudo inverse allocation



(f) Rudder command - Blended inverse allocation



(g) Aft servo command - Weighted pseudo inverse allocation



(h) Aft servo command - Blended inverse allocation

Figure 5.21: Actuator command histories for transition to forward flight attitude control phase

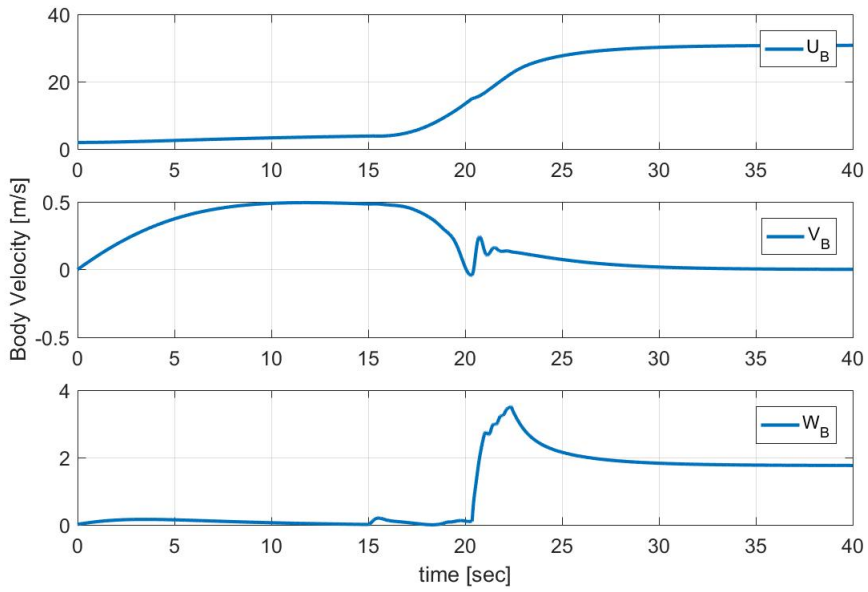


Figure 5.22: Body Velocities - Weighted pseudo inverse allocation

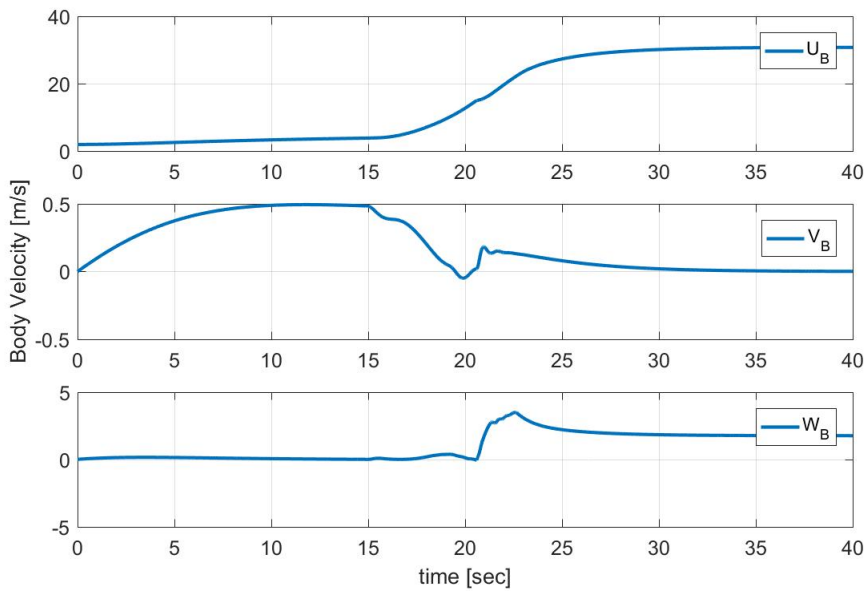


Figure 5.23: Body Velocities - Blended inverse allocation

5.6 VTOL Platform Forward Flight Control Simulations

Simulations are carried out in the forward flight mode for attitude commands. Figure (5.24), Figure (5.27) and Figure (5.30) shows attitude command and responses.

5.6.1 Roll Control

Attitude controller simulations are carried out for 15 [deg] roll command with 45% collective input where theta and yaw commands are zero. Response of the platform is given in Figure (5.24) for positive and negative roll commands. Simulation results show that aileron deflection command can hold system in desired state which is shown in the Figure (5.25). The success of the controller is evident in these simulations

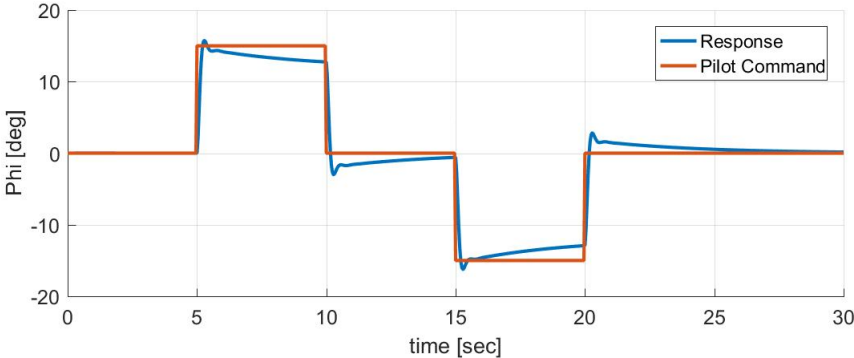


Figure 5.24: Roll command and roll angle response during forward flight

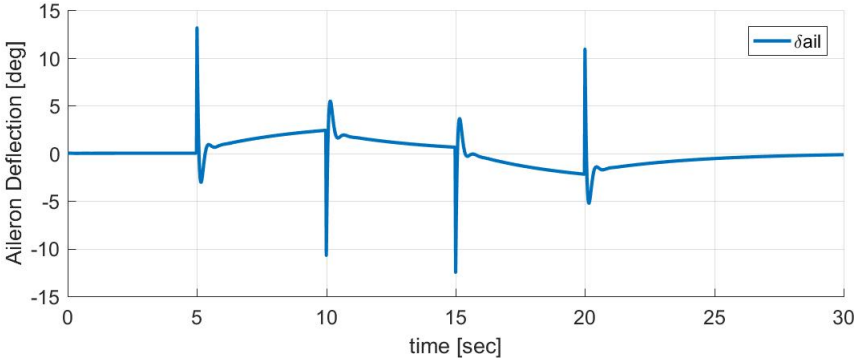
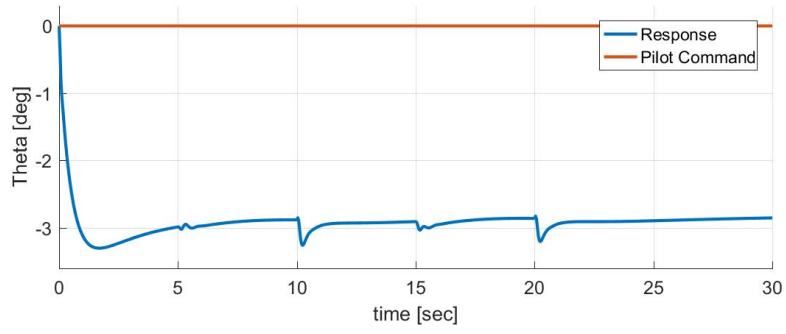
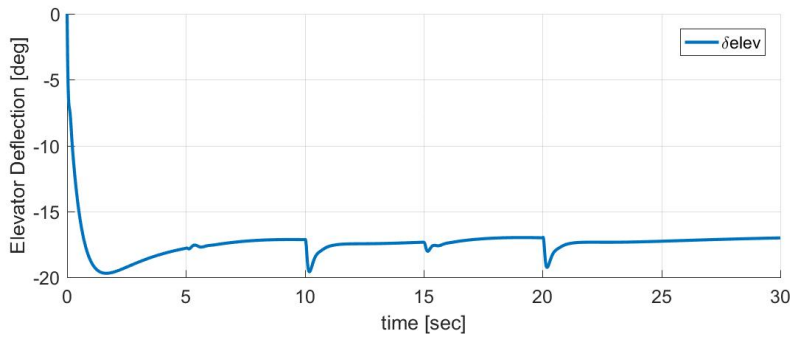


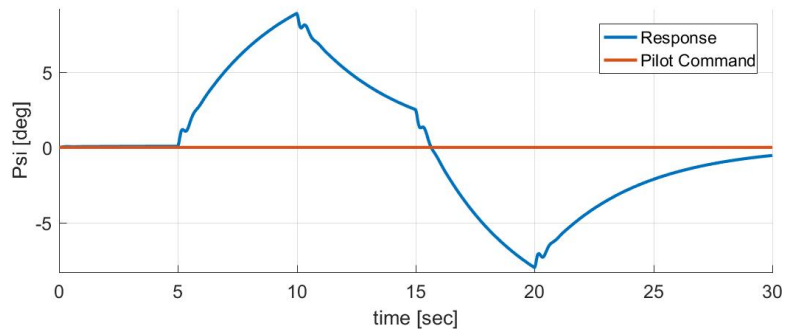
Figure 5.25: Aileron deflection command due to given roll command



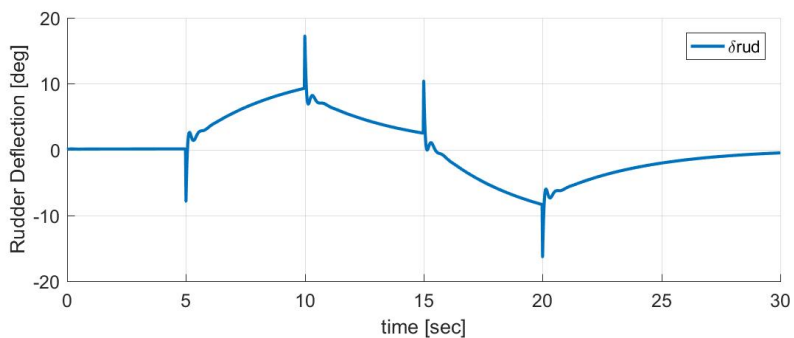
(a) LQT control result for given zero pitch command



(b) LQT control result for elevator deflection



(c) LQT control result for given zero yaw command



(d) LQT control result for rudder deflection

Figure 5.26: VTOL frame responses during 15 [deg] roll command in forward flight

5.6.2 Pitch Control

Attitude controller simulations are carried out for 15 [deg] pitch command with 45% collective input where roll and yaw commands are zero. Response of the platform is given in Figure (5.27) for positive and negative pitch commands. Simulation result shows that elevator deflection command can hold system in desired state with offset which is shown in the Figure (5.27).

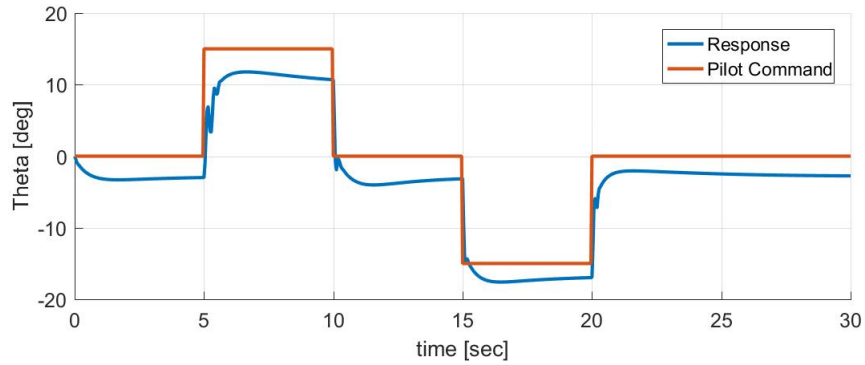


Figure 5.27: Pitch command and pitch angle response during forward flight

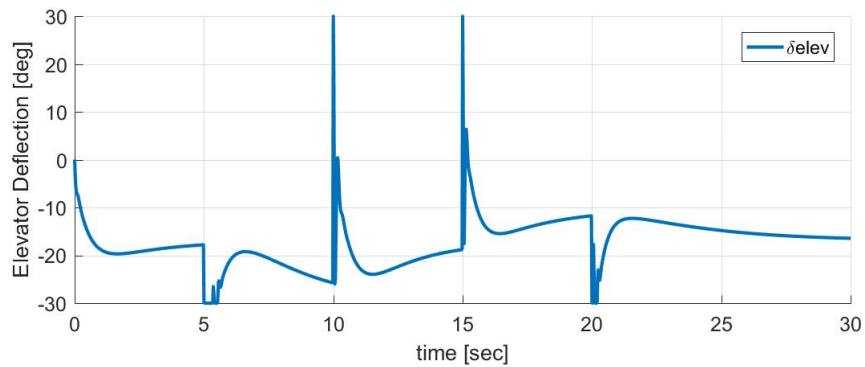
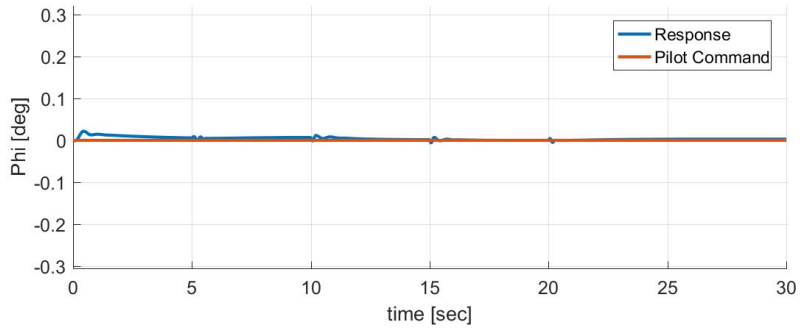
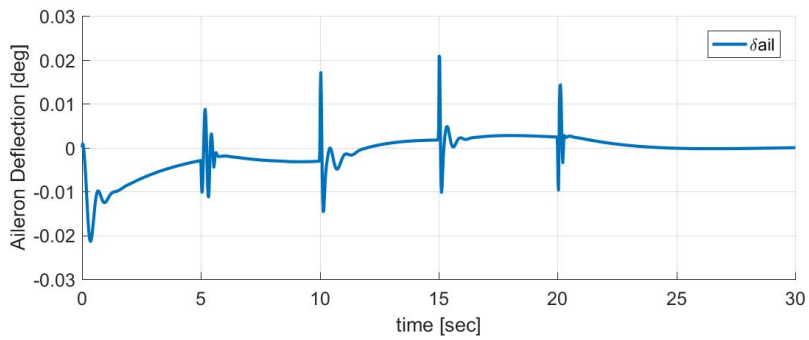


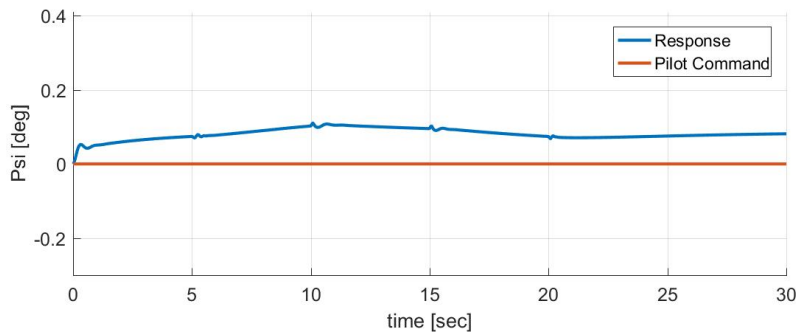
Figure 5.28: Elevator deflection command due to pitch command forward flight



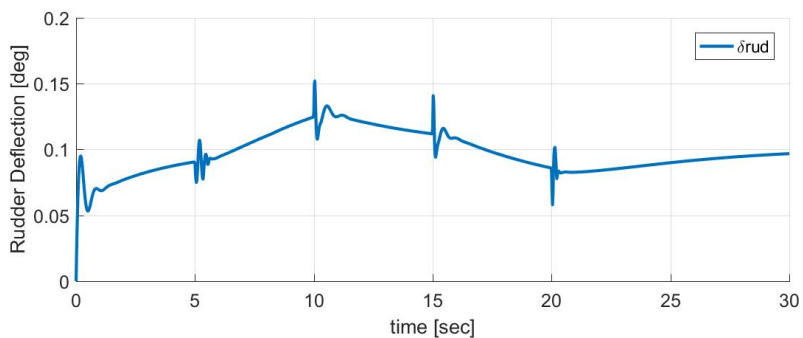
(a) LQT control result for given zero roll command



(b) LQT control result for aileron deflection



(c) LQT control result for given zero yaw command



(d) LQT control result for rudder deflection

Figure 5.29: VTOL frame responses during 15 [deg] pitch command in forward flight

5.6.3 Yaw Control

Attitude controller simulations are carried out for yaw commands where roll and yaw commands are zero. Response of the platform is given in Figure (5.30) for yaw command gradually increasing to 50 degrees with 45% collective input. Simulation result shows that rudder deflection command can follow desired state

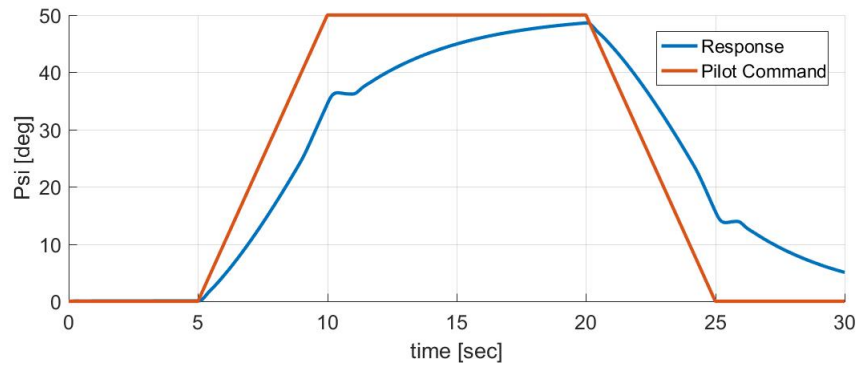


Figure 5.30: Yaw command and yaw angle response during forward flight

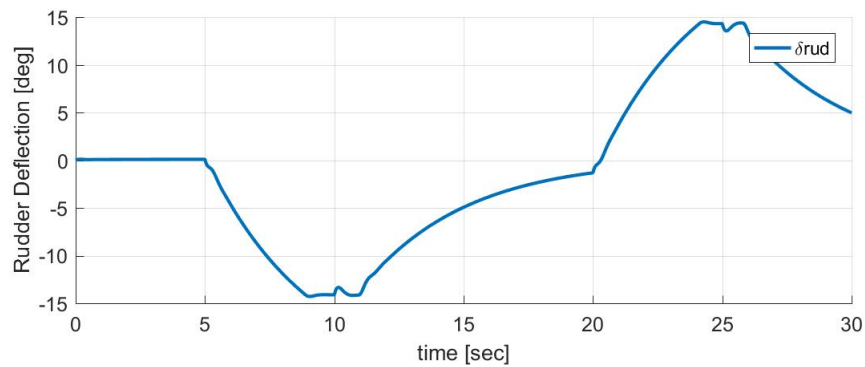
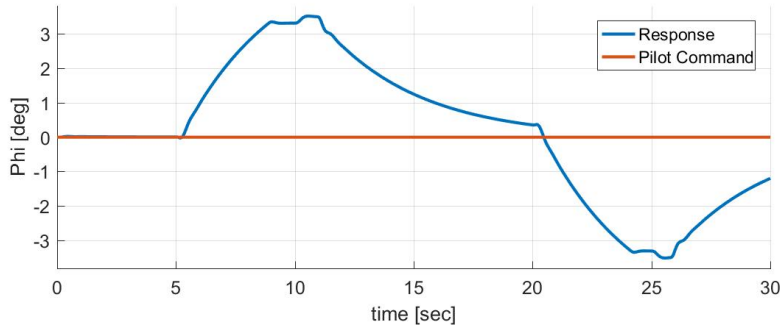
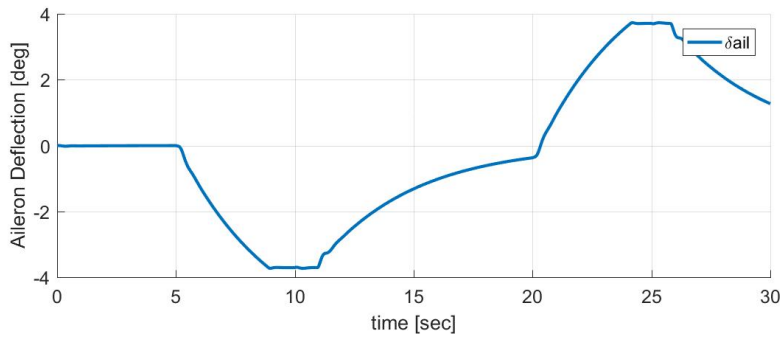


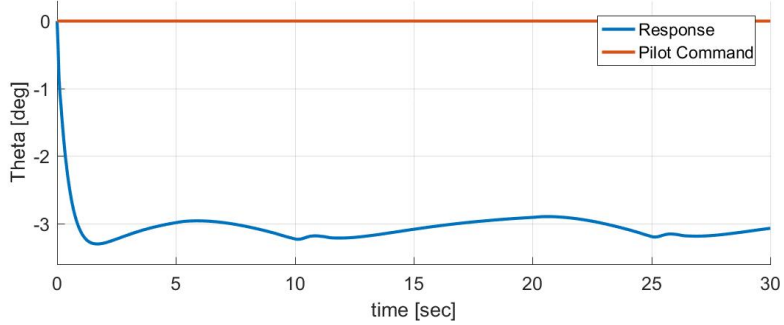
Figure 5.31: Rudder deflection command due to yaw command during forward flight



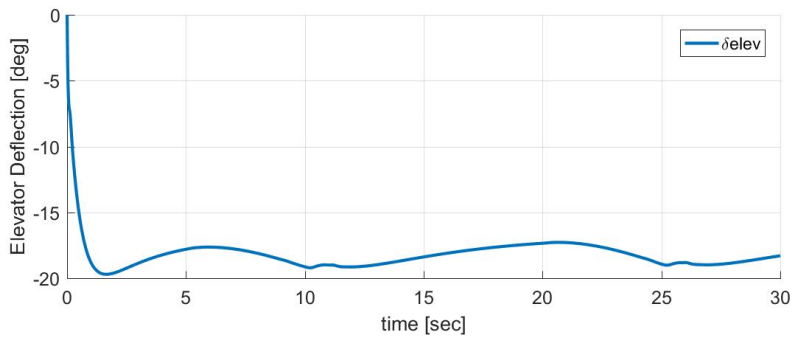
(a) LQT control result for given zero roll command



(b) LQT control result for aileron deflection



(c) LQT control result for given zero pitch command



(d) LQT control result for rudder deflection

Figure 5.32: VTOL frame responses during heading commands in forward flight

5.7 VTOL Platform Transition to Tri-coper Mode Attitude Control Simulations

5.7.1 Transition Control

Forward flight transition is controlled by given gradually increasing pitch command from current reference to 45 [deg]. The reason to give positive gradually increasing pitch command is to decrease speed, since the system is controlled only by attitude controller. This command directs the system to lose lift and airspeed while it tries to hold pitch command.

Transition pulse is triggered at 15 seconds and during transition front motors tilt from horizontal position, $\sigma = 90$ [deg] to $\sigma = 30$ [deg] as specific in flight management tricopter mode in Figure (4.7). Transition has two phases. First phase involves front tilt range from $\sigma = 90$ [deg] to $\sigma = 50$ [deg]. At this phase forward flight controller is still active and it tries to sustain attitude commands. Front motors produce same amount of throttle output, control surface deflections are active, and aft motor and aft tilt servo are inactive. Second phase starts when front tilt reaches to $\sigma = 50$ [deg] and control allocation is activated. Aft motor and aft tilt servo becomes also active in this phase. Front tilt servo continues to tilt to $\sigma = 30$ [deg]. Tricopter mode attitude control becomes active when transition phase ends, such that airspeed of the system decreases below 15 [m/s]. Observation may be made from the results that as the system loses speed while controller tries to hold platform at desired pitch attitude, elevator deflection command decreases as shown in Figure (5.40). Simulations results showed that both weighted pseudo inverse (WPI) and blended inverse (BI) transition responses are enough to hold system stable. During the second phase front motors' and aft motor's throttle outputs increase. Control allocation starts at 22 seconds and it may observed that during the transition phase both of the control allocation approaches leads system to gain altitude as shown in Figure (5.39). WPI and BI response characteristics for theta command are similar, but BI performs smoother theta response as it may be seen comparing Figure (5.35) with Figure (5.36). Beside that, system can hold the desired roll and yaw commands with some small variations for both approaches as shown in Figure (5.37). Another difference is that aft mo-

tor's throttle output gradually increases in BI control allocation, whereas WPI control allocation starts with sudden increment in aft motor's throttle output.

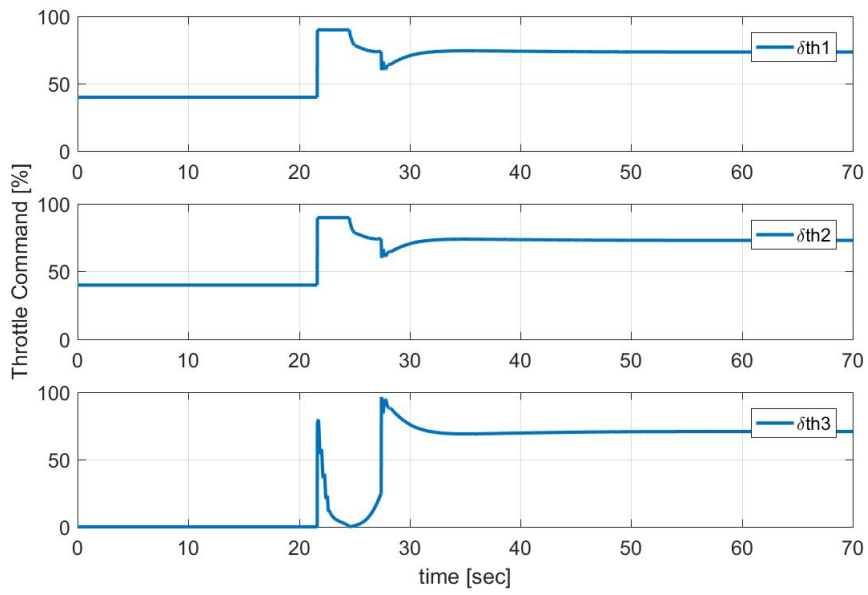


Figure 5.33: Throttle outputs - Weighted pseudo inverse allocation

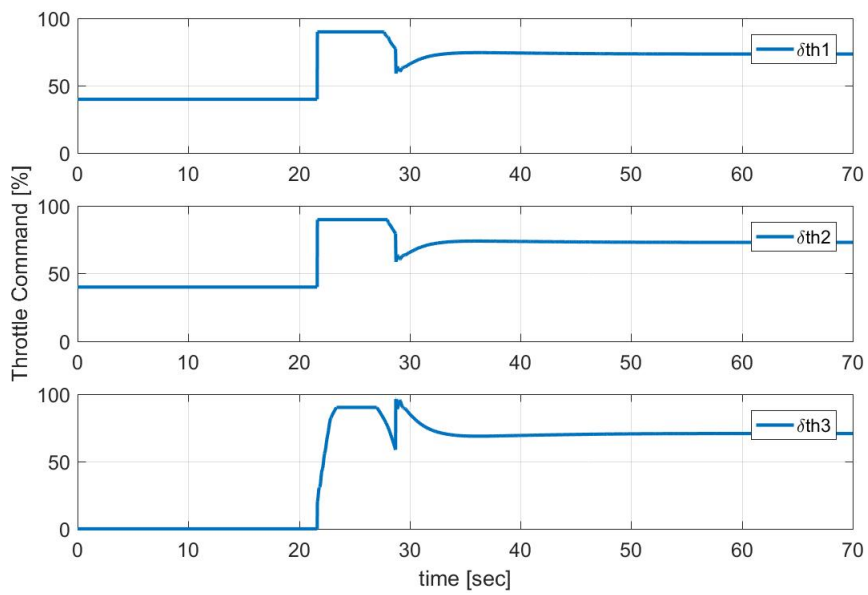


Figure 5.34: Throttle outputs - Blended inverse allocation

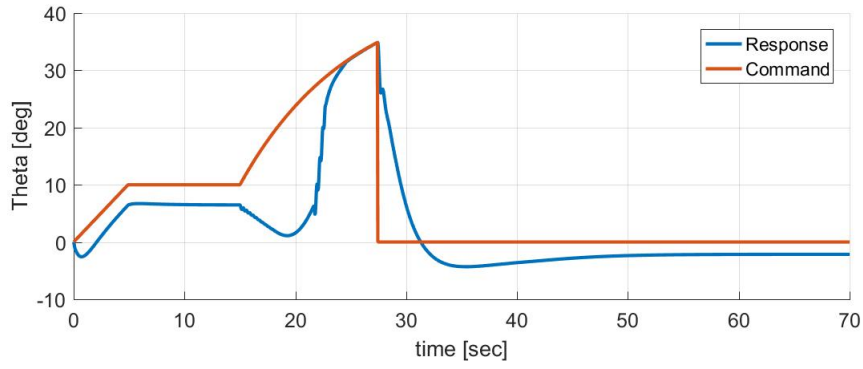


Figure 5.35: Theta Response - Weighed Pseudo Inverse allocation

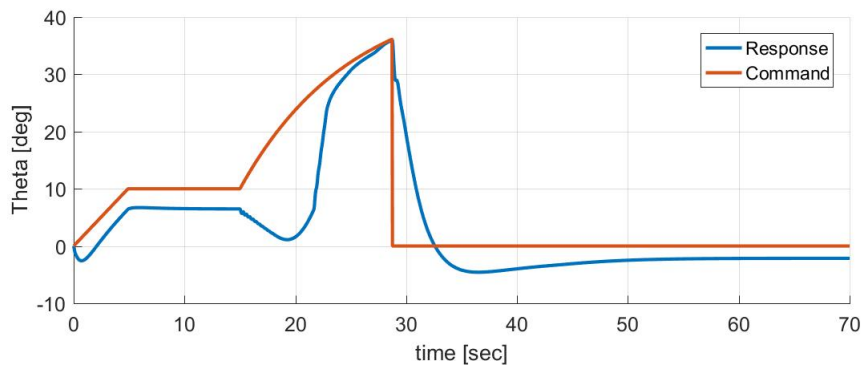
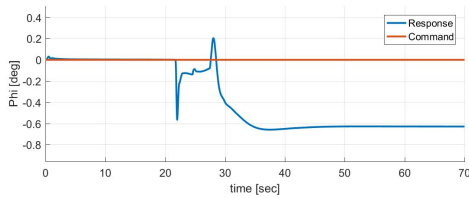
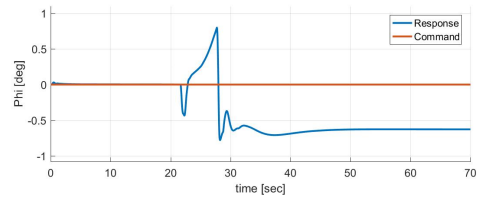


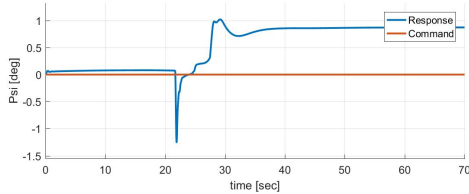
Figure 5.36: Theta Response - Blended Inverse allocation



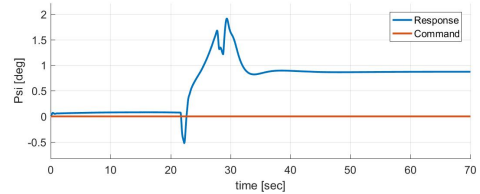
(a) Phi response - Weighted pseudo inverse allocation



(b) Phi response - Blended inverse allocation



(c) Psi response - Weighted pseudo inverse allocation



(d) Psi response - Blended inverse allocation

Figure 5.37: Commands and platform response histories for transition to tricopter attitude control phase

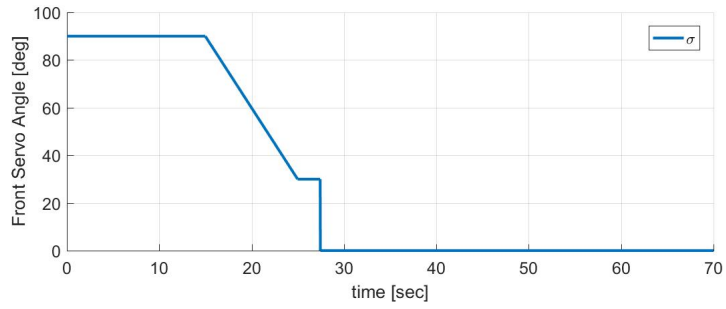
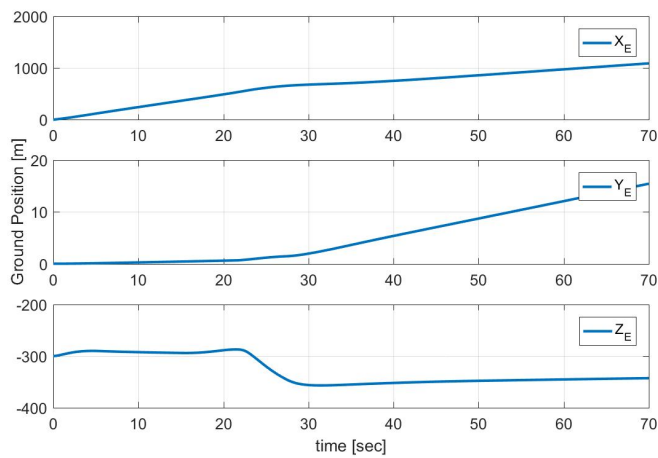
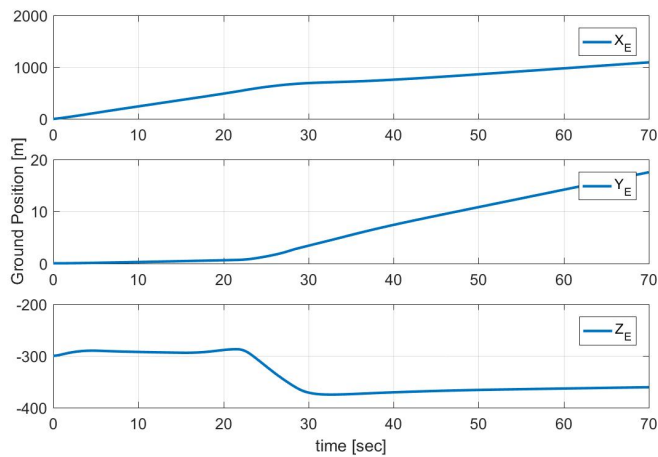


Figure 5.38: Front tilt servo command history during transition to tricopter attitude control phase

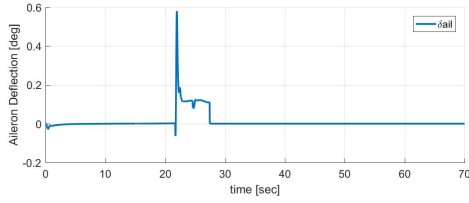


(a) Ground Position - Weighted pseudo inverse allocation

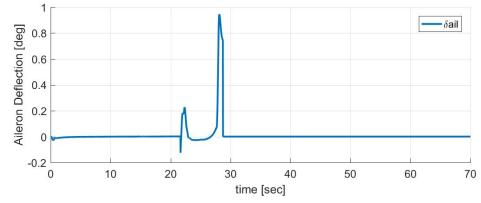


(b) Ground Position - Blended inverse allocation

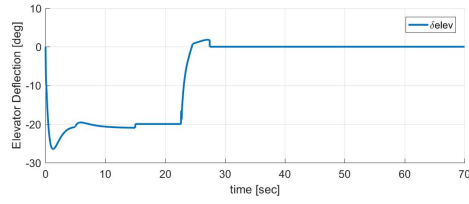
Figure 5.39: Ground position change histories for transition to tri-coper mode attitude control phase



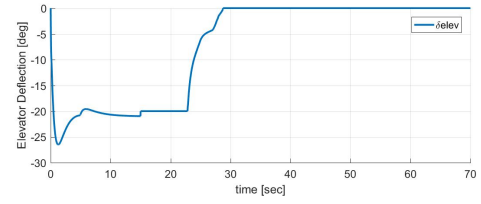
(a) Aileron command - Weighted pseudo inverse allocation



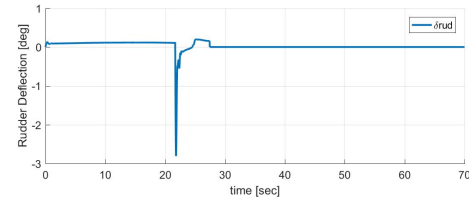
(b) Aileron command - Blended inverse allocation



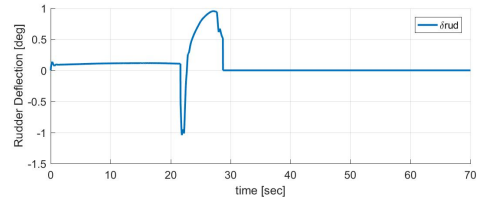
(c) Elevator command - Weighted pseudo inverse allocation



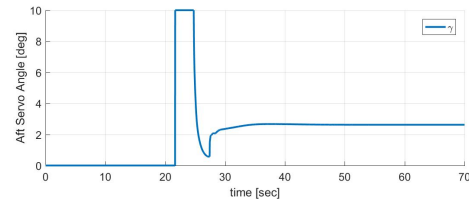
(d) Elevator command - Blended inverse allocation



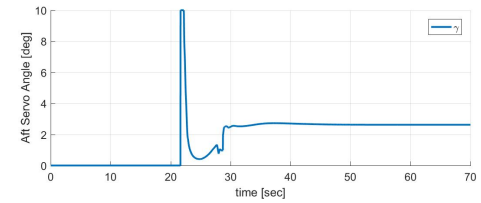
(e) Rudder command - Weighted pseudo inverse allocation



(f) Rudder command - Blended inverse allocation



(g) Aft servo command - Weighted pseudo inverse allocation



(h) Aft servo command - Blended inverse allocation

Figure 5.40: Actuator command histories for transition to tricopter attitude control phase

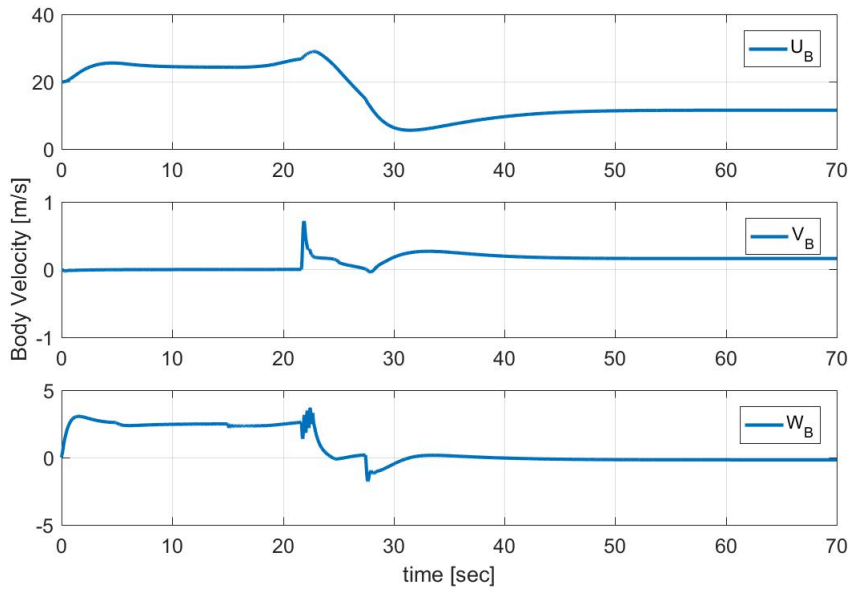


Figure 5.41: Body Velocities - Weighted pseudo inverse allocation

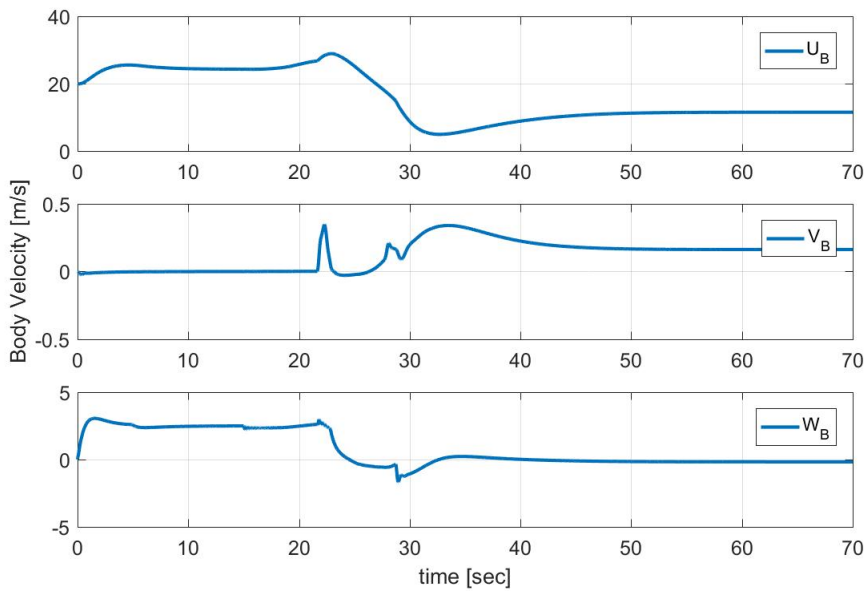


Figure 5.42: Body Velocities - Blended inverse allocation

CHAPTER 6

HARDWARE COMPONENTS AND SOFTWARE ENVIRONMENT

6.1 Avionics

This chapter presents the avionic hardware and software components that are used to build up the tilt-rotor tricopter VTOL platform during thesis studies. Development platform is chosen for autopilot implementation is Pixhawk 2.1 board. Platform provides shared libraries that include sensor drivers, attitude and position estimation and controllers. Software components are modular and provide flexibility for changes. For the scope of this thesis, motor library is changed and controller libraries are removed to implement LQT controller. GPS module is used for correction and calibration of position, velocity and angular orientation with the use of filter libraries. Pixhawk board drives front and aft motors via ESCs, tilt and control surface servos. Board takes pilot control commands to control vehicle movement (throttle, yaw, pitch, roll and safety-switch) and flight mode control (transition between tricopter and plane modes) via receiver. Thus, it communicates with ground control station through telemetry to observe flight data. Detailed information about hardware and software components will explained in the following sections. General scheme of avionic setup is shown in Figure (6.1).

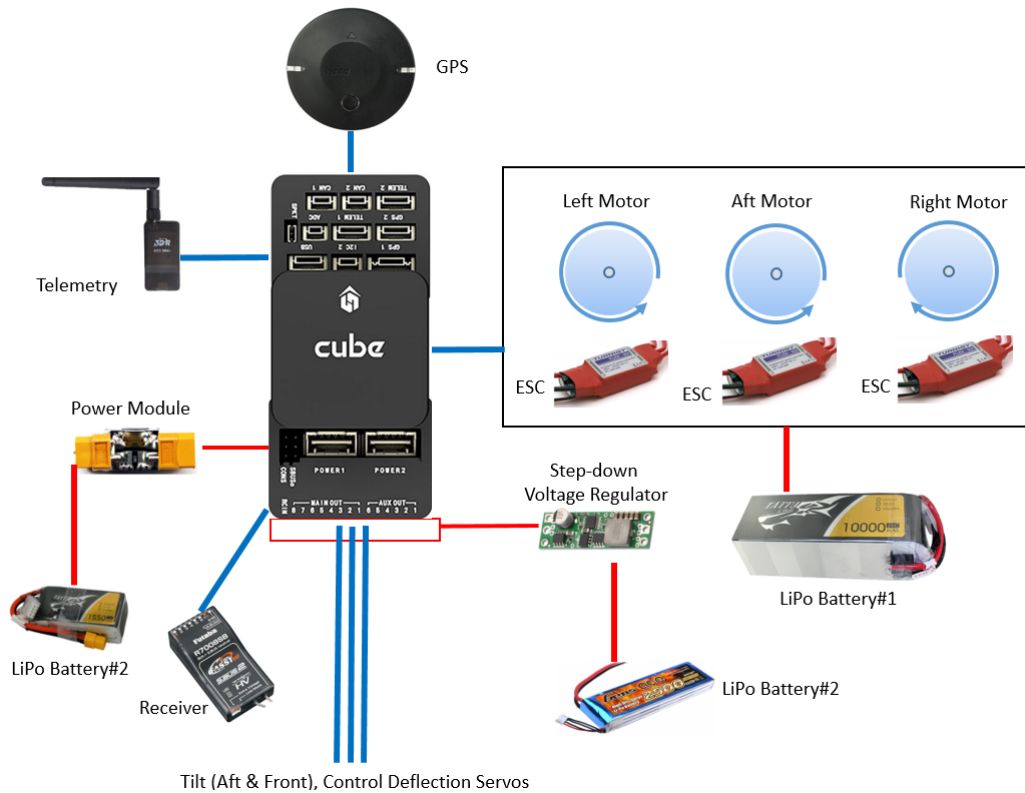


Figure 6.1: Avionic Setup

6.1.1 Autopilot Platform

Pixhawk 2.1 is an open hardware project that it is aimed to provide hardware environment for developers, academics and industry with low costs sustaining many peripheral support [29]. It is shown in Figure (6.2).



Figure 6.2: Pixhawk board

Pixhawk 2.1 is using 32bit STM32 Cortex MF4 core with 168MHZ clock frequency. It has Floating Point Unit (FPU) such that complex trigonometric algorithms can

be handled without latency. On-board 2MB flash stores configuration parameters, mission database and logger data. Board has 256 KB RAM such that it gives enough space for programme variables and temporary data.

Power module is triple redundant such that it can be supplied from power module input, servo pinout port and USB port at the same time. Thus, its operating range is limited 4.8V to 5.4V.

Pixhawk 2.1 has a gyroscope, accelerometer - magnetometer, barometric pressure sensor and additional 3-axis gyroscope-accelerometer. ST Micro L3GD20H gyroscope can measure three-axis angular rate with 16 bit resolution and it consumes low power and it is resistant to high shocks. ST Micro LSM303D accelerometer/magnetometer can measure 3D linear motion and magnetic field with 16 bit resolution. MEAS MS5611 is barometer with a 24 bit resolution. Barometric pressure sensor has augmented precision capability for measurements with 10 [cm] resolution. InvenSense MPU 6000 is a motion tracking system with three axis accelerometer and three axis gyroscope. Besides its internal sensors, it accepts external three-axis magnetometer data which enable on-board fusion. It can track both fast and slow motions precisely.

System has hardware interfaces to communicate with external sources ,such as sensors, receiver, servos and telemetry. It has a support for serial bus communication (SBUS) using one channel for receiver that comes from user stick commands. Moreover, this can also be accomplished by using external PPM encoder which is used to convert multiple PWM inputs into one PPM signal. For serial communication, five UART ports and additionally I2C and SPI ports exist. Analogue input port can be fed from 3.3V up to 6.6V.

6.1.2 Telemetry

Communication between tricopter and ground control is implemented using telemetry. There are several approaches to do data transmission, such as radio, satellite and GSM/LTE modems. Among these, 3DR - 433 MHz radio modem set is chosen, since its performance is accepted and it is an affordable solution. There are two units in a

set, one for ground and one for air platform, both can be replaceable for each others role. They allow wireless transfer such that operator monitors and ground control software logs flight data from tricopter and operator can send tuning commands. Air modem connects to Pixhawk via UART port.

6.1.3 GPS Module

Global positioning system is a satellite aided radio navigation system which provides estimated real world location of a receiver. Location is commonly referred as latitude, longitude and elevation. System works independently without requiring any request of data. Here+ NEO-M8N GPS and compass module are chosen since it is configured for multi-rotor and fixed-wing platforms. It is shown in Figure (6.3). It is critical



Figure 6.3: GPS+Mag module

for autopilot to control heading, such that receiving clean signal from source is important. Board has HMC5883l compass which is designed to measure both direction and magnitude of magnetic fields with accuracy of 1° to 2° , which is well enough for reference input. Compass is mounted on GPS board, and module is placed closer to front shaft, so that it is away both from other electronic sources and blades which generate magnetic and spinning interferences respectively. Position and magnetic direction obtained from GPS module are used as parameter input to Extended Kalman Filter(EKF) algorithm sustained by autopilot software to estimate position, velocity and attitude of tricopter additional to on board sensors.

6.2 Software Development Environment and Architecture

Ardupilot is a ready to fly, open source autopilot system [2]. It has been developed for years by growing society. It has a wide range of application areas varying from helicopter, multicopters, planes, boats, ground vehicles and submarines. It is compatible with Pixhawk hardware. With many peripheral support, many sensors can be integrated as plug-in and use method. Besides its autopilot code, ground control station software is also open source, such that desired functionality may be edited to both autopilot and ground control station code to work as it is intended. APM Copter-3.5.0 stable version is used development for activities.

Autopilot code is written in C++, and development environment is QT Creator IDE. QT Creator is a cross platform development kit to develop applications for embedded, desktop, and mobile systems [35]. To build the code necessary environment variables are linked. Ardupilot code is imported to the IDE and ArduCopter module is selected as an active working platform. The code with classes related to arming, channel assignment, parameter configuration is modified for VTOL platform. Attitude Controllers are written in *UserCode.cpp* file and its functions are decelerated in *Copter.h*. All the previous control algorithms are removed. Similar to Matlab/Simulink model running frequency, controller function is added to run for 50Hz. Main motor class *AP_Motor.cpp*, is modified and new derived class *AP_MotorsVTOL.cpp* is added. Motor class function is designed just to drive servos and ESCs. Channel assignments are selected to control platform both for tricopter mode using there motors and aft angle control, and for forward flight mode using front motors, wing deflection surface servos. Transition from tricopter attitude control to level flight mode is implemented by additional front tilt servo output. Channel parameter values assigned directly from *UserCode.cpp*, controller outputs scaled to valid PWM range and updated with main function call.

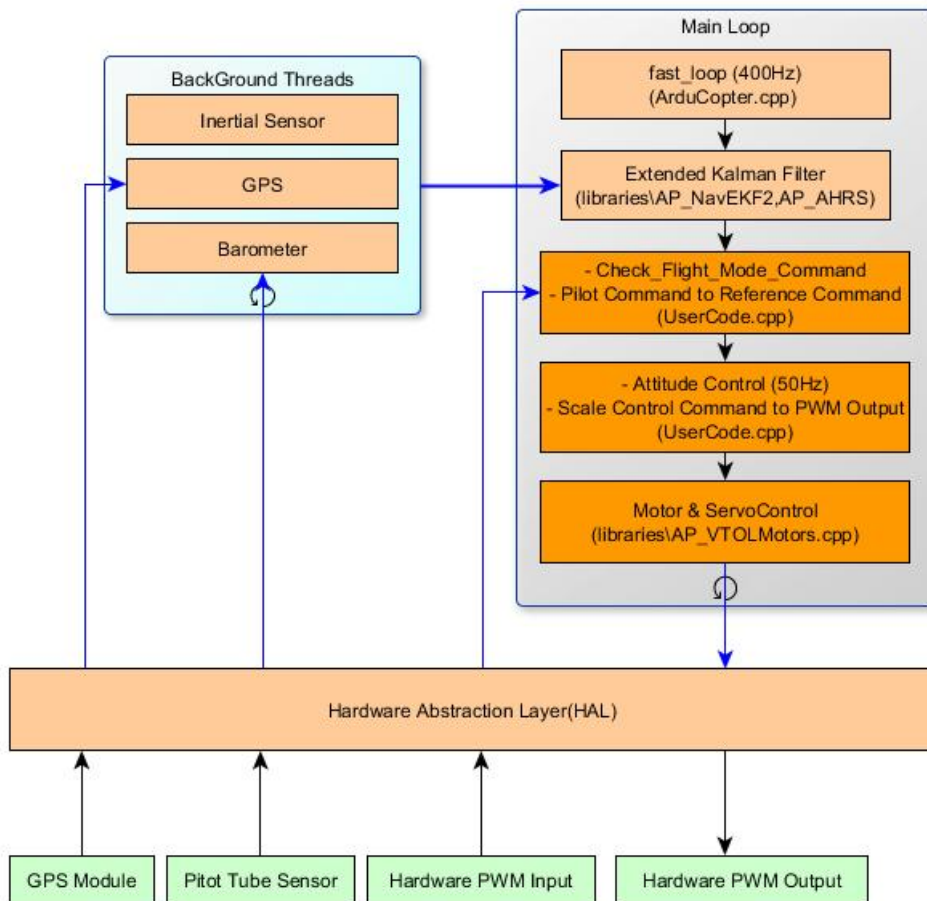


Figure 6.4: Pixhawk board

CHAPTER 7

SYSTEM CONFIGURATION TESTS

7.1 Introduction

In Chapter 5, simulation results are represented. In Chapter 6, avionics are defined and software approach for design is presented. According to simulation results, controller gains are embedded with developed codes. Prior to the flight tests, laboratory experiments are performed to test and validate the simulation results. Tests for tri-copter and dummy-wing configurations are carried out using telescopic bars of which are hanging from ceiling and attached to the CG of the configuration. Controller gains in simulation environment tuned after recorded data evaluation. Flight tests are performed after sufficient performance is demonstrated in the laboratory.

7.2 Lab Tests and Results

Test setup in laboratory environment is employed by telescopic bars hanging from ceiling and it is assisted with a metal cable that is attached to the CG of the frame. This setup helps to observe the controller outputs with varying throttle command inputs and platform reaction according to given inputs. It helps for tuning the controller gains and avoided possible harm to platform. Telescopic bars are assisted with metal cable suspended enables platform to swing freely, so that all attitude control inputs to throttle outputs can be observed. Dummy-Wing solution is emerged from the concern that VTOL frame can not be tested in laboratory environment due to the fact that the wing can be broken in trials and movement of free-swing effect can not be sustained due to wing sizing.

7.2.1 Tricopter Lab Tests

The controller gains verified through simulations are hard-coded to Pixhawk micro-controller to validate the simulation results. Test is started after steady condition for free hanging state is sustained. Thus, test data is evaluated after platform gained enough lift to carry out attitude commands. Pilot input throttle command is shown in Figure (7.5). Attitude commands and throttle command are given through RC Transmitter to observe reaction of tricopter platform.

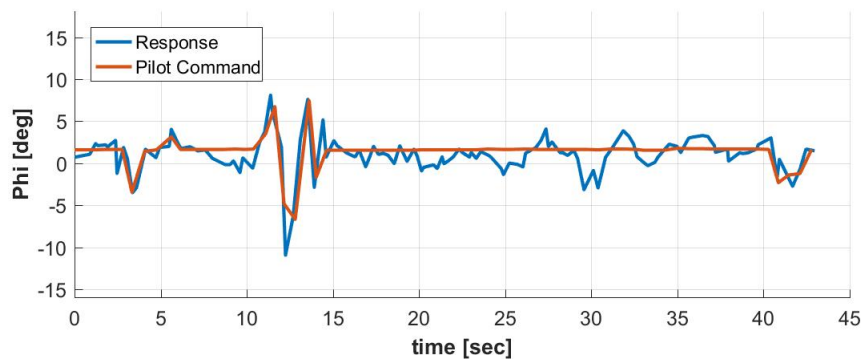


Figure 7.1: Tricopter lab test result for the given roll command



Figure 7.2: Tricopter lab test photo

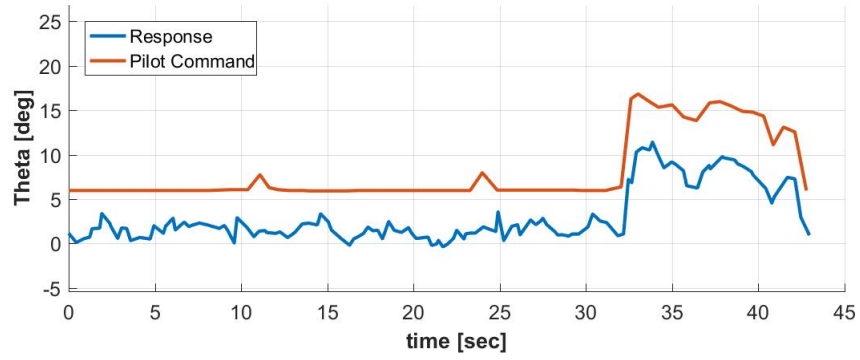


Figure 7.3: Tricopter lab test result for the given theta command

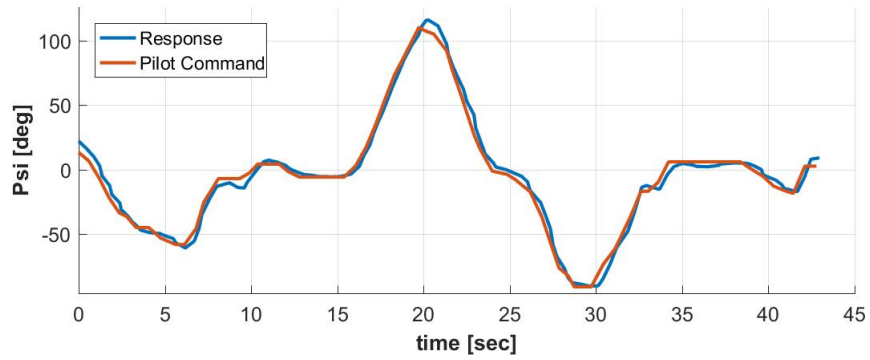


Figure 7.4: Tricopter lab test result for the given yaw command

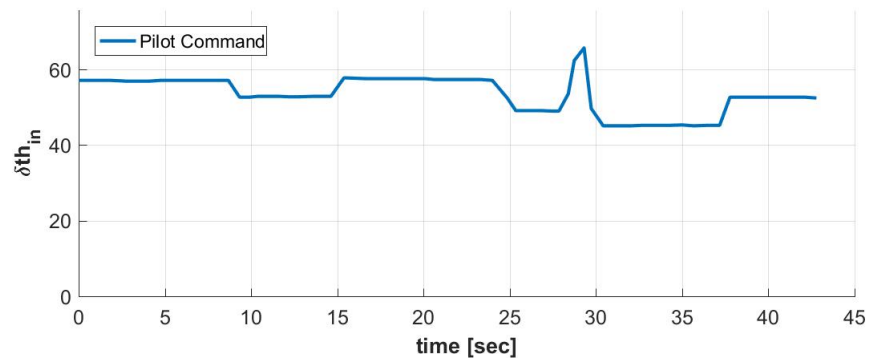


Figure 7.5: Tricopter lab test - throttle input command

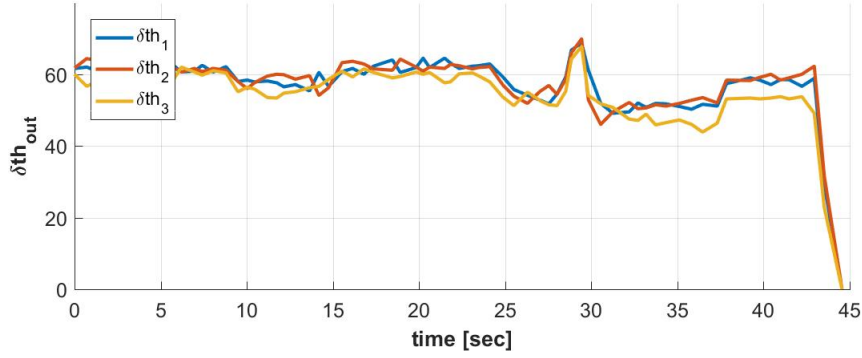


Figure 7.6: Tricopter lab test throttle responses of motors

The platform responses are shown in Figure (7.1), Figure (7.3), and Figure (7.4). Platform throttle responses relative to given pilot commands are shown in Figure (7.6). Test results show that the pilot commands are followed by the platform and the idle state commands for roll and pitch commands followed by the controller as steady state reference. Heading command for idle input state can be observed from test results that platform retains its current heading.

7.2.2 Dummy-Wing VTOL Configuration Lab Tests

In order to test the VTOL configuration for safe conditions, dummy-wing is designed with same inertia properties as the flying wing. Dummy-wing dimensions are calculated according to base XPS material and carbon tube specifications [24]. Carbon tube is used as a backbone to attach the dummy-wing to the tricopter frame and increases the strength of XPS prism. Function is derived from inertia of the wing, maximum and minimum limitation in dimensions for XPS and length for carbon tube are defined. Additional mass required to meet the inertia properties of wing is also calculated. Wheel balance weights are used for additional mass and located to the edges of XPS as function outcome indicated. Dummy-wing is located to point where CG of wing should be. Thus, wing inertia is moved to CG of tricopter frame, which is also the point where aerodynamic forces acting on the wing, by using parallel-axis theorem. Detailed information about dummy-wing calculations can be found in Appendix-B. Before trying the VTOL tricopter mode attitude control flight, it is required to validate calculations and simulation results. Tests are carried out with freely

swinging configuration in the laboratory environment.



Figure 7.7: Dummy-Wing configuration lab test photo

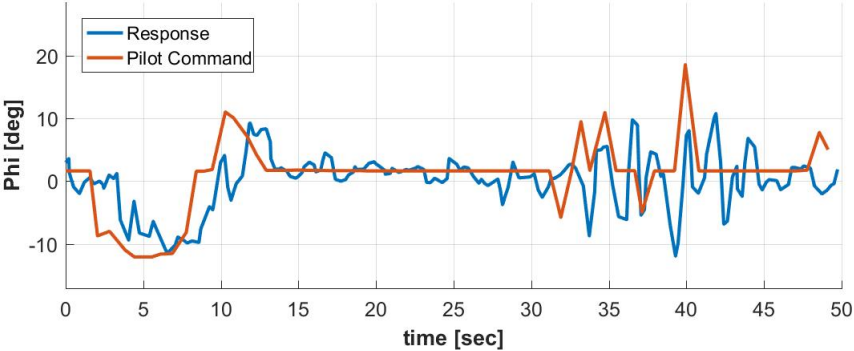


Figure 7.8: Dummy-Wing configuration lab test result for the given roll command

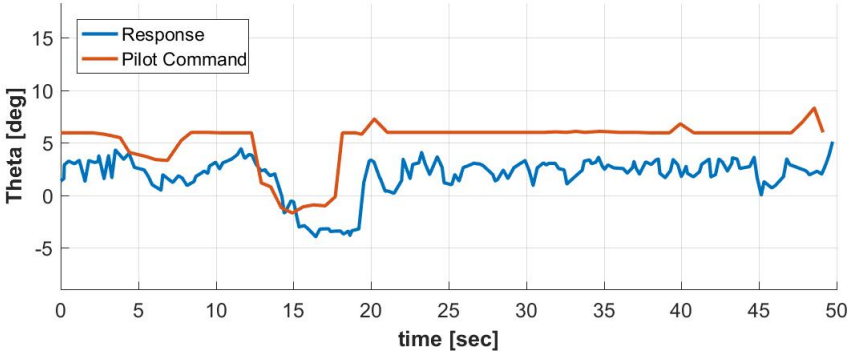


Figure 7.9: Dummy-Wing configuration lab test result for the given theta command

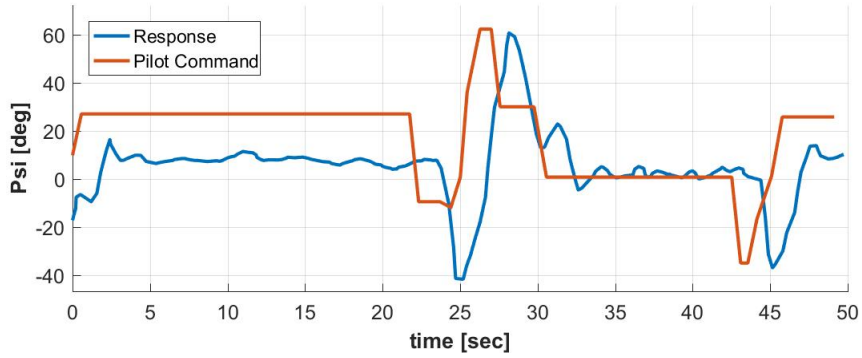


Figure 7.10: Dummy-Wing configuration lab test result for the given yaw command

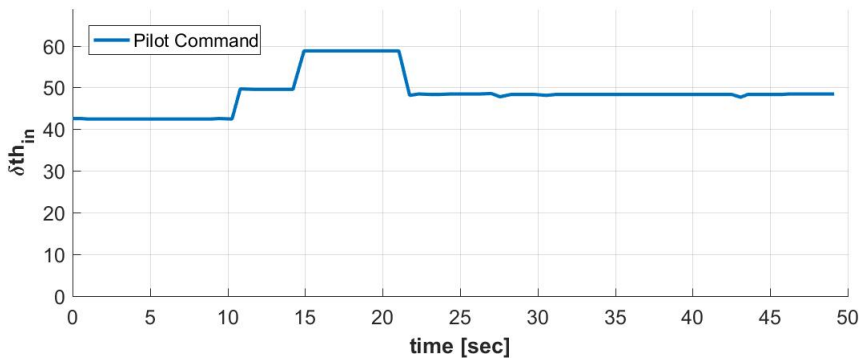


Figure 7.11: Dummy-Wing configuration lab test - throttle input command

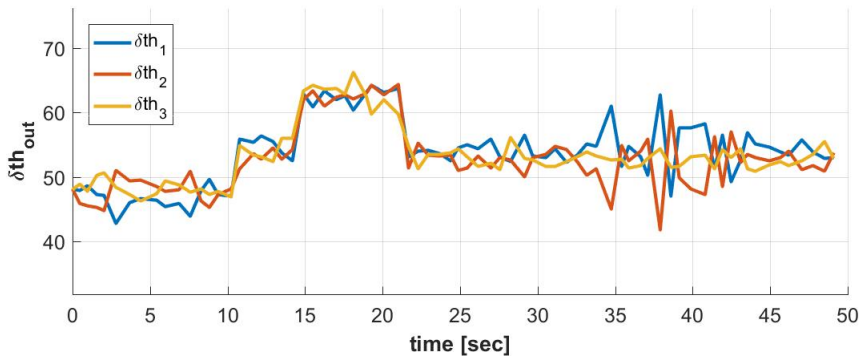


Figure 7.12: Dummy-Wing configuration lab test - throttle responses of motors

The platform responses are shown in Figure (7.8), Figure (7.10), and Figure (7.10). Pilot input throttle command is shown in Figure (7.11) and platform motor outputs relative to given pilot commands are shown in Figure (7.12). During the lab tests, it is observed that dummy-wing configuration is oscillating independent from main

frame especially against counter input commands. It may be due to the increment of mass and effect of wing inertia at the aft frame which causes twisting like movements at back. These effects can be observed most likely in the roll commands in Figure (7.8) between 37[sec] and 43[sec] duration. Beside these results, it is observed that dummy-wing configuration gives enough information about handling capabilities of VTOL configuration, such that flight tests can be performed. Dummy-wing configuration flight tests are also performed but due to reactive effect of dummy-wing, it is decided to move on VTOL configuration for flight tests, since both lab and flight tests give enough confidence that controller performs as intended.

7.3 Flight Tests and Results

Flight tests are performed with the same platform configurations and validated controller gains that are used in laboratory tests. In the following sections tricopter and VTOL configurations' flight results can be examined.

7.3.1 Tricopter Flight Tests

Tricopter frame is tested outside covering all control commands. It is observed during the flight that pilot commands are followed easily by the system, and the pilot stated that it is agile. Flight log is examined to confirm the flight observation.



Figure 7.13: Tricopter flight test photo

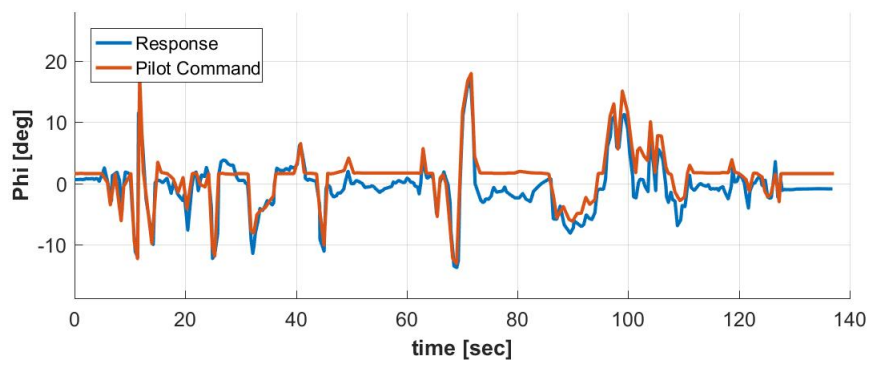


Figure 7.14: Tricopter flight test result for the given roll command

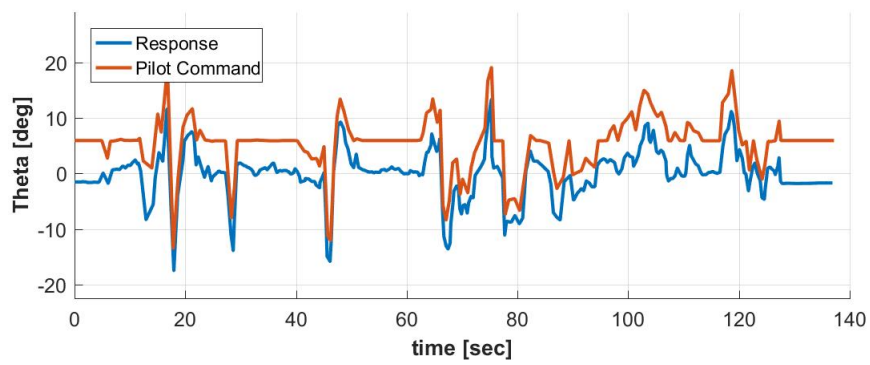


Figure 7.15: Tricopter flight test result for the given theta command

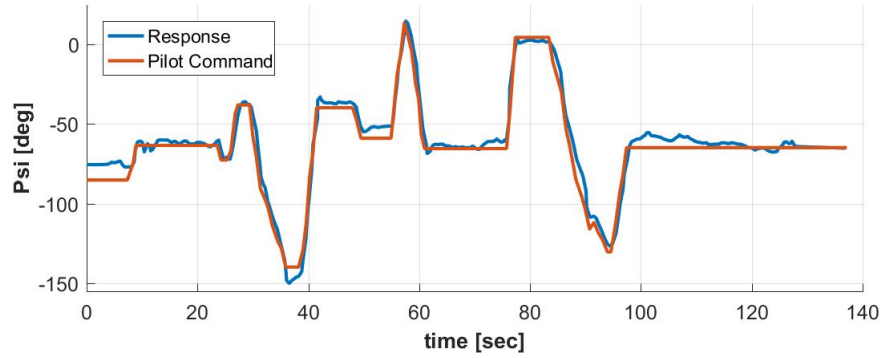


Figure 7.16: Tricopter flight test result for the given yaw command

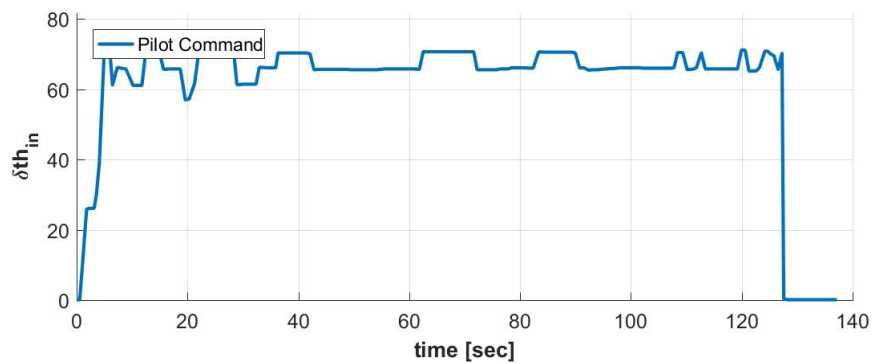


Figure 7.17: Tricopter flight test - throttle input command

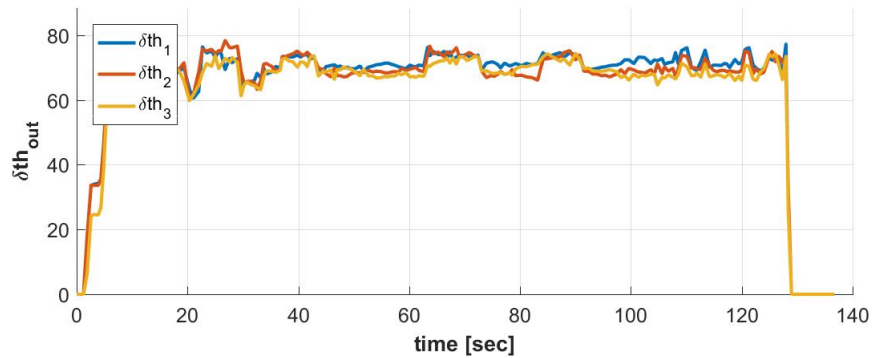


Figure 7.18: Tricopter flight test - throttle responses of motors

The flight test results for tricopter frame are presented in Figure (7.14), Figure (7.15) and Figure (7.16) which show that the tricopter tracks commands as close as possible. Results also indicate that pilot can achieve to lift the tricopter above 60% throttle input as shown in Figure (7.17). Motor outputs also vary around the reference throttle

percentage which are given in Figure (7.18). Handling capabilities and stability of the controller give confidence to move on to the winged tricopter VTOL configuration which is examined in the following sub-section.

7.3.2 VTOL Configuration Flight Tests

After performing flight test of tricopter and laboratory test of dummy-wing configuration, wing is replaced with dummy-wing and tests are performed with VTOL configuration. Beside dummy-wing, desired configuration frame is aligned with tricopter main frame, so that during tests no aft body oscillations are observed.



Figure 7.19: VTOL tricopter mode attitude control flight test photo

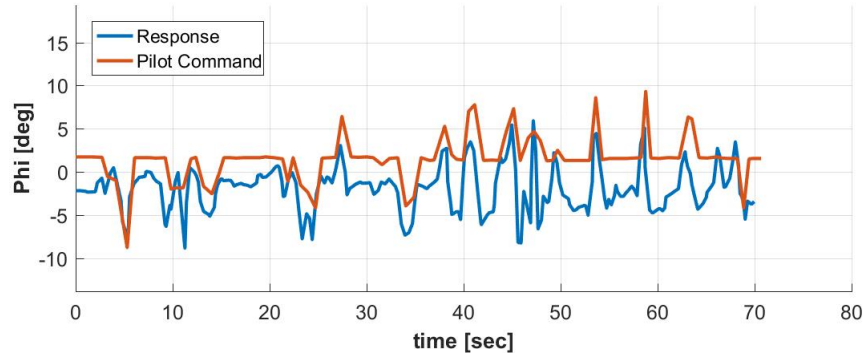


Figure 7.20: VTOL tricopter mode attitude control flight test result for the given roll command

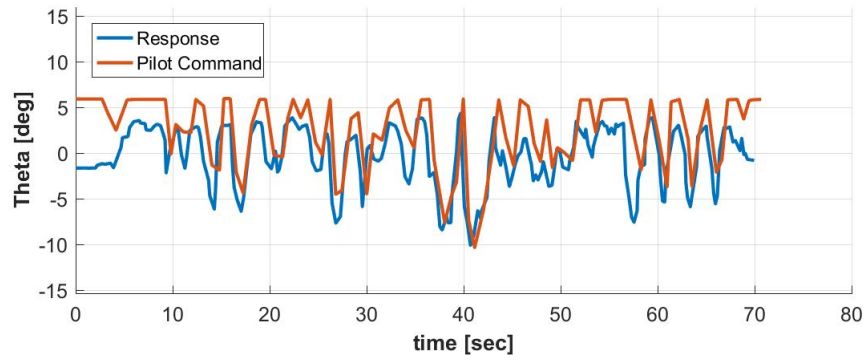


Figure 7.21: VTOL tricopter mode attitude control flight test result for the given theta command

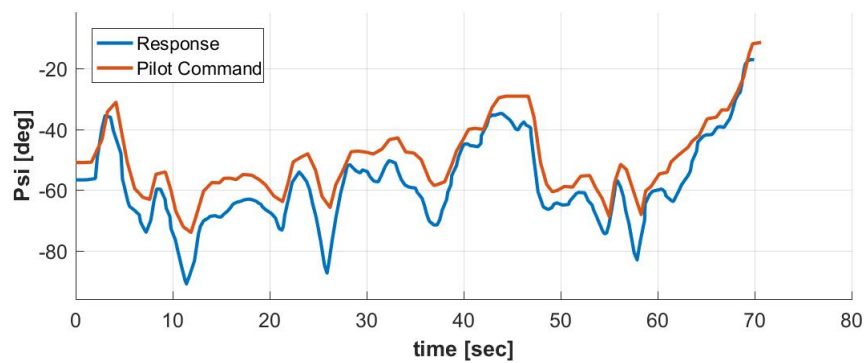


Figure 7.22: VTOL tricopter mode attitude control flight test result for the given yaw command

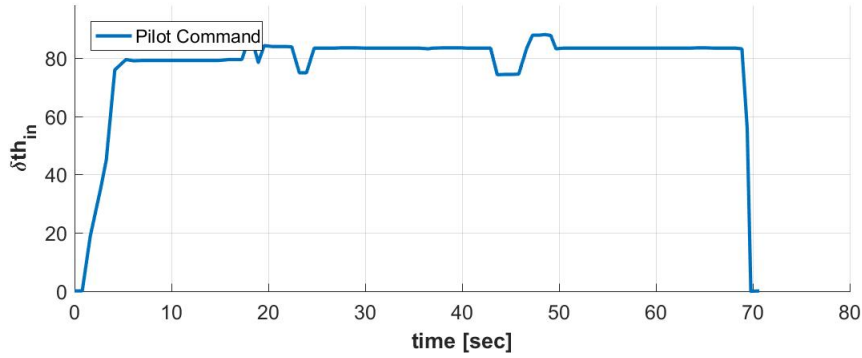


Figure 7.23: VTOL tricopter mode attitude control flight test - throttle input command

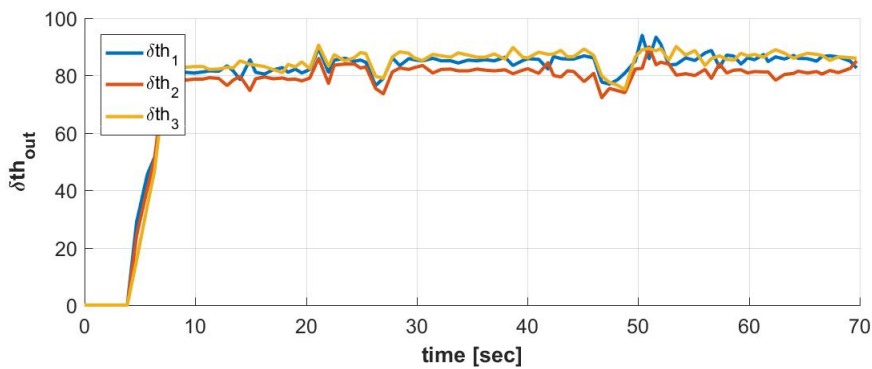


Figure 7.24: VTOL tricopter mode attitude control flight test - throttle responses of motors

The tricopter mode attitude control flight test results for VTOL configuration are presented in Figure (7.20), Figure (7.21) and Figure (7.22) which show that the VTOL tracks the pilot commands for all given commands with some offset. However, the platform is controllable and responds to all commands. Results also indicate that pilot can achieve to lift the tricopter above 80% throttle input as shown in Figure (7.23). Motor outputs also varies around the reference throttle percentage which are given in Figure (7.24). Pilot observed that heading control of platform can be enhanced but it is not a drawback, and system is stable enough.

CHAPTER 8

CONCLUSION

Aviation plays an important role on civilian and military areas and UAVs are becoming important players with their growing diverse capabilities. Hybrid VTOL aircrafts are designed to meet the need for effective VTOL and cruise flight capabilities with improved performance. In this thesis, tilt-rotor approach with flying wing configuration is proposed. Concept is to control take-off with differential thrust of three motors with the help of aft tilt mechanism to sustain stability. After take-off platform gains speed with all three motors and during transition to forward flight stage front motors smoothly tilt and as the platform gains speed, wing surfaces become active for both creating lift and attitude control. In order to model the proposed concept, wind tunnel tests were performed to get motor-propeller characteristics, and test data is analysed. Non-linear mathematical equations, aerodynamic and propulsion models are applied to simulation environment.

In order to reduce complexity and increase the awareness of the each added features and their outcomes, development stage is separated into tricopter and VTOL configurations. Model trim conditions are defined and MATLAB scripts for this purposes are created. According to linearized equations, controller is designed. Control modes (copter and plane), flight phases (tricopter attitude control, transition to forward flight, forward flight, transition to tricopter attitude control), and methodologies are defined. Blended inverse and weighted pseudo inverse approaches are applied for transition control. Due to simulation results, both blended inverse and weighted pseudo inverse control allocations performs well in transition to plane mode. However, blended inverse control allocation performs more smooth transition characteristics for transition to tricopter mode, considering stability of the platform. For the tricopter attitude con-

trol and forward flight controllers LQT and LQR-I are designed. Simulation tests are performed to find the controller gains that meet desired attitude control outputs. In order to avoid crashes, a freely-swinging setup is used for lab tests to validate model results. After many failures, lab tests showed that proposed solution for the simulation side does not completely reflect real-world conditions as expected. As test results are analysed, responsiveness of motors are decreased and optimum gains are obtained. After each successful lab test, flight tests are performed. First, using previous platform and its motor-propeller wind tunnel test results, as proposed in [26], new LQT controller is designed as described in Appendix A. Lab and flight tests are performed successfully. Speed hold controller is designed to be used both for altitude control and transition control. However, flight test resulted in crash. Due to the difficulty in purchasing same motors, a new motor and a propeller combination is selected and wind tunnel tests are performed. Control strategy is differentiated from the previous study and LQR-I approach is left due to unforeseeable outcomes of integral wind-ups. Current controller tests are performed for attitude controller in tricopter, dummy-wing and winged VTOL configurations successfully. Hardware selected for the studies gives flexibility to develop and implement controller. Since, embedded platform itself is open source, build-in libraries for sensors and actuators come with it. The code is written with C++ in QT Creator under Ubuntu. Motor classes are modified and autopilot source code is eliminated. LQT controller, simulation gains and design logic are implemented to system.

For the future work, sensor models and motor-actuator responses will be modelled to obtain simulation results relatively close to real-world. More precise GPS solutions will be implemented to avoid sensor related control failures in altitude control using speed control strategy. Forward flight tests will be performed and then transition control allocation strategy will be tried. These will also enable to implement waypoint navigation capabilities to system. Furthermore, full-autonomous take-off and landing, cruise flights, and predefined waypoint actions may be performed during flight.

REFERENCES

- [1] Bob Allen. Ten-Engine Electric Plane Completes Successful Flight Test, 2015.
- [2] ArduPilot Dev Team. ArduPilot, 2019.
- [3] Ozlem Armutcuoglu, Mehmet Serif Kavsaoglu, and Ozan Tekinalp. Tilt Duct Vertical Takeoff and Landing Uninhabited Aerial Vehicle Concept Design Study. *Journal of Aircraft*, 2008.
- [4] Reg Austin. *Unmanned Aircraft Systems: UAVS Design, Development and Deployment*. John Wiley & Sons, Ltd, 2010.
- [5] Deperrois C. A. About XFLR5 calculations and experimental measurements, 2009.
- [6] Vinny Devine. Cypher ® Unmanned Aerial Vehicle (UAV), 2016.
- [7] James Drew. New search for VTOL UAVs may resurrect Bell tiltrotor, 2016.
- [8] Duc Anh Ta, I. Fantoni, and R. Lozano. Modeling and control of a tilt tri-rotor airplane. In *2012 American Control Conference (ACC)*, pages 131–136. IEEE, jun 2012.
- [9] S. Durand, B. Boisseau, J.J. Martinez-Molina, N. Marchand, and T. Raharijaona. Event-based LQR with integral action. In *Proceedings of the 2014 IEEE Emerging Technology and Factory Automation (ETFA)*, pages 1–7. IEEE, sep 2014.
- [10] Wayne Durham. *Aircraft Flight Dynamics and Control*. John Wiley & Sons, Ltd, 2013.
- [11] Bernard Etkin and Llyod Duff Reid. *Dynamics of Flight Stability and Control*. Wiley, 3rd edition, 1996.
- [12] Paul Gerin Fahlstrom and Thomas James Gleason. *Introduction to UAV Systems*. John Wiley & Sons, Ltd, 4th edition, 2012.

- [13] Mike Hanlon. SkyTote - the VTOL UAV that transitions into horizontal flight, 2006.
- [14] M. Hassanalian and A. Abdelkefi. Classifications, applications, and design challenges of drones: A review, 2017.
- [15] Tor A. Johansen, Andrea Cristofaro, Kim Sorensen, Jakob M. Hansen, and Thor I. Fossen. On estimation of wind velocity, angle-of-attack and sideslip angle of small UAVs using standard sensors. In *2015 International Conference on Unmanned Aircraft Systems, ICUAS 2015*, 2015.
- [16] Derya Kaya, Ali T. Kutay, and Ozan Tekinalp. Experimental Investigation of Optimal Gap Distance between Rotors of a Quadrotor UAV. 2017.
- [17] Derya Kaya and Ali Turker Kutay. Modeling and Simulation of a Quadrotor using Curve Fitting Method. 2015.
- [18] Nick Lavars. Lilium's full-sized electric jet flies for the first time, 2019.
- [19] Hanmant G. Malkapure and M. Chidambaram. Comparison of Two Methods of Incorporating an Integral Action in Linear Quadratic Regulator. *IFAC Proceedings Volumes*, 47(1):55–61, 2014.
- [20] Donald McLean. *Automatic Flight Control Systems*. Prentice Hall International (UK), Cambridge, 1990.
- [21] J.L. Meriam, L.G. Kraige, and J.N. Bolton. *Engineering Mechanics: Dynamics*. John Wiley & Sons, Inc, 2015.
- [22] J. Milan. Thrust allocation techniques for dynamically positioned vessels. Technical report, National Research Council Canada. Institute for Ocean Technology, St. John's, NL, 2008.
- [23] Desineni Subbaram Naidu. *Optimal Control Systems*. CRC Press, Florida, 2002.
- [24] Erik Oberg, Franklin D. Jones, Holbrook L. Horton, and Henry H. Ryffel. *Machinery's Handbook - 29th Edition*. Industrial Press, New York, 29th edition, 2012.

- [25] Shea O'Donnell. *A Short History of Unmanned Aerial Vehicles (UAVs)*, 2017.
- [26] Anil Sami Onen, Levent Cevher, Murat Senipek, Talha Mutlu, Osman Gungor, Ismail Ozdemir Uzunlar, Dilek Funda Kurtulus, and Ozan Tekinalp. Modeling and controller design of a VTOL UAV. In *2015 International Conference on Unmanned Aircraft Systems, ICUAS 2015*, 2015.
- [27] Anil Sami Önen. *Modeling and Controller Design of a VTOL UAV*. PhD thesis, Middle East Technical University, 2015.
- [28] K. P. Valavanis P. Spanoudakis, L. Doitsidis, N. C. Tsourveloudis. Market Overview of the Vertical Take-Off and Landing Vehicles. 2003.
- [29] PX4 Dev Team. Cube (Pixhawk 2) · PX4 v1.9.0 User Guide, 2019.
- [30] Jan Roskam. *Airplane Flight Dynamics and Automatic Flight Controls - Part I*. 3rd edition, 2001.
- [31] Hugh Schmittle. *The Pivoting Wing Paradigm*, 2016.
- [32] Yasmina Bestaoui Sebbane. *Smart autonomous aircraft: Flight control and planning for UAV*. 2015.
- [33] Ozan Tekinalp and Anna Prach. Development of a State Dependent Riccati Equation based Tracking Flight Controller for an Unmanned Aircraft. 2013.
- [34] Ozan Tekinalp and Emre Yavuzoglu. A new steering law for redundant control moment gyroscope clusters. *Aerospace Science and Technology*, 2005.
- [35] The QT Company. Qt Creator IDE – Making software development fast, easy & fun, 2019.
- [36] Tuğba Ünlü. *Flight Control of a Tilt Duct UAV with Emphasis on The Over Actuated Transition Flight Phase*. PhD thesis, Middle East Technical University, 2009.

Appendix A

A.1 Previous Platform Studies

In this section, previous platform studies are explained. Thesis studies started firstly using given methodology and then applied to the new platform and developed.

A.1.1 Dynamic Model of Motor

Applying Equation (2.4) and Equation (2.5) to Axi 2826/10 motor and Xoar 11x4 propeller combination, fitting results can be observed in the following figures:

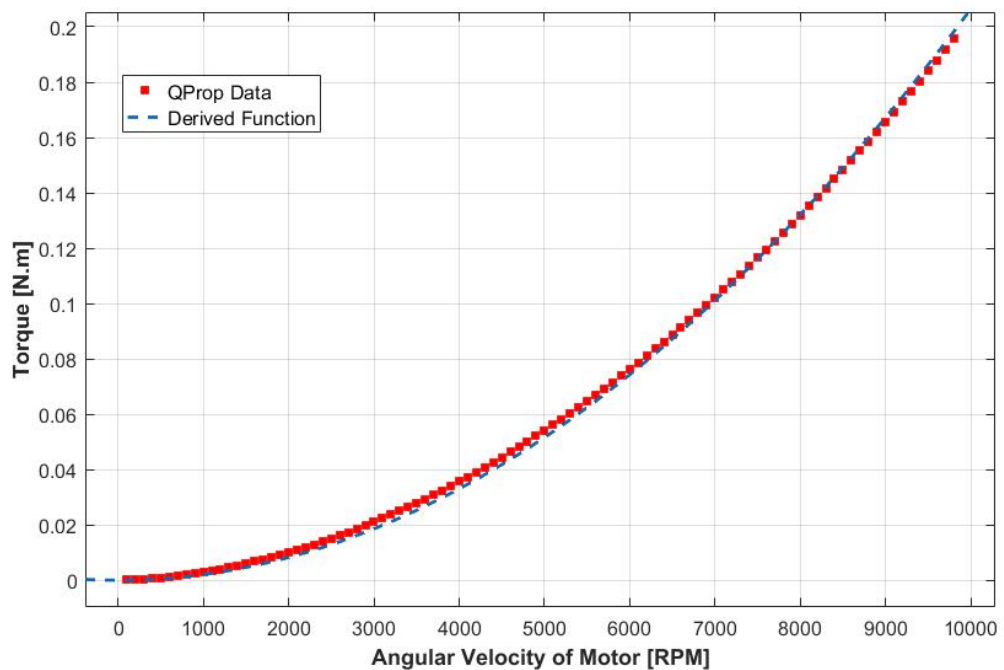


Figure A.1: Torque[N.m] vs. RPM relation with Axi 2826/10 motor and Xoar 11x4 propeller

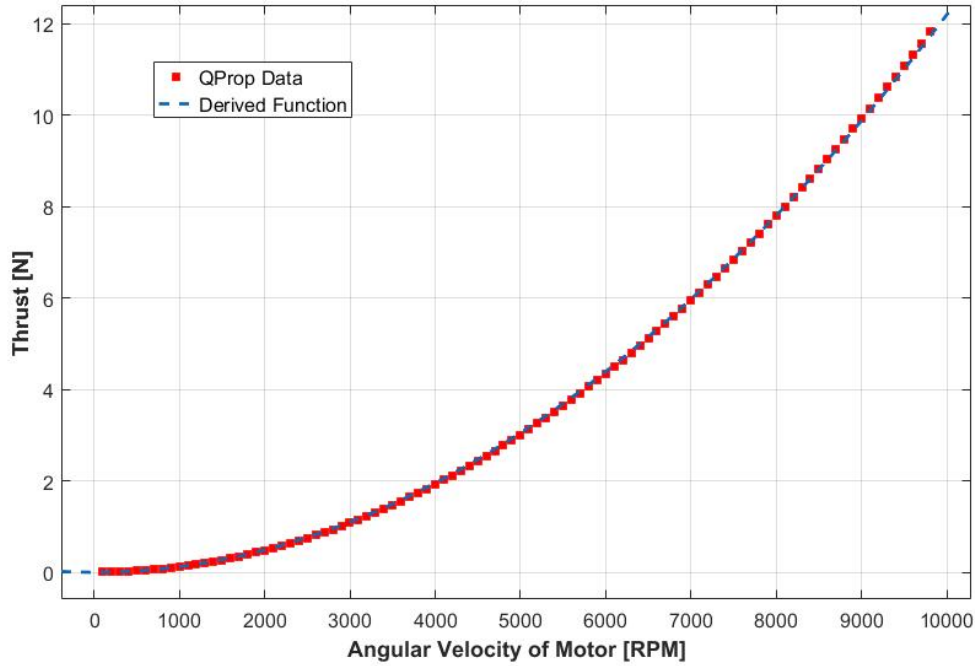


Figure A.2: Thrust[N] vs. RPM relation with Axi 2826/10 motor and Xoar 11x4 propeller

In the previous study [26], Torque - RPM, and Thrust - RPM relations were obtained as shown in Figure (A.1) and Figure (A.2). QPROP model for Axi 2826/10 motor and Xoar 11x4 propeller combination were tested and for this thesis, proper 2nd order model was obtained with following thrust and torque coefficients:

$$\begin{aligned}
 k_{axi} &= 1.22e - 07[N./RPM^2] \\
 l_{axi} &= 2.065e - 09[N.m/RPM^2]
 \end{aligned}
 \tag{A.1}$$

RPM-throttle and RPM-torque relations must be defined in order to be used both in mathematical model of the system and conversions between thrust and torque parameters. Extracting from the experimental data as given in the Figure A.3, relation can be expressed as follows:

$$RPM = -0.2299\delta_{th}^2 + 103.2\delta_{th} + 1907
 \tag{A.2}$$

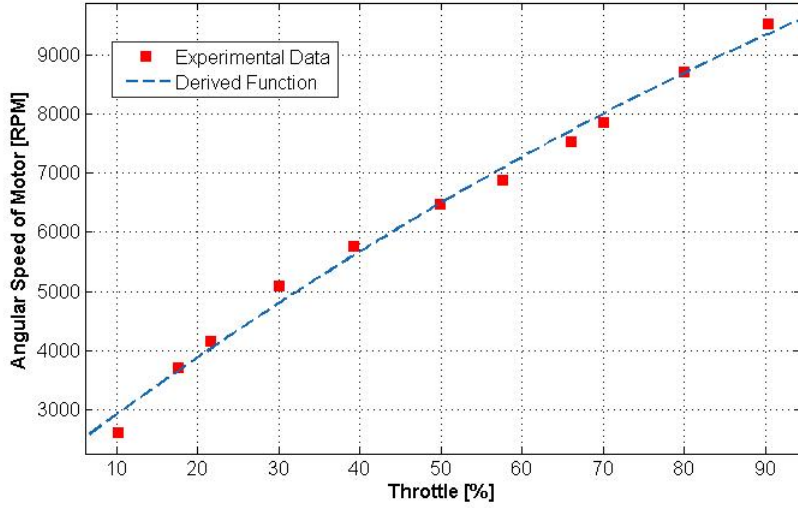


Figure A.3: RPM vs. Throttle[%] relation with Scorpion 3020-780kv and APC 11x5.5 propeller combination

A.1.2 Dynamic Model

Referencing Equation (2.31), translational motion can be expressed to find an equation related to ground speed of tricopter:

$$\dot{V}_E = \begin{bmatrix} \dot{u}_E \\ \dot{v}_E \\ \dot{w}_E \end{bmatrix} = \dot{L}_{EB}.V_B + L_{EB}.\dot{V}_B \quad (\text{A.3})$$

Derivative of L_{EB} as given in Equation (A.3) can be obtained using orthogonality of matrix L_{EB} as stated in [11]:

$$\dot{L}_{EB} = \tilde{\omega}_E.L_{EB} \quad (\text{A.4})$$

$\tilde{\omega}_E$ can expressed as following:

$$\tilde{\omega}_E = \begin{bmatrix} 0 & -\tilde{\omega}_z & \tilde{\omega}_y \\ \tilde{\omega}_z & 0 & -\tilde{\omega}_x \\ -\tilde{\omega}_y & \tilde{\omega}_x & 0 \end{bmatrix} \quad (\text{A.5})$$

Hence, angular velocity notation can be represented as $\tilde{\omega}_E.R = \omega_E x R$

Angular velocity transformation from earth fixed to body fixed frame can be ex-

pressed as following:

$$\omega_B = L_{EB} \cdot \omega_E \quad (\text{A.6})$$

Using the skew-symmetric property of $\tilde{\omega}_B$, the expression $(L_{BE} \cdot \tilde{\omega}_B) \times L_{EB}$ can be written as:

$$\tilde{\omega}_E = L_{BE}^T \cdot \tilde{\omega}_B \cdot L_{BE} \quad (\text{A.7})$$

By substituting Equation (A.7) into Equation (A.4), \dot{L}_{EB} can be represented as following:

$$\dot{L}_{EB} = L_{EB} \cdot \tilde{\omega}_B \quad (\text{A.8})$$

From Equation (A.8) and Equation (A.3) using reexpression of \dot{L}_{EB} , \dot{V}_B can expressed as following:

$$\dot{V}_B = L_{BE} \cdot (\dot{V}_E - L_{EB} \cdot \tilde{\omega}_B \cdot V_B) \quad (\text{A.9})$$

Substituting Equation (A.9) into Equation (2.31), external forces can be defined as following:

$$\begin{aligned} F_B^{ext} &= m \cdot (L_{BE} \cdot \dot{V}_E - L_{BE} \cdot L_{EB} \cdot \tilde{\omega}_B \cdot V_B + \tilde{\omega}_B \cdot V_B) \\ &= m \cdot (L_{BE} \cdot \dot{V}_E) \end{aligned} \quad (\text{A.10})$$

Alternatively using Equation (2.38) and Equation (A.10), forces acting on body fixed frame can be expressed in terms of earth fixed frame velocity vectors, considering $L_{BE}^{-1} = L_{EB}$.

$$m \cdot \dot{V}_E = \begin{bmatrix} 0 \\ 0 \\ mg \end{bmatrix} + L_{EB} \cdot \begin{bmatrix} (F_1 + F_2) \cdot \sin(\sigma) \\ F_3 \cdot \sin(\gamma) \\ -(F_1 + F_2) \cdot \cos(\sigma) - F_3 \cdot \cos(\gamma) \end{bmatrix} \quad (\text{A.11})$$

Velocity vector of tricopter in earth fixed inertial frame is represented as V_E vector, so that it can be used to calculate ground speed reference into the system during simulations.

A.1.3 Trimming Approach for Hover Position

Solving Equation (3.5) for characteristics of AXI 2826/10 motor and Xoar 11x4 wooden propeller combination, trim results for tricopter are obtained as following:

Table A.1: Trim values for hover with AXI 2826/10 - Xoar 11x4 combination

Φ_0 [deg]	Θ_0 [deg]	Ψ_0 [deg]	γ_0 [deg]	$\Omega_{0,1}$ [rpm]	$\Omega_{0,2}$ [rpm]	$\Omega_{0,3}$ [rpm]
-0.7625	2.802e-08	-3.1944	2.2876	9149	7846	8523

A.1.4 Linearization of Hover Flight Equations

Change in angular rates will be derived from perturbed moments as shown in Equation (3.8). Thus, perturbed motion of moment generated by propellers can be derived by substituting Equation (3.1) and Equation (3.5) into total moment equation given by Equation (2.48) and Equation (2.49). After simplification, constant part for each equation will be neglected. Function becomes as follows:

$$\begin{bmatrix} \Delta L \\ \Delta M \\ \Delta N \end{bmatrix} = [T_{C2M}] \begin{bmatrix} \Delta\Omega_{0,1} \\ \Delta\Omega_{0,2} \\ \Delta\Omega_{0,3} \\ \Delta\gamma \\ \Delta\sigma \end{bmatrix} \quad (\text{A.12})$$

Where T_{C2M} is a $[3 \times 5]$ transformation matrix and functional relations used in T_{C2M} are defined in Matlab. Considering that, in attitude control front motors are positioned vertically according to body axes, such that value of σ is zero. In other words, equations defined in T_{C2M} with σ_0 parameter will be taken zero and $\Delta\sigma$ state will be omitted. Applying these changes angular rates can be represented as following:

$$\begin{bmatrix} \Delta\dot{p} \\ \Delta\dot{q} \\ \Delta\dot{r} \end{bmatrix} = \begin{bmatrix} \frac{1}{I_x} & 0 & 0 \\ 0 & \frac{1}{I_y} & 0 \\ 0 & 0 & \frac{1}{I_z} \end{bmatrix} [T_{C2M}^H] \begin{bmatrix} \Delta\Omega_{0,1} \\ \Delta\Omega_{0,2} \\ \Delta\Omega_{0,3} \\ \Delta\gamma \end{bmatrix} \quad (\text{A.13})$$

Derivation of dynamic model for translational motion is given in Equation (A.11). Linearizations of the equations are obtained by applying assumptions in Equation (3.1) on body fixed to earth fixed frame L_{EB} . Propeller forces acting on body axes are replaced by relative trim and perturbed portions. Also it is assumed that platform

is in hover. When given information applied into Equation (A.11), following equation is obtained:

$$m. \begin{bmatrix} \Delta \dot{u} \\ \Delta \dot{v} \\ \Delta \dot{w} \end{bmatrix} = [T_{C2V}] \begin{bmatrix} \Delta \Phi \\ \Delta \Theta \\ \Delta \Psi \\ \Delta F_{X_B}^{Prop} \\ \Delta F_{Y_B}^{Prop} \\ \Delta F_{Z_B}^{Prop} \end{bmatrix} + [C_{C2V}] + \begin{bmatrix} 0 \\ 0 \\ mg \end{bmatrix} \quad (\text{A.14})$$

Where T_{C2V} is a [3x6] transformation matrix and C_{C2V} is a [3x1] constant vector. Results showed that sum of vector C_{C2V} and gravitational force acting on body are negligibly small:

$$0 \cong [C_{C2V}] + \begin{bmatrix} 0 \\ 0 \\ mg \end{bmatrix} \quad (\text{A.15})$$

For attitude control case, equations defined in T_{C2V} with σ_0 parameter will be replaced by zero, such that there will be no propeller force acting on (X_B), x-axis of body fixed frame. Moreover, linearization results also showed that rate of change in Ψ has almost no effect on variations in ground speed, so $\Delta \Psi$ command will be omitted. Applying these changes angular rates can be represented as:

$$\begin{bmatrix} \Delta \dot{u} \\ \Delta \dot{v} \\ \Delta \dot{w} \end{bmatrix} = \frac{1}{m} [T_{C2V}^H] \begin{bmatrix} \Delta \Phi \\ \Delta \Theta \\ \Delta F_{Y_B}^{Prop} \\ \Delta F_{Z_B}^{Prop} \end{bmatrix} \quad (\text{A.16})$$

A.1.5 Linear Quadratic Tracking Control

LQT and LQR-I are chosen to be used for the controller design. Since both of them are linear controllers, linear state space approach is required to be used. As control strategy guided, attitude commands is used to hold system in desired attitude.

The state space approach used for linearized solutions obtained in Equation (3.7), (3.8) and Equation (A.13), states and inputs of the system for attitude control can be

defined as follows:

$$\Delta x = \begin{bmatrix} \Delta p & \Delta q & \Delta r & \Delta \Phi & \Delta \Theta & \Delta \Psi \end{bmatrix}' \quad (\text{A.17})$$

$$\Delta u_h = \begin{bmatrix} \Delta \Omega_1 & \Delta \Omega_2 & \Delta \Omega_3 & \Delta \gamma \end{bmatrix}' \quad (\text{A.18})$$

Linearized solution for states and inputs for ground-speed control can be defined as follows:

$$\Delta x_s = \begin{bmatrix} \Delta u & \Delta v & \Delta w \end{bmatrix}' \quad (\text{A.19})$$

$$\Delta u_s = \begin{bmatrix} \Delta \Phi & \Delta \Theta & \Delta F_Y^{Prop} & \Delta F_Z^{Prop} \end{bmatrix}' \quad (\text{A.20})$$

A.1.5.1 Linear Quadratic Tracking (LQT) Controller

A.1.5.1.1 LQT Controller - Attitude Control

From Equation (4.4), attitude control, where state and input vectors which are given in Equation (A.17) and Equation (A.18) respectively, can be represented as follows:

$$\Delta \dot{x}_h(t) = \begin{bmatrix} A_d \end{bmatrix} \begin{bmatrix} \Delta p(t) \\ \Delta q(t) \\ \Delta r(t) \\ \Delta \Phi(t) \\ \Delta \Theta(t) \\ \Delta \Psi(t) \end{bmatrix} + \begin{bmatrix} B_d \end{bmatrix} \begin{bmatrix} \Delta \Omega_1(t) \\ \Delta \Omega_2(t) \\ \Delta \Omega_3(t) \\ \Delta \gamma(t) \end{bmatrix} \quad (\text{A.21})$$

LQT optimal control approach for attitude control case can be derived by applying Equation (4.12) into Equation (A.21) as follows:

$$u(t) = \begin{bmatrix} \Delta \Omega_1(t) \\ \Delta \Omega_2(t) \\ \Delta \Omega_3(t) \\ \Delta \gamma(t) \end{bmatrix} = \begin{bmatrix} -K_H \end{bmatrix} \begin{bmatrix} \Delta p(t) \\ \Delta q(t) \\ \Delta r(t) \\ \Delta \Phi(t) \\ \Delta \Theta(t) \\ \Delta \Psi(t) \end{bmatrix} + \begin{bmatrix} K_{zH} \end{bmatrix} \begin{bmatrix} \Delta \Phi(t) \\ \Delta \Theta(t) \\ \Delta \Psi(t) \end{bmatrix} \quad (\text{A.22})$$

The gain matrices for attitude control are given in Appendix D.

A.1.5.1.2 LQT Controller - Ground Speed Control

Ground speed control state space representation can be derived by applying Equation (A.16) into Equation (4.4), where state and input vectors are Equation (A.19) and Equation (A.20) can respectively be represented as follows:

$$\Delta \dot{x}_h(t) = [A_d] \begin{bmatrix} \Delta u(t) \\ \Delta v(t) \\ \Delta w(t) \end{bmatrix} + [B_d] \begin{bmatrix} \Delta \Phi(t) \\ \Delta \Theta(t) \\ \Delta F_Y^{Prop}(t) \\ \Delta F_Z^{Prop}(t) \end{bmatrix} \quad (A.23)$$

LQT optimal control approach for ground speed control case can be derived by applying Equation (4.12) into Equation (A.23) as follows:

$$u(t) = \begin{bmatrix} \Delta \Phi \\ \Delta \Theta \\ \Delta F_Y^{Prop} \\ \Delta F_Z^{Prop} \end{bmatrix} = [-K_H] \begin{bmatrix} \Delta u_{E_{nav}}(t) \\ \Delta v_{E_{nav}}(t) \\ \Delta w_{E_{nav}}(t) \end{bmatrix} + [K_{z_H}] \begin{bmatrix} \Delta u_{E_d}(t) \\ \Delta v_{E_d}(t) \\ \Delta w_{E_d}(t) \end{bmatrix} \quad (A.24)$$

The gain matrices for ground speed control are given in Appendix D.

A.1.5.2 Linear Quadratic Regulator Control with Integral Action (LQR-I)

Linear quadratic controller is chosen to get desired output not just by controlling desired states, but also minimizing steady state tracking errors. LQR approach tends to hold outputs in desired reference, but in some cases it is unavoidable to reach zero steady state error. More robust approach is to add external control that is defined as integral action, such that even disturbances and model uncertainties exist in the model. In order to use external loop output, error vector is needed to be defined. Let's define error using the notation as follows [19, 9]:

$$\begin{aligned} \Delta e(t) &= \Delta u_d(t) - C_d \Delta x(t) \\ \Delta \dot{z}(t) &= \Delta e(t) \end{aligned} \quad (A.25)$$

Where $u_d(t)$ is a $[m \times 1]$ output setpoint vector and $x(t)$ is a $[n \times 1]$ state vector. Integral feedback is given such that error integrator provides zero steady state as an input.

Dynamic equation with new states can be defined as follows:

$$\Delta\bar{x}(t) = \begin{bmatrix} \Delta x(t) & \Delta z(t) \end{bmatrix} \quad (\text{A.26})$$

Where, $\bar{x}(t)$ is a $[(n+m) \times 1]$ state vector. Equation (4.4) becomes:

$$\begin{aligned} \dot{\bar{x}}(t) &= \bar{A}_d \bar{x}(t) + \bar{B}_d \bar{u}(t) + \bar{E}_d \bar{u}_d(t) \\ y(t) &= \bar{C}_d \bar{x}(t) \end{aligned} \quad (\text{A.27})$$

State, input and output matrices in Equation (A.28) can be represented as follows:

$$\begin{aligned} \dot{\bar{x}}(t) &= \begin{bmatrix} A & 0 \\ -C & 0 \end{bmatrix} \bar{x}(t) + \begin{bmatrix} B \\ 0 \end{bmatrix} \bar{u}(t) + \begin{bmatrix} 0 \\ I_m \end{bmatrix} \bar{u}_d(t) \\ y(t) &= \begin{bmatrix} C & 0 \end{bmatrix} \bar{x}(t) \end{aligned} \quad (\text{A.28})$$

Augmented system applied in quadratic performance index is chosen for infinite time case and it can be defined as follows:

$$J_d = \frac{1}{2} \sum_{t=t_0}^{\infty} \left\{ \Delta\bar{x}(t)^T \bar{Q} \Delta\bar{x}(t) + \Delta u(t)^T R \Delta u(t) \right\} \quad (\text{A.29})$$

Where Q is positive semi-definite $[(n+m) \times (n+m)]$ state weight matrix, R is positive definite $[m \times m]$ control weight matrix. The optimal control obtained from Hamiltonian form is given as

$$u^*(t) = -R^{-1} \bar{B}_d^T \lambda^*(t) \quad (\text{A.30})$$

States are related to optimal costate by a transformation as follows:

$$\lambda^*(t) = P x^*(t) \quad (\text{A.31})$$

Equation (A.31) is satisfied by eliminating the costate, by P which is a Riccati coefficient matrix that satisfies the following differential Riccati equation:

$$0 = -P \bar{A}_d - \bar{A}_d^T P + P \bar{B}_d R^{-1} \bar{B}_d^T P - Q \quad (\text{A.32})$$

Applying Equation (A.32) and Equation (A.31) into optimal control equation (A.30) eliminating costate $\lambda^*(t)$, optimal control becomes as follows:

$$u^*(t) = -R^{-1} \bar{B}_d^T P x(t) \quad (\text{A.33})$$

Where Kalman gain $\bar{K} = R^{-1}\bar{B}_d^T P$ can be grouped into corresponding state and error output vectors as follows:

$$\begin{aligned}\bar{K} &= \begin{bmatrix} K & -K_I \end{bmatrix} \\ \bar{u} &= - \begin{bmatrix} K\Delta x(t) - K_I\Delta z(t) \end{bmatrix}\end{aligned}\tag{A.34}$$

where K is state control gain and K_I is integral term.

A.1.5.2.1 Attitude Controller

LQR-I control approach for attitude control can be derived by applying Equation (A.34) into Equation (A.21) where state and input vectors are Equation (4.1) and Equation (4.2) respectively:

$$\Delta u(t) = \begin{bmatrix} \Delta\Omega_1(t) \\ \Delta\Omega_2(t) \\ \Delta\Omega_3(t) \\ \Delta\gamma(t) \end{bmatrix} = \begin{bmatrix} -K_H \end{bmatrix} \begin{bmatrix} \Delta p(t) \\ \Delta q(t) \\ \Delta r(t) \\ \Delta\Phi(t) \\ \Delta\Theta(t) \\ \Delta\Psi(t) \end{bmatrix} + \begin{bmatrix} K_{IH} \end{bmatrix} \Delta z(t)\tag{A.35}$$

$$\begin{aligned}\Delta z(t) &= \Delta z(t-1) + \Delta e(t)\Delta t \\ \Delta e(t) &= \begin{bmatrix} \Delta\Phi_d(t) \\ \Delta\Theta_d(t) \\ \Delta\Psi_d(t) \end{bmatrix} - \begin{bmatrix} \Delta\Phi_{nav}(t) \\ \Delta\Theta_{nav}(t) \\ \Delta\Psi_{nav}(t) \end{bmatrix}\end{aligned}\tag{A.36}$$

The gain matrices for attitude control are given in Appendix D.

A.1.6 Control Allocation Approach

Simulations tests are based on two approaches. First approach is using controller output as presented in Equation (A.18) and converting RPM commands to throttle commands from deriving Equation (A.2).

Second approach is used for ground speed hold controller as a conversion approach, which produces roll and pitch commands and beside that, it also produces force deviations in x and y axis to hold the desired speeds as given in Equation (A.18). Attitude

controller takes roll, pitch and yaw commands and creates control outputs as stated in Equation (A.20). In order to apply the force deviations to attitude control outputs, control allocation equations are derived. Attitude controller outputs in Equation (A.18) are converted to force and moments required to hold the system in desired attitude by applying to the Equation (2.28), Equation (2.29) and Equation (2.26). Total-moment outputs of controller are defined as L_{TC} , M_{TC} and N_{TC} for roll, pitch and yaw moments respectively. Thus, force outputs of controller are defined $F_{Y_C}^P$ and $F_{Z_C}^P$ for y and z body-axis respectively. Thrust generated in x-axis is omitted. In hover position, motors do not create force in x-axis direction. Using the information given for second approach, forces and moments required to hold tricopter in desired states is given as below:

$$\begin{bmatrix} F_{Y_d}^P \\ F_{Z_d}^P \\ L_{T_d} \\ M_{T_d} \\ N_{T_d} \end{bmatrix} = \begin{bmatrix} F_{Y_C}^P \\ F_{Z_C}^P \\ L_{T_C} \\ M_{T_C} \\ N_{T_C} \end{bmatrix} + \begin{bmatrix} \Delta F_{Y_B}^P \\ \Delta F_{Z_B}^P \\ 0 \\ 0 \\ 0 \end{bmatrix} \quad (\text{A.37})$$

Relation between Equation (A.37) and control inputs can be obtained using moment and force equations, Equation (2.45), Equation(2.46) and Equation (2.44) respectively, for tricopter frame as following:

$$\begin{bmatrix} Y \\ Z \\ L \\ M \\ N \end{bmatrix} = \begin{bmatrix} 0 & 0 & 0 & k \\ -k\cos(\sigma) & -k\cos(\sigma) & -k & 0 \\ -k\cos(\sigma)r_{y,1} - l\sin(\sigma) & -k\cos(\sigma)r_{y,2} + l\sin(\sigma) & -kr_{y,3} & -kr_{z,3} \\ k(\sin(\sigma)r_{z,1} + \cos(\sigma)r_{x,1}) & k(\sin(\sigma)r_{z,2} + \cos(\sigma)r_{x,2}) & kr_{x,3} & -l \\ -k\sin(\sigma)r_{y,1} + l\cos(\sigma) & -k\sin(\sigma)r_{y,2} - l\cos(\sigma) & l & kr_{x,3} \end{bmatrix} \cdot \begin{bmatrix} \Omega_1^2 \\ \Omega_2^2 \\ \Omega_3^2 \cos(\gamma) \\ \Omega_3^2 \sin(\gamma) \end{bmatrix} \quad (\text{A.38})$$

Total forces and moments are required to hold system in desired states are given in Equation (A.38). Thus conversion between desired force and moment outputs can be

converted to control inputs as below:

$$\begin{bmatrix} \Omega_1^2 \\ \Omega_2^2 \\ \Omega_3^2 \cos(\gamma) \\ \Omega_3^2 \sin(\gamma) \end{bmatrix} = [T_{C2M}] \begin{bmatrix} Y \\ Z \\ L \\ M \\ N \end{bmatrix} \quad (\text{A.39})$$

where T_{C2M} is a [5x4] transformation matrix. Aft servo angle will be derived from vectorial force components of aft motor, of which is a result of change in aft servo angle as it is presented in Equation (4.17) Aft servo angle will be derived from vectorial force components of aft motor as proposed in Equation (4.17)

A.1.7 Simulation Tests and Results

In this sub-section laboratory test results for previous platform are presented. Period of Inner loop controllers were taken 50Hz, whereas outer loop control runs at 10Hz. Test scenarios are created to observe LQT and LQR-I controllers' performance. Dynamic and system models shown in Figure (A.4) and Figure (A.5) respectively.

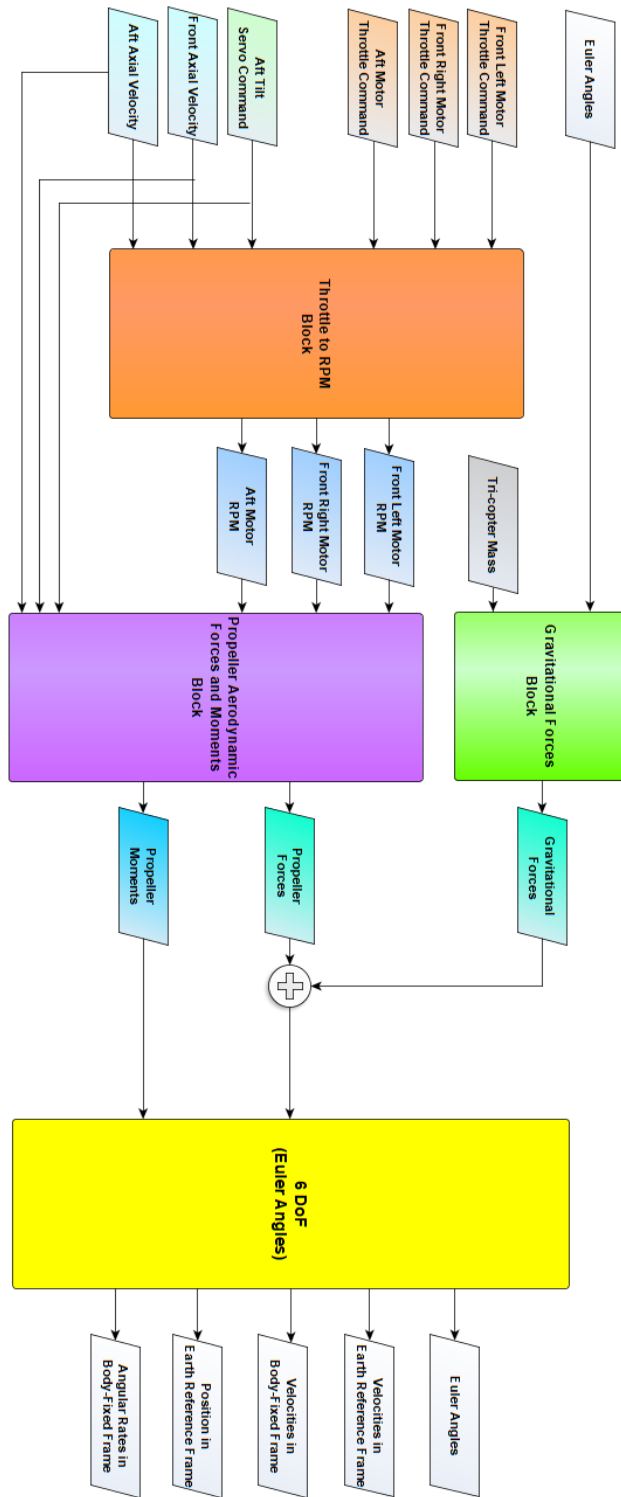


Figure A.4: Dynamic model of tricopter

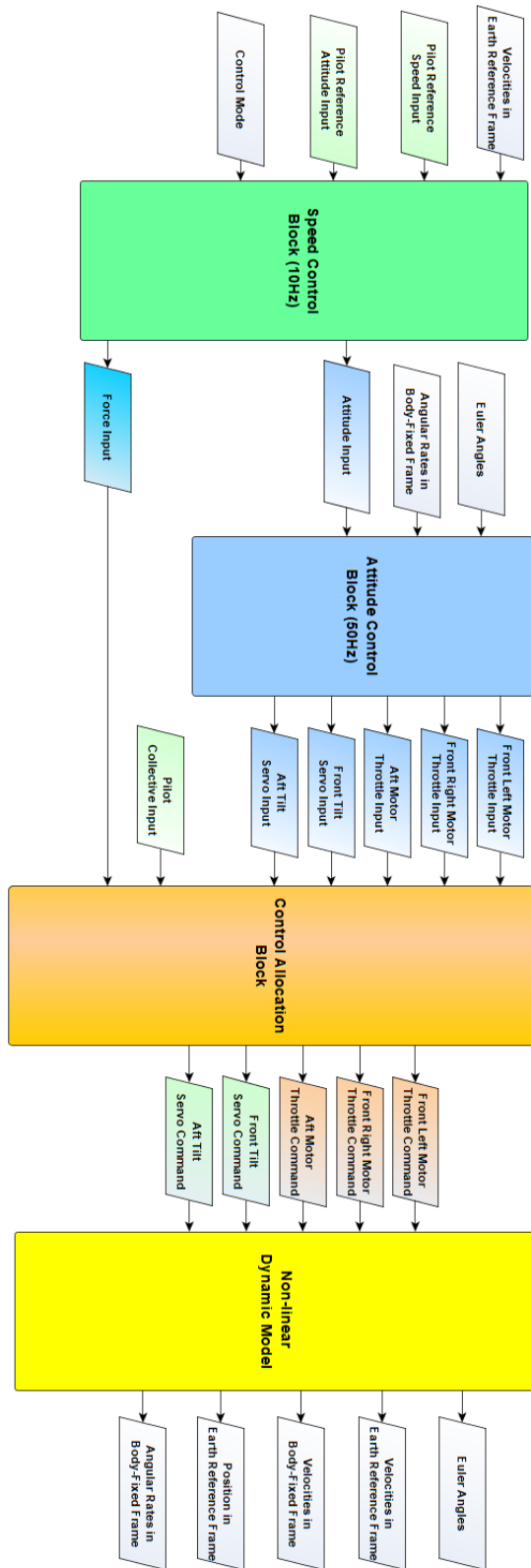
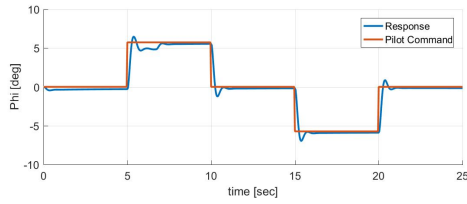
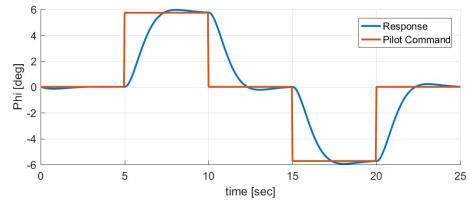


Figure A.5: System model of ground speed hold and attitude controllers

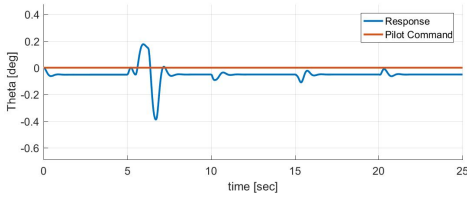
A.1.7.1 Tricopter Roll Control



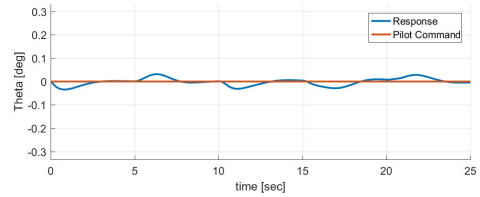
(a) LQT control result for the given roll command



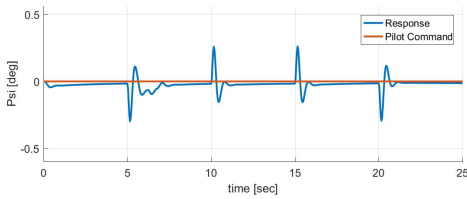
(b) LQR-I control result for the given roll command



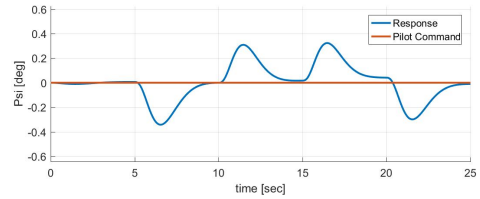
(c) LQT control result for the given zero pitch command



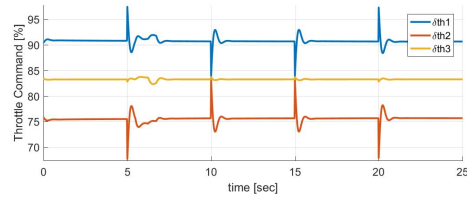
(d) LQR-I control result for the given zero pitch command



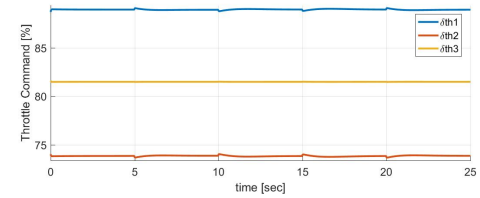
(e) LQT control result for the given zero yaw command



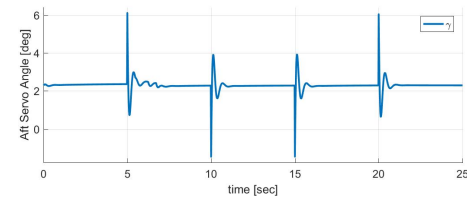
(f) LQR-I control result for the given zero yaw command



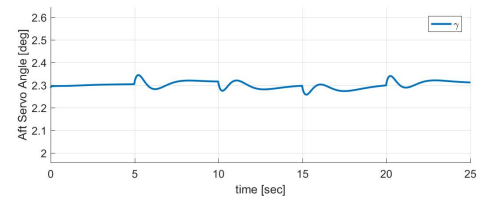
(g) LQT - Throttle output of motors for the given roll command



(h) LQR-I - Throttle output of motors for the given roll command



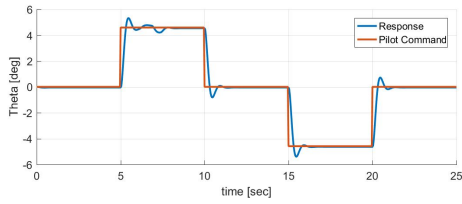
(i) LQT - Aft servo output for the given roll command



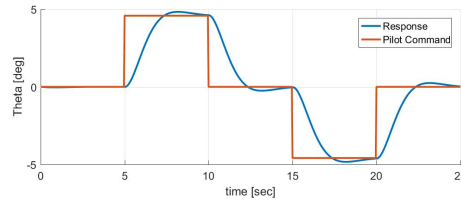
(j) LQR-I - Aft servo output for the given roll command

Figure A.6: Simulation results of LQT and LQR-I controllers for roll command

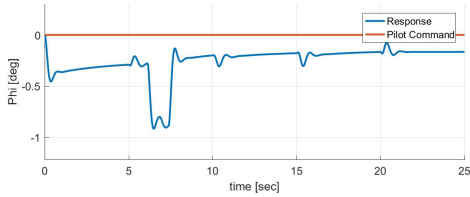
A.1.7.2 Tricopter Pitch Control



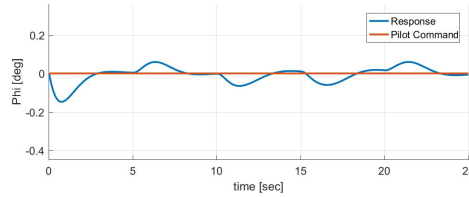
(a) LQT control result for the given pitch command



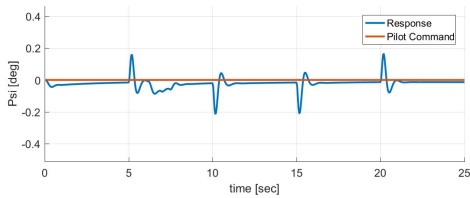
(b) LQR-I control result for the given pitch command



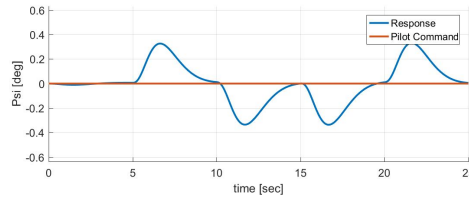
(c) LQT control result for the given zero roll command



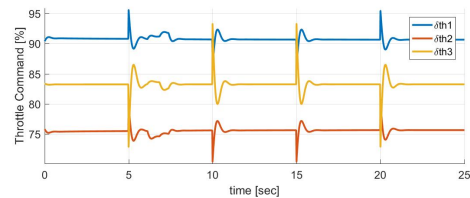
(d) LQR-I control result for the given zero roll command



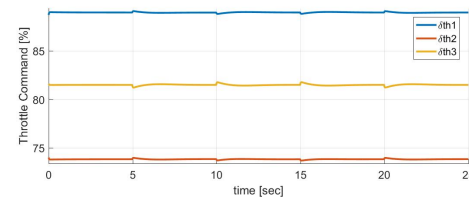
(e) LQT control result for the given zero yaw command



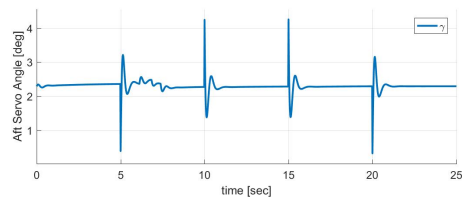
(f) LQR-I control result for the given zero yaw command



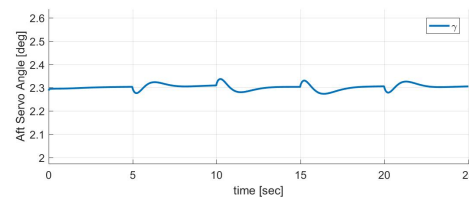
(g) LQT - Throttle output of motors for the given pitch command



(h) LQR-I - Throttle output of motors for the given pitch command



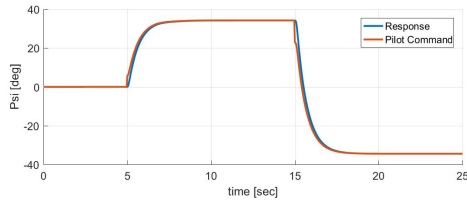
(i) LQT - Aft servo output for the given pitch command



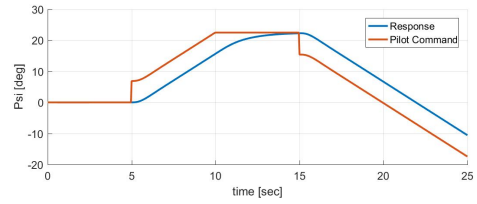
(j) LQR-I - Aft servo output for the given pitch command

Figure A.7: Simulation results of LQT and LQR-I controllers for pitch command

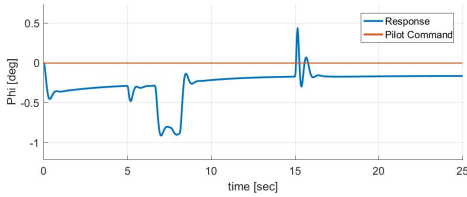
A.1.7.3 Tricopter Yaw Control



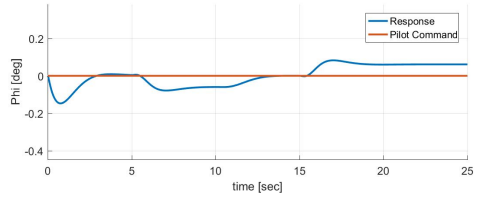
(a) LQT control result for the given yaw command



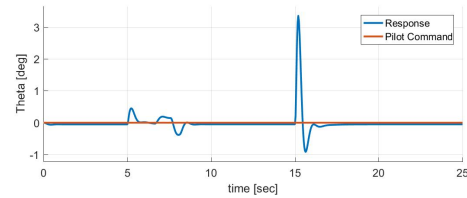
(b) LQR-I control result for the given yaw command



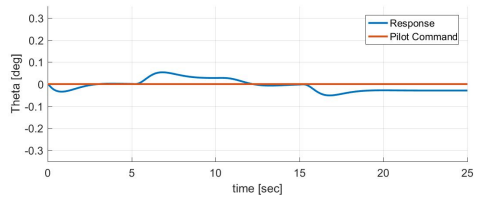
(c) LQT control result for the given zero roll command



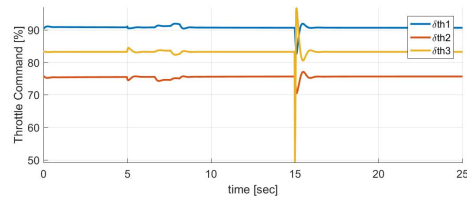
(d) LQR-I control result for the given zero roll command



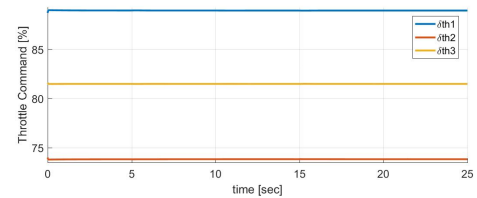
(e) LQT control result for the given zero pitch command



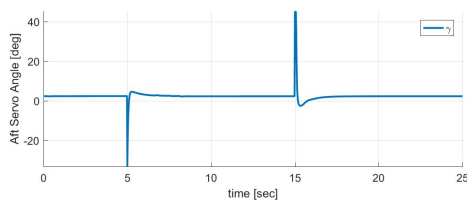
(f) LQR-I control result for the given zero pitch command



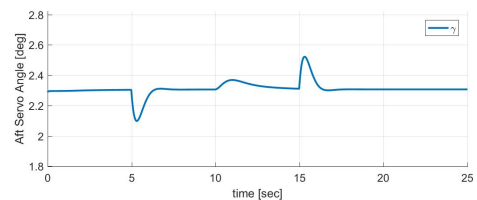
(g) LQT - Throttle output of motors for the given yaw command



(h) LQR-I - Throttle output of motors for the given yaw command



(i) LQT - Aft servo output for the given yaw command



(j) LQR-I - Aft servo output for the given yaw command

Figure A.8: Simulation results of LQT and LQR-I controllers for yaw command

A.1.7.4 Tricopter Ground Speed Hold Control

Ground speed hold controller simulations are carried out for zero velocity commands. Controller is activated at 6 [sec] in simulation. Before ground speed controller is activated, attitude controller is active feed with zero reference commands. Speed controller produces roll and pitch commands and differential forces required to hold speed. Period of inner loop attitude controller is 50 [Hz], and for outer loop, ground speed hold control is 10 [Hz]. Attitude controller outputs converted by control allocation block to drive motors and aft servo. Response of the platform is given in Figure (A.9) for given speed commands. Simulation result shows that system hold desired states with small offsets. Due to small offsets drifts in ground positions can be observed in Figure (A.10).

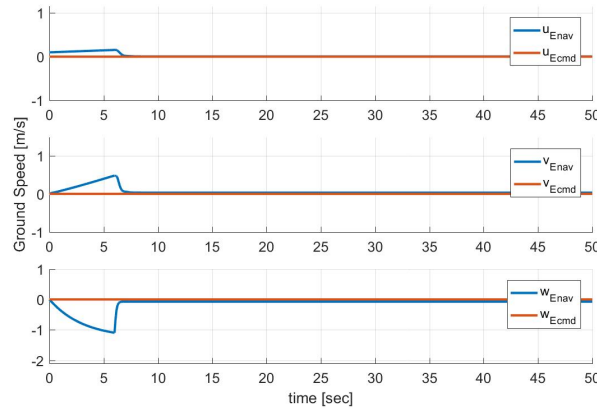


Figure A.9: LQT-Tricopter ground velocity responses for given reference commands

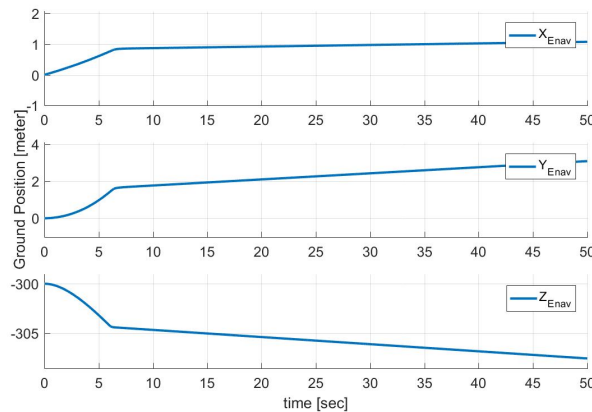
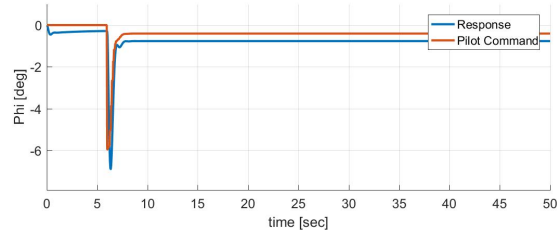
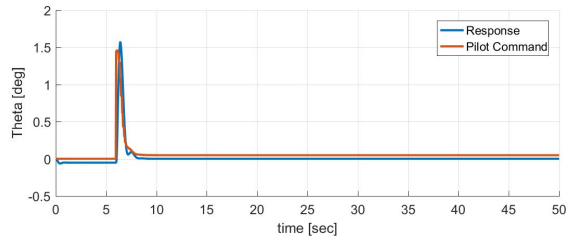


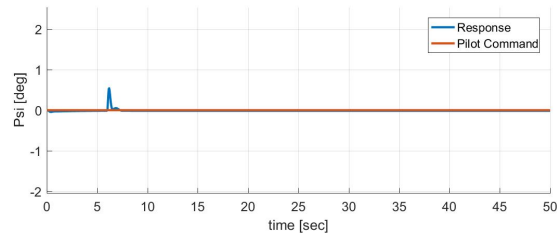
Figure A.10: LQT-Tricopter ground position changes for given reference commands



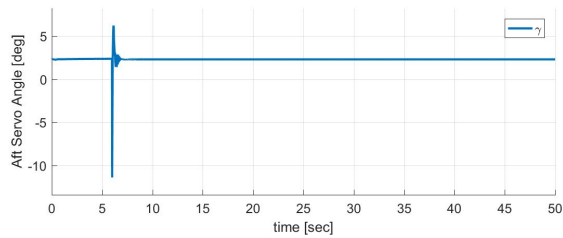
(a) LQT - Response for roll command by ground speed controller



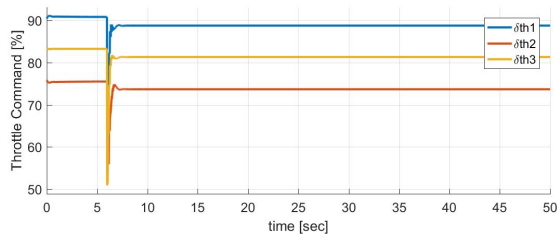
(b) LQT - Response for pitch command by ground speed controller



(c) LQT - Response for yaw command by ground speed controller



(d) LQT - Aft servo output for given attitude commands



(e) LQT - Throttle output of motors for given attitude commands

Figure A.11: Simulation results of LQT ground speed hold and attitude controllers for given speed commands

A.1.8 Flight Tests and Results

In this sub-section, flight test results for previous platform with LQT controller approach are presented. Period of inner loop controller is run at 50Hz.

A.1.8.1 Tricopter Flight Tests

Tricopter frame was tested outside covering all control commands. It was observed during the flight that pilot commands were followed by the system and the platform was responsive to the control inputs. Flight log was examined to compare how controller was performed during flight test.



Figure A.12: Tricopter (Axi-Xoar configuration) flight test photo

A.1.8.1.1 LQT Tri-coper Attitude Controller - Approach-1

Flight tests were performed according to first approach as suggested in subsection (A.1.6), and its results are given as following:

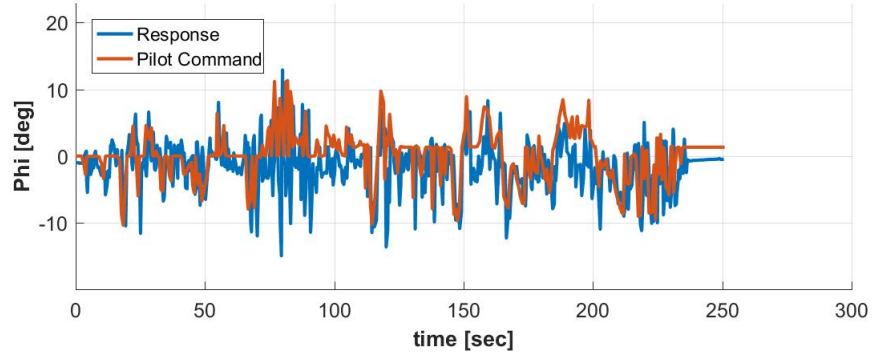


Figure A.13: Tricopter flight test result for given roll command

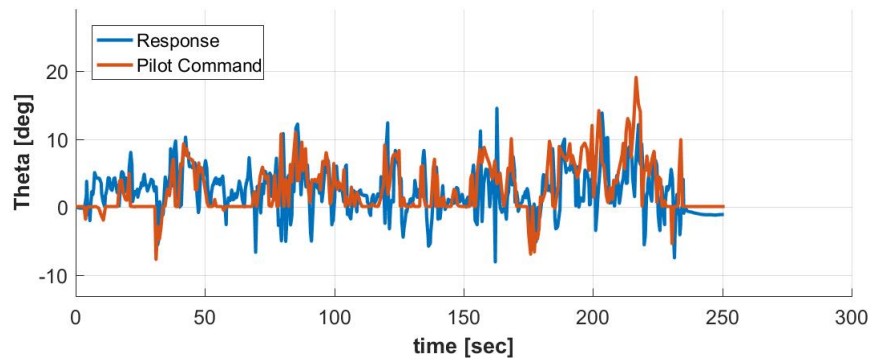


Figure A.14: Tricopter flight test result for given pitch command

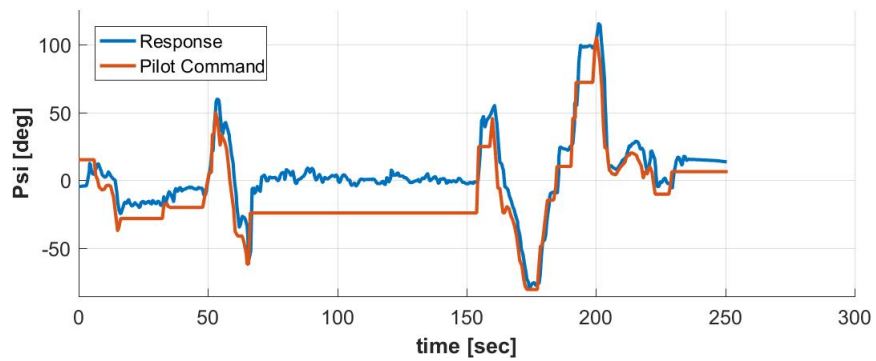


Figure A.15: Tricopter flight test result for given yaw command

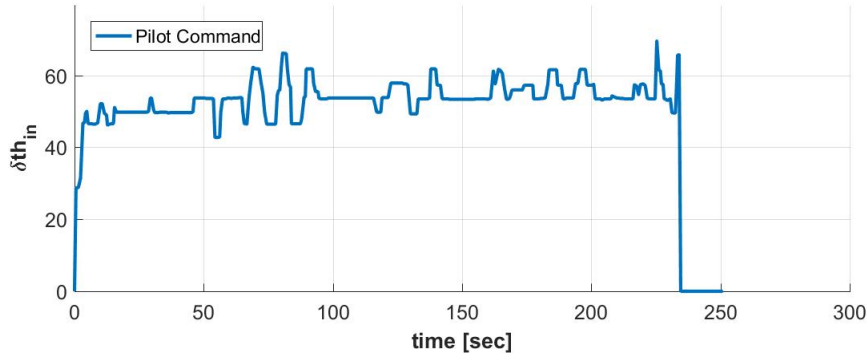


Figure A.16: Tricopter flight test - throttle input command

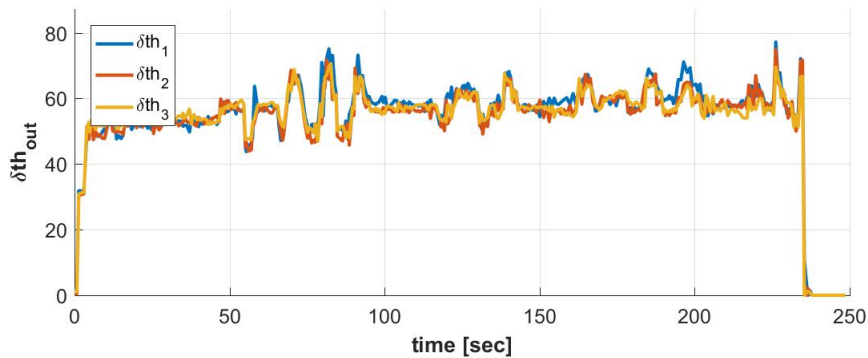


Figure A.17: Tricopter flight test - throttle responses of motors

The flight test results for tricopter frame are presented in Figure (A.13), Figure (A.14) and Figure (A.15) which show that the tricopter tracks commands as intended. Results also indicate that pilot can achieve to lift the tricopter with approximately 50% throttle input as shown in Figure (A.16). Motor outputs also vary around the reference throttle percentage which are given in Figure (A.17).

A.1.8.1.2 LQT Tricopter Attitude Controller - Approach-2

Flight test were performed according to second approach as given in subsection (A.1.6), and its results are given as following:

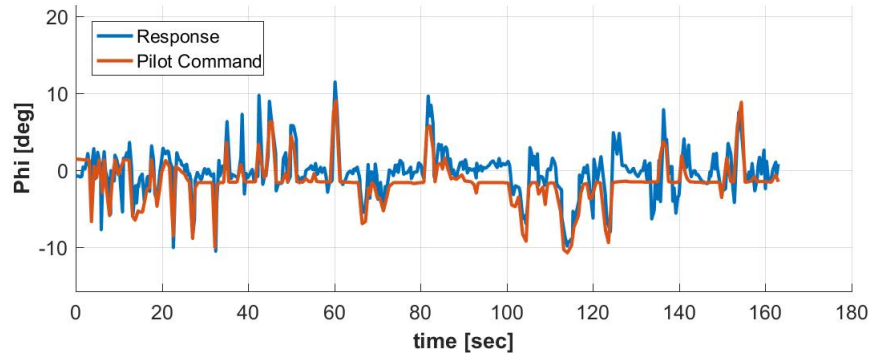


Figure A.18: Tricopter flight test result for given roll command

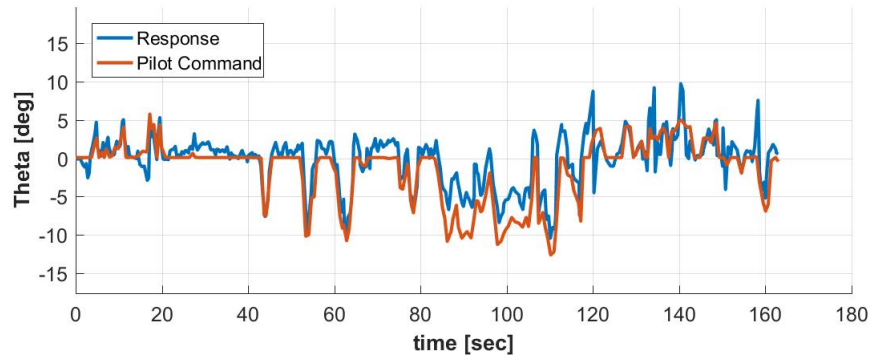


Figure A.19: Tricopter flight test result for given pitch command

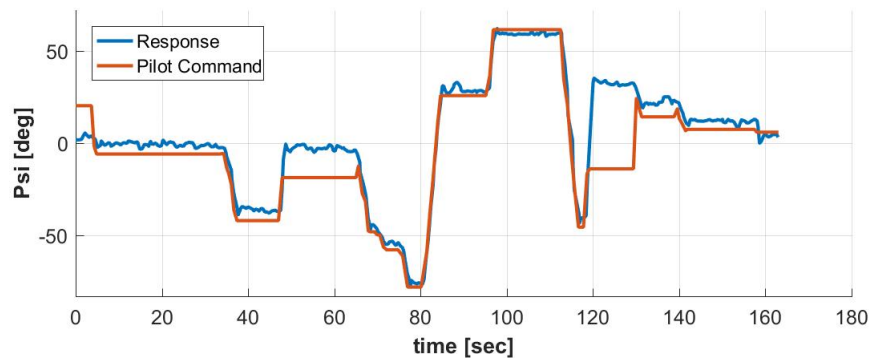


Figure A.20: Tricopter flight test result for given yaw command

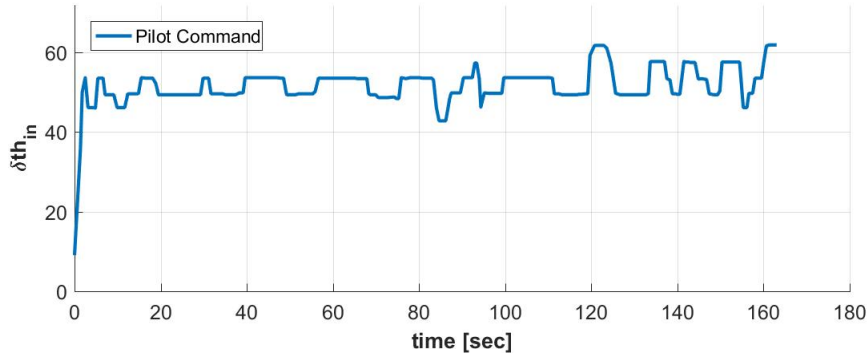


Figure A.21: Tricopter flight test - throttle input command

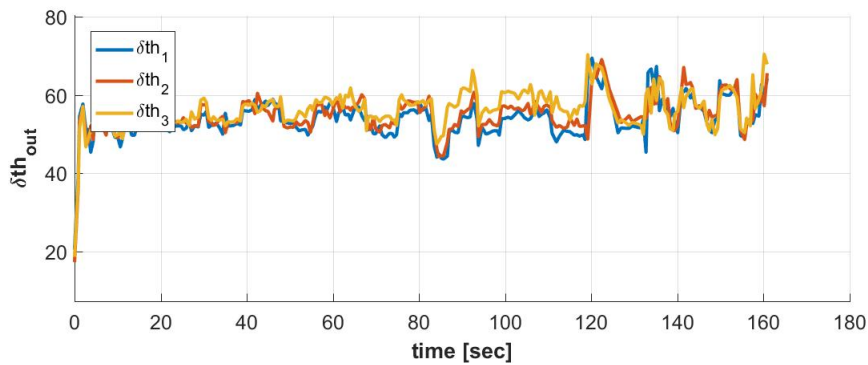


Figure A.22: Tricopter flight test - throttle responses of motors

The flight test results for tricopter frame are presented in Figure (A.18), Figure (A.19) and Figure (A.20) which show that the tricopter tracks commands as intended. Results also indicate that pilot can achieve to lift the tricopter with approximately 50% throttle input as shown in Figure (A.21). Motor outputs also vary around the reference throttle percentage which are given in Figure (A.22).

During attitude control, only attitude control outputs are converted to forces and moments as an input to control allocation block as it is suggested in Equation (A.37), and ground speed hold control output parameters are given as zero. Results prove that control allocation presented in subsection (A.1.6) works as intended. Ground speed hold controller had been activated during this flight test, but it did not work and the tricopter crashed. It is evaluated that both controller gains and ground speed source device may be the reason for crash. Controller gains were tested for the first time, since laboratory test environment is not eligible for tests. Thus, controller gains

may be too responsive to control the tricopter. GPS, ground speed source device, does not guarantee accuracy for sensor results. There are GPS receivers with Real-Time-Kinematic (RTK) capability to achieve centimetre level correction and positional accuracy, which can give more accurate ground speed results. Tests may continue with RTK-GPS and outdoor test stand may be required before performing flight tests.

Appendix B

B.2 Dummy-wing Mass and Inertia Calculation

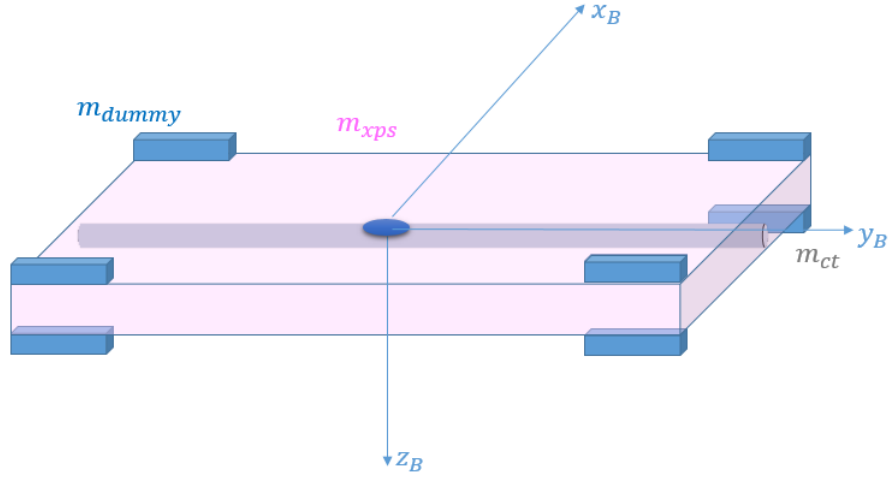


Figure B.23: Dummy-wing configuration layout

B.2.1 Mass Moment of Inertia of Prism

Mass moment of inertia of rectangular prism is calculated according to Equation (B.40) is given below [24]:

$$\begin{aligned}
 I_x^{xps} &= \frac{m_{xps}(z_{xps}^2 + y_{xps}^2)}{12} \\
 I_y^{xps} &= \frac{m_{xps}(z_{xps}^2 + x_{xps}^2)}{12} \\
 I_z^{xps} &= \frac{m_{xps}(x_{xps}^2 + y_{xps}^2)}{12}
 \end{aligned} \tag{B.40}$$

Where I_x^{xps} , I_y^{xps} , I_z^{xps} presents the mass moment of inertia about x, y and z axes respectively. Mass of prism is presented as m_{xps} . Thus, dimensions of the prism are presented as x_{xps} , y_{xps} , z_{xps} . Density is calculated according to sample XPS prism's weight and dimension of which same radii properties used for dummy-wing construction. Due to material dimensional restrictions, its length y_{xps} is predefined

before the calculations. Although the material itself is non-uniform, for simplicity and considering its weight and inertia contribution onto overall construction, it is assumed to be uniform.

B.2.2 Dummy Weights

Weights and inertias of XPS prism and carbon tube are not enough to meet the wing mass and inertia properties. Due to that reason, identical dummy masses are required. Each of the masses are predefined and chosen as 95 [gr]. Dummy mass is presented as m_{dummy} and they are located on the edges of XPS prism. Mass moment of inertia is calculated for each of the dummy masses according to equations given in [21] considering the positions according to body fixed frame as shown in Figure (B.23).

B.2.3 Mass Moment of Inertia of Hollow Cylinder

Mass moment of inertia of hollow cylinder is calculated according to equation (B.41) as given below [24]

$$\begin{aligned} I_x^{ct} &= \frac{m_{ct}}{12}(3(R_1^2 + R_2^2) + h_{ct}^2) \\ I_y^{ct} &= \frac{m_{ct}}{12}(3(R_1^2 + R_2^2) + h_{ct}^2) \\ I_z^{ct} &= \frac{m_{ct}}{2}(R_1^2 + R_2^2) \end{aligned} \quad (B.41)$$

Where I_x^{ct} , I_y^{ct} , I_z^{ct} presents the mass moment of inertia about x, y and z axes respectively. Mass of carbon tube is presented as m_{ct} . Inner and outer radii are presented as R_1 and R_2 respectively. Thus, length of the carbon tube is presented as h_{ct} . Mass of carbon tube is calculated as given equation (B.42) below:

$$m_{ct} = d_{ct}[kg/m].h_{ct}[m] \quad (B.42)$$

Where d_{ct} presents linear density of tube. Density is calculated according to sample tube's weight and length of which same radius properties used for dummy-wing construction. Furthermore, it is assumed to be uniform.

Appendix C

In this appendix, LQT control weight matrices, controller gains and eigen vectors of closed loop state matrix is given for Scorpion SII-3020-780Kv motor and 11x5.5 APC configuration of tilt rotor tricopter VTOL platform. Moreover, transition weight matrices are given both weighted pseudo inverse and blended inverse approach.

C.3 LQT - Weighting Matrices and Gains for Tricopter Attitude Control

$$R_{tricopter_v2} = \begin{bmatrix} 0.1920 & 0 & 0 \\ 0 & 0.0979 & 0 \\ 0 & 0 & 0.04496 \end{bmatrix} \quad (C.43)$$

$$Q_{tricopter_v2} = \begin{bmatrix} 5.1876 & 0 & 0 \\ 0 & 5.1876 & 0 \\ 0 & 0 & 1.0537 \end{bmatrix} \quad (C.44)$$

$$K_{tricopter_v2} = \begin{bmatrix} 1.1671 & 0 & 0 & 5.1876 & 0 & 0 \\ 0 & 2.1317 & -0.0042 & 0 & 5.1876 & 0.0462 \\ 0 & -0.0146 & 1.1368 & 0 & -0.1514 & 4.8407 \end{bmatrix} \quad (C.45)$$

$$K_{Ztricopter_v2} = \begin{bmatrix} 5.1876 & 0 & 0 \\ 0 & 5.1876 & 0.0462 \\ 0 & -0.1514 & 4.8407 \end{bmatrix} \quad (C.46)$$

$$eig(A_{triv2_{closedloop}}) = \begin{bmatrix} -4.4534 + 4.4534i \\ -4.4534 - 4.4534i \\ -3.5192 + 3.5192i \\ -3.5192 - 3.5192i \\ -3.4126 + 3.4126i \\ -3.4126 - 3.4126i \end{bmatrix} \quad (C.47)$$

C.4 LQT - Weighting Matrices and Gains for Forward Flight Control

$$R_{plane} = \begin{bmatrix} 0.01 & 0 & 0 \\ 0 & 0.0003 & 0 \\ 0 & 0 & 0.0004 \end{bmatrix} \quad (C.48)$$

$$Q_{plane} = \begin{bmatrix} 29.1805 & 0 & 0 \\ 0 & 29.1805 & 0 \\ 0 & 0 & 3.0396 \end{bmatrix} \quad (C.49)$$

$$K_{plane} = \begin{bmatrix} 5.0278 & 0 & 0.3656 & 53.6200 & 0 & -2.1150 \\ 0 & -13.4263 & 0 & 0 & -341.6460 & 0 \\ -1.8312 & 0 & -13.5750 & -31.0836 & 0 & -82.0886 \end{bmatrix} \quad (C.50)$$

$$K_{Z_{plane}} = \begin{bmatrix} 53.6200 & 0 & -2.1150 \\ 0 & -341.6460 & 0 \\ -31.0836 & 0 & -82.0886 \end{bmatrix} \quad (C.51)$$

$$eig(A_{plane_{closedloop}}) = \begin{bmatrix} -10.7535 + 10.7535i \\ -10.7535 - 10.7535i \\ -6.2210 + 6.2210i \\ -6.2210 - 6.2210i \\ -25.4461 + 25.4461i \\ -25.4461 - 25.4461i \end{bmatrix} \quad (C.52)$$

C.5 Weighted Pseudo Inverse - Transition to Forward Flight Control

$$W_{WPI_{t2p}} = \begin{bmatrix} \frac{e_1}{9650^4} & & & & & & \\ & \frac{e_1}{9650^4} & & & & & \\ & & \frac{e_1}{9650^4} & & & & \\ & & & \frac{e_1}{9650^4 \sin(\pi/4)^2} & & & \\ & & & & \frac{0.5e_2}{20^2} & & \\ & & & & & \frac{0.5e_2}{20^2} & \\ & & & & & & \frac{0.5e_2}{20^2} \end{bmatrix} \quad (C.53)$$

$$e_1 = 0.1 + \frac{V_\infty^2}{30^2 0.9} \quad (C.54)$$

$$e_2 = 1 - e_1 \quad (C.55)$$

C.6 Blended Inverse - Transition to Forward Flight Control

$$q_{t2p} = I_{7 \times 7} \quad (C.56)$$

$$W_{BI_{t2p}} = \begin{bmatrix} \frac{1}{9650^4} & & & & & & \\ & \frac{1}{9650^4} & & & & & \\ & & \frac{6}{9650^4 \cos(\pi/12)^2} & & & & \\ & & & \frac{6}{9650^4 \sin(\pi/4)^2} & & & \\ & & & & \frac{0.5}{20^2} & & \\ & & & & & \frac{1}{30^2} & \\ & & & & & & \frac{0.5}{20^2} \end{bmatrix} \quad (C.57)$$

Appendix D

In this appendix, weight matrices, controller gains and eigen vectors of closed loop state matrix of LQT and LQR-I controllers are given for AXI 2826/10 motor - Xoar 11x4 propeller configuration of tricopter platform.

D.9 LQT - Weighting Matrices and Gains for Tricopter Attitude Control

$$R_{lqt_{v1}} = \begin{bmatrix} 5.64e-6 & 0 & 0 & 0 \\ 0 & 5.64e-6 & 0 & 0 \\ 0 & 0 & 5.64e-6 & 0 \\ 0 & 0 & 0 & 0.1862 \end{bmatrix} \quad (\text{D.65})$$

$$Q_{lqt_{v1}} = \begin{bmatrix} 12.7324 & 0 & 0 \\ 0 & 19.0986 & 0 \\ 0 & 0 & 7.1620 \end{bmatrix} \quad (\text{D.66})$$

$$K_{lqt_{v1}} = \begin{bmatrix} 118.077 & 114.870 & 5.050 & 1011.244 & 737.389 & 46.737 \\ -132.231 & 126.988 & -15.666 & -1102.118 & 767.173 & -79.579 \\ -5.0116 & -240.529 & 9.0150 & -70.890 & -1499.780 & 23.137 \\ 0.047 & -0.023 & -0.708 & 0.654 & -0.301 & -6.180 \end{bmatrix} \quad (\text{D.67})$$

$$K_{Zlqt_{v1}} = \begin{bmatrix} 1011.244 & 737.389 & 46.737 \\ -1102.118 & 767.173 & -79.579 \\ -70.890 & -1499.780 & 23.137 \\ 0.654 & -0.301 & -6.180 \end{bmatrix} \quad (\text{D.68})$$

$$eig(A_{lqtv1_{closedloop}}) = \begin{bmatrix} -8.8925 + 8.8925i \\ -8.8925 - 8.8925i \\ -8.3203 + 8.3203i \\ -8.3203 - 8.3203i \\ -6.2118 + 6.2118i \\ -6.2118 - 6.2118i \end{bmatrix} \quad (D.69)$$

D.10 LQR-I - Weighting Matrices and Gains for Attitude Control

$$R_{lqri_{v1}} = \begin{bmatrix} 0.0043 & 0 & 0 & 0 \\ 0 & 0.0043 & 0 & 0 \\ 0 & 0 & 0.0043 & 0 \\ 0 & 0 & 0 & 47.7465 \end{bmatrix} \quad (D.70)$$

$$Q_{lqri_{v1}} = \begin{bmatrix} 0.25 & 0 & 0 & 0 & 0 & 0 & 0 & 0 & 0 \\ 0 & 0.25 & 0 & 0 & 0 & 0 & 0 & 0 & 0 \\ 0 & 0 & 0.25 & 0 & 0 & 0 & 0 & 0 & 0 \\ 0 & 0 & 0 & 0.5 & 0 & 0 & 0 & 0 & 0 \\ 0 & 0 & 0 & 0 & 0.25 & 0 & 0 & 0 & 0 \\ 0 & 0 & 0 & 0 & 0 & 0.5 & 0 & 0 & 0 \\ 0 & 0 & 0 & 0 & 0 & 0 & 32.8 & 0 & 0 \\ 0 & 0 & 0 & 0 & 0 & 0 & 0 & 73.9 & 0 \\ 0 & 0 & 0 & 0 & 0 & 0 & 0 & 0 & 8.9 \end{bmatrix} \quad (D.71)$$

$$K_{lqri_{v1}} = \begin{bmatrix} 28.7782 & 32.6318 & 1.1965 & 58.3043 & 52.7302 & 2.3514 \\ -32.6125 & 36.3399 & -4.3948 & -63.7028 & 53.8004 & -4.6397 \\ -0.8668 & -68.5734 & 2.7655 & -3.9406 & -106.2715 & 1.7501 \\ 0.0184 & -0.0125 & -0.1989 & 0.0905 & -0.0662 & -0.4277 \end{bmatrix} \quad (D.72)$$

$$K_{Z_{lqr}^{i_{v1}}} = \begin{bmatrix} 58.3043 & 52.7302 & 2.3514 \\ -63.7028 & 53.8004 & -4.6397 \\ -3.9406 & -106.2715 & 1.7501 \\ 0.0905 & -0.0662 & -0.4277 \end{bmatrix} \quad (\text{D.73})$$

D.11 LQT - Weighting Matrices and Gains for Tricopter Ground Speed Hold Control

$$R_{V_{hold}^{v1}} = \begin{bmatrix} 146.4225 & 0 & 0 & 0 \\ 0 & 146.4225 & 0 & 0 \\ 0 & 0 & 1.0963 & 0 \\ 0 & 0 & 0 & 0.0470 \end{bmatrix} \quad (\text{D.74})$$

$$Q_{V_{Hold}^{v1}} = \begin{bmatrix} 4 & 0 & 0 \\ 0 & 8 & 0 \\ 0 & 0 & 10 \end{bmatrix} \quad (\text{D.75})$$

$$K_{V_{hold}^{v1}} = \begin{bmatrix} 0 & 0.2145 & -0.0006 \\ -0.1653 & 0 & 0 \\ 0 & 1.0729 & -0.0199 \\ 0 & 0.0637 & 14.5890 \end{bmatrix} \quad (\text{D.76})$$

$$K_{Z_{V_{hold}^{v1}}} = \begin{bmatrix} 0 & 0.2145 & -0.0006 \\ -0.1653 & 0 & 0 \\ 0 & 1.0729 & -0.0199 \\ 0 & 0.0637 & 14.5890 \end{bmatrix} \quad (\text{D.77})$$

$$eig(A_{V_{hold}^{closedloop}}) = \begin{bmatrix} -1.6216 \\ -5.3586 \\ -2.4976 \end{bmatrix} \quad (\text{D.78})$$

Appendix E

E.12 Coefficients of Motor-Propeller Surface Fit Equations

Table E.2: Coefficients of Force Surface Fit Equations

σ [deg]	a_0	a_1	a_2	a_3	a_4	a_5
90	1.912	-0.09383	-0.0008031	-0.01711	7.427e-06	2.48e-07
70	1.915	-0.03305	-0.0009265	-0.01537	4.467e-07	2.647e-07
50	1.641	-0.04156	-0.0007519	-0.009203	3.486e-06	2.492e-07
30	1.703	-0.1408	-0.0006502	5.586e-06	1.575e-05	2.319e-07
0	0.5811	-0.1043	-0.0002887	-0.006627	1.553e-05	2.056e-07

Table E.3: Coefficients of Torque Surface Fit Equations

σ [deg]	b_0	b_1	b_2	b_3	b_4	b_5
90	-0.07316	0.0009318	3.35e-05	0.0002711	-4.82e-07	-6.15e-09
70	-0.05737	0.0004911	2.80e-05	0.0002637	-4.33e-07	-5.81e-09
50	-0.05253	0.0001433	2.57e-05	0.0001469	-3.62e-07	-5.55e-09
30	-0.0481	-0.0002621	2.54e-05	6.695e-05	-2.91e-07	-5.51e-09
0	-0.04425	0.0008161	2.35e-05	-3.198e-05	-3.88e-07	5.38e-09

Table E.4: Coefficients of RPM Surface Fit Equations

σ [deg]	c_0	c_1	c_2	c_3	c_4	c_5
90	2217	-26.42	103.4	6.774	-1.646	-0.1651
70	1833	57.04	91.7	2.592	-1.195	-0.108
50	1887	25.24	102.1	1.288	-0.6223	-0.2128
30	1783	12.67	106.1	-0.6159	-0.1332	-0.2615
0	1735	-18.3	113	-0.6369	0.2276	-0.3325

E.13 Aerodynamic Coefficients

Aerodynamic coefficients that are given below are multiplied with relative control surface deflections, α and β values. Unit of these parameters is degree.

Table E.5: C_X aerodynamic coefficients

C_{X_0}	$\Delta C_{X_{\delta_{elev}}}$	$\Delta C_{X_{\delta_{ail}}}$	$\Delta C_{X_{\alpha}}$	$\Delta C_{X_{\alpha^2}}$
-0.0299	0.003	-0.0028	7.1703e-04	4.9220e-04

Table E.6: C_Y aerodynamic coefficient

$\Delta C_{Y_{\beta}}$	-0.0035
------------------------	---------

Table E.7: C_Z aerodynamic coefficients

C_{Z_0}	$\Delta C_{Z_{\delta_{elev}}}$	$\Delta C_{Z_{\alpha}}$
-0.0657	-0.0162	-0.0523

Table E.8: C_l aerodynamic coefficients

$\Delta C_{l_{\delta_{ail}}}$	$\Delta C_{l_{\beta}}$
0.0053	-9.8137e-04

Table E.9: C_m aerodynamic coefficients

C_{m_0}	$\Delta C_{m_{\delta_{elev}}}$	$\Delta C_{m_{\alpha}}$
-0.0548	-0.0248	-0.0398

Table E.10: C_n aerodynamic coefficients

$\Delta C_{n_{\delta_{rud}}}$	$\Delta C_{n_{\beta}}$
-0.0017	0.0012

E.14 VTOL and Tricopter Parameters

$$I_{vtol} = \begin{bmatrix} 0.2995 & -0.0004 & 0.0096 \\ -0.0004 & 0.3756 & 0.0004 \\ 0.0096 & 0.0004 & 0.4238 \end{bmatrix} [kg.m^2] \quad (E.79)$$

$$m_{vtol} = 4 [kg] \quad (E.80)$$

$$I_{tri} = \begin{bmatrix} 0.1310 & -0.0004 & 0.0020 \\ -0.0004 & 0.3121 & 0.0004 \\ 0.0020 & 0.0004 & 0.1958 \end{bmatrix} [kg.m^2] \quad (E.81)$$

$$m_{tri} = 3 [kg] \quad (E.82)$$

Table E.11: Position vectors of each motor according to Center of Gravity (CG)

	x	y	z
r_1	0.2700	-0.4450	-0.0384
r_2	0.2700	0.4450	-0.0384
r_3	-0.5400	0	-0.0384

The unit of measurement that is given in Table (E.11) is meter.